2009

Imaging of Tyramine-Substituted Hydrogels for Tissue Replacement

Ediuska V. Laurens
Cleveland State University

IMAGING OF TYRAMINE-SUBSTITUTED HYDROGELS FOR TISSUE REPLACEMENT

EDIUSKA V. LAURENS

Bachelor of Science in Aerospace Engineering

State University of New York at Buffalo

May 2003

Master of Science in Mechanical Engineering

State University of New York at Buffalo

May 2005

submitted in partial fulfillment of requirements for the degree

DOCTORATE OF ENGINEERING IN BIOMEDICAL ENGINEERING

at the

CLEVELAND STATE UNIVERSITY

December 2009

This dissertation has been approved

for the Department of **CHEMICAL AND BIOMEDICAL ENGINEERING**

and the College of Graduate Studies by

_____

Dissertation Committee Chairperson, *Anthony Calabro, Ph.D.*

Chemical and Biomedical Engineering
Department / Date

_____

Nolan Holland, Ph.D.

Chemical and Biomedical Engineering
Department / Date

_____

Lars Gilbertson, Ph.D.

Chemical and Biomedical Engineering
Department / Date

_____

Miron Kaufman, Ph.D.

Physics
Department / Date

_____

Mark Kayanja, M.D.,Ph.D.

Chemical and Biomedical Engineering
Department / Date

I dedicate this dissertation work to my beloved family: mom and dad Rosa and Aquiles Laurens, brothers Ybsen and Aquiles J., and sister Nadeska. Their unconditional love and support have been the driving force for accomplishing my most ambitious goals and dreams; at the cost of being apart from them.

Esta disertación esta dedicada a mi querida familia: mama y papa Rosa y Aquiles Laurens, hermanos Ybsen y Aquiles J, y hermana Nadeska. Su amor y apoyo incondicional han sido la fuerza que me ha llevado a alcanzar mis metas y sueños mas ambiciosos, al costo de estar apartado de ellos.

ACKNOWLEDGEMENTS

Nothing is too big or small of a dream, anything you want, you can make yours, anything you want in the world!

This very long, but so worthy journey would have been next to impossible without the guidance of my committee members, help from friends, and support from my family.

I would like to express my deepest gratitude to my advisor, Dr. Anthony Calabro, for his excellent guidance, patience, caring, and providing me with an exceptional atmosphere for doing research. I would have not wanted to be in any other lab!

I would also like to thank:

My committee members, Dr. Nolan Holland, Dr. Lars Gilbertson, Dr. Mark Kayanja, and Dr. Miron Kaufman for their guidance and accepting nothing less than the best research I could produce.

Dr. Erika Schneider and Dr. Carl Winalski for providing me with their outstanding MRI expertise and showing me the beauty of T1 and T2 maps. Dr. Schneider, I will miss you picking me up at 5 am to get the imaging going!

Dr. Brian Davis for being such an amazing research and life mentor and continuously inspiring me to be the BEST scientist and person that I can be!

The amazing people at CCF who have made these past four years an incredible experience for me. Especially, Amit Vasanji for always helping me when I needed him both as an engineer and as a friend; Jackie Loftis for being such a great labmate and friend always trying to ease the long and sometimes frustrating process of dissertation writing; and finally, Aniq Darr for teaching me the basics and giving me clever advice every time.

Everyone at CSU, in particular, Becky, Darlene, and Dr. Gatica for being so caring and supportive all these years.

My wonderful friends, especially those residing in Cleveland, who have become my family: Uma for being the best ER and yoga companion, Smruta for being my soul-minded friend, and Elie for your honest friendship and most importantly providing transportation for all of us to meet when required.

Finally, I deeply thank my dearly loved family for all they have sacrificed to provide me with everything I needed to succeed and fulfill my dreams.

IMAGING OF TYRAMINE-SUBSTITUTED HYDROGELS
FOR TISSUE REPLACEMENT

EDIUSKA V. LAURENS

ABSTRACT

Novel tyramine-based hyaluronan (HA) and collagen hydrogels have been developed in which cross-linking is accomplished via peroxidase-mediated dityramine linkages allowing direct cross-linking *in vivo*. These TB hydrogels possess advantageous physical properties, which include excellent biocompatibility and the ability to mimic the biological, structural and mechanical properties of normal, healthy tissues, including cartilage, and thus provide for synthetic, implantable biomaterials suitable for a wide range of tissue types. The efficacy of these TB-hydrogels has been previously tested in a number of clinically relevant animal models, which have evaluated their applicability for the repair/replacement of various tissues, including cartilage. Nevertheless, there exists a fundamental need for non-destructive methods to identify, distinguish, quantify and trace these biomaterials *in vivo*. Magnetic Resonance Imaging (MRI) is a broadly used non-invasive clinical imaging methodology that allows direct visualization of soft tissues. Our results indicated that T1 and T2 mapping can differentiate and measure changes in HA and collagen concentration both alone and in combination with composite materials, composed of HA and collagen at the concentrations found in cartilage resulting in T1 values representative of cartilage. Furthermore, the dGEMRIC technique was able to quantify the HA concentration in phantoms of known HA concentration. These MRI techniques could detect and differentiate the tyramine-based hydrogels in implanted joints, and accurately quantify their volumes.

TABLE OF CONTENTS

LIST OF TABLES

Table **Page**

LIST OF FIGURES

Figure **Page**

CHAPTER I

BACKGROUND

1.1 Macromolecules in Cartilage

Cartilage is an avascular tissue consisting of cells (chondrocytes) in an extensive extracellular matrix (ECM) composed mainly of proteoglycans (PG), collagen, and water. The properties of the tissue depend on the structure and organization of the macromolecules in the ECM. The collagen, primarily type II, but also type IX and XI, forms a dense fibrillar network that is embedded in a high concentration of PGs (up to 100 mg/ml), **Fig 1.1**. The PG, because of its polyanionic glycosaminoglycan (GAG) chains, creates a large osmotic pressure that draws water into the tissue and expands the collagen network. The balance between the osmotic swelling pressure of the PGs and the tension in the collagen fibers produces the compressive properties characteristic of this tissue. The biomechanical properties of cartilage are critically dependent on the integrity of the collagen network and on the maintenance of a high concentration of PGs

within the matrix **[21]**. Hence, any loss of, for instance, PG from the cartilage matrix due to physiologic or pathologic processes must be balanced by *de novo* synthesis of PGs by the chondrocytes. Failure of this compensatory synthesis and decrease of the effective concentration of PGs within the matrix will cause alteration of the biomechanical properties of the tissue, thereby affecting the biologic function of cartilage, as in osteoarthritis **[46]**.

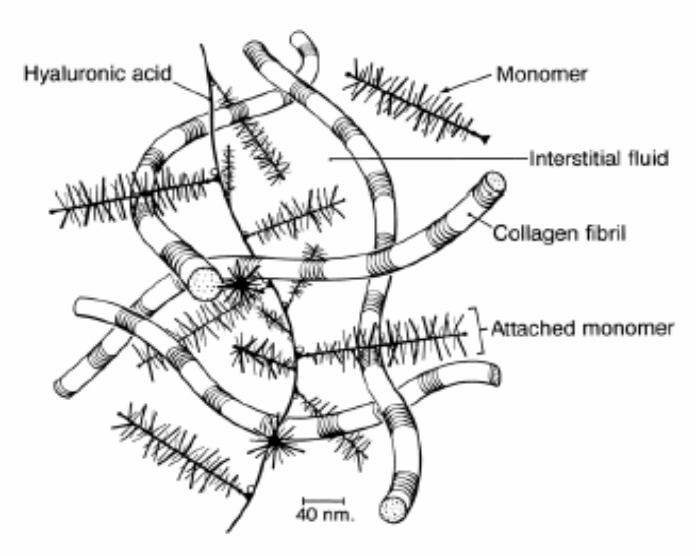

Figure 1.1. Molecular Organization of the Extracelullar Matrix of Articular Cartilage [34].

The most abundant PG in cartilage is aggrecan, which consists of a long, extended protein core with up to 100 chondroitin sulfate (CS) and 50 keratan sulfate (KS) GAG chains covalently bound to the protein core. At the N-terminal end of the protein core, one of the globular domains (G1) has the specific function of binding to hyaluronan (HA). The functions of the other domains of aggrecan are unknown. The link protein (LP), which is a separate smaller molecule, binds to both the G1 domain of aggrecan and HA, stabilizing the bond, and subsequently forming the aggrecan-HA-LP complexes referred to as PG aggregates **(Fig 1.2)**. Aggregation helps stabilize the aggrecan molecules within the ECM, and since each HA chain is long and unbranched, many aggrecan molecules can bind to a single HA to form a large PG aggregate **(Fig 1.3) [34]**.

HA is a linear, non-sulfated GAG composed of repeating disaccharide units linked with β-1-4, β-1-3 bonds between D-glucuronic acid and N-acetyl-D-glucosamine **(Fig 1.4).**

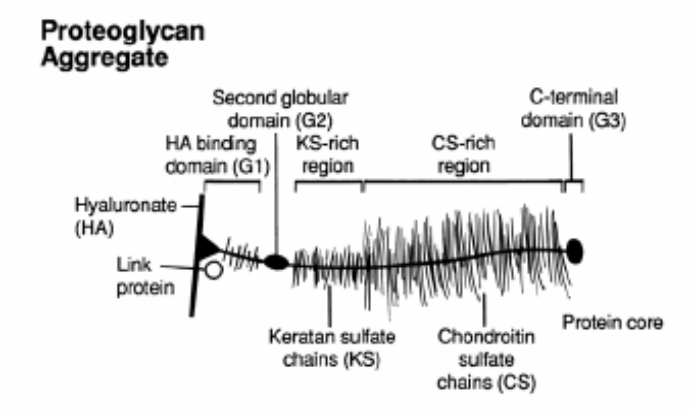

Figure 1.2. Aggrecan and its Binding to Hyaluronan. The protein core has several globular domains (G1, G2, and G3), with other regions containing the keratan sulfate and chondroitin sulfate glycosaminoglycan chains. The N-terminal G1 domain is able to bind specifically to hyaluronan and is stabilized by link protein **[34].**

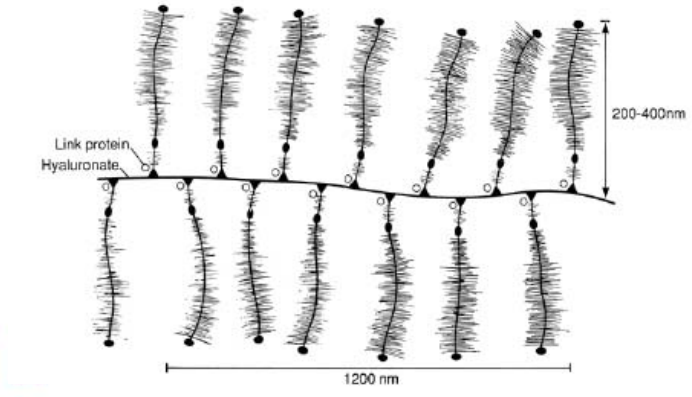

Figure 1.3. Aggrecan Molecules Arranged as a Proteoglycan Aggregate [34].

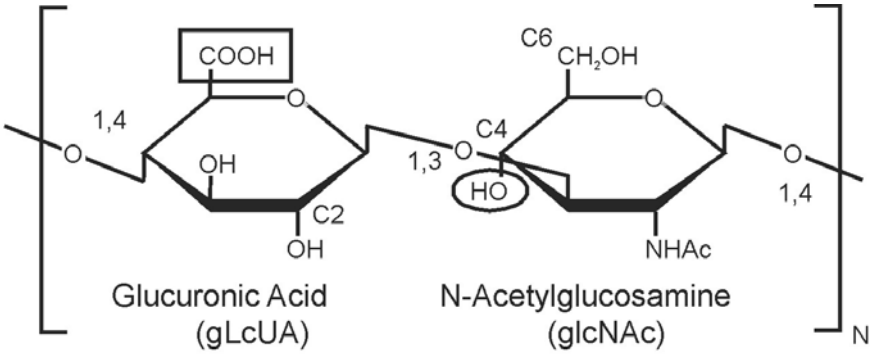

Figure 1.4. Chemical Structure of the Repeat Disaccharide of Hyaluronan.

The HA in cartilage has repeating carboxyl (COOH) **(Fig 1.4)**. In solution, these groups become ionized (COO^-), and in the physiologic environment, they attract positive counterions such as Ca^{2+} and Na^+ to maintain overall electroneutrality. These free-floating ions within the interstitial water are present at a higher concentration than that found in the surrounding fluids (i.e. synovial fluid) giving rise to an osmotic pressure (Donnan pressure). Normally, ions flow out of a tissue to equilibrate their concentration with the surrounding fluid, but in cartilage they are prevented from doing so by the fixed nature of their negative counter ions (i.e. the COO^- groups on the HA), and the need to maintain electroneutrality. Alternatively, water would flow into the tissue from the surrounding fluids thus equilibrating the tissue's free-floating positive counter ion concentration with that in the surrounding fluids. However, additional swelling is again resisted by the inextensible nature of the collagen meshwork. In addition, the tight packing of the cartilage aggregates, causes their fixed-negative charge groups to be spaced only 10 to 15 angstroms apart, resulting in strong charge-to-charge repulsive forces (electrorepulsive forces). As with the Donnan effect, the tendency to swell to lessen these repulsive forces is resisted by the inextensible nature of the collagen meshwork. Upon compression, the distance between the fixed-negative charge groups on the GAGs decrease, which increases the charge-to-charge repulsive forces as well as increasing the concentration of the free-floating positive counter ions **[34]**. Thus both the Donnan and electrorepulsion effects are intensified by compression. Both effects contribute to the swelling pressure of

articular cartilage and its ability to resist deformation and absorb compressive loads **[4,33,39,50]**.

Articular cartilage is often described as a viscoelastic, biphasic material, composed of a solid phase (cartilage aggregates and collagen) and a fluid phase (water and dissolved ions) **[13,17,16,27]**. An important feature of articular cartilage is how the organization of its ECM is designed to deflect the forces applied during loading from the load susceptible solid phase of the tissue to the load resistant fluid phase of water. This phenomenon is referred to as stress shielding of the solid matrix, and results as follows. The nature of the cartilage ECM produces a material with very low permeability (very small pores), which creates drag during interstitial fluid flow. Interstitial fluid pressure is thus generated during compressive loading, and during dynamic loading it is the primary force responsible for supporting the applied load while matrix compression is a minor factor. During compression, the porosity is reduced further, which increases the already high frictional drag forces. Under constant load, creep due to the exit of water from the tissue continues **(Fig 1.5)** until the load support is gradually transferred from the fluid phase (as the fluid pressure dissipates) to the solid phase.

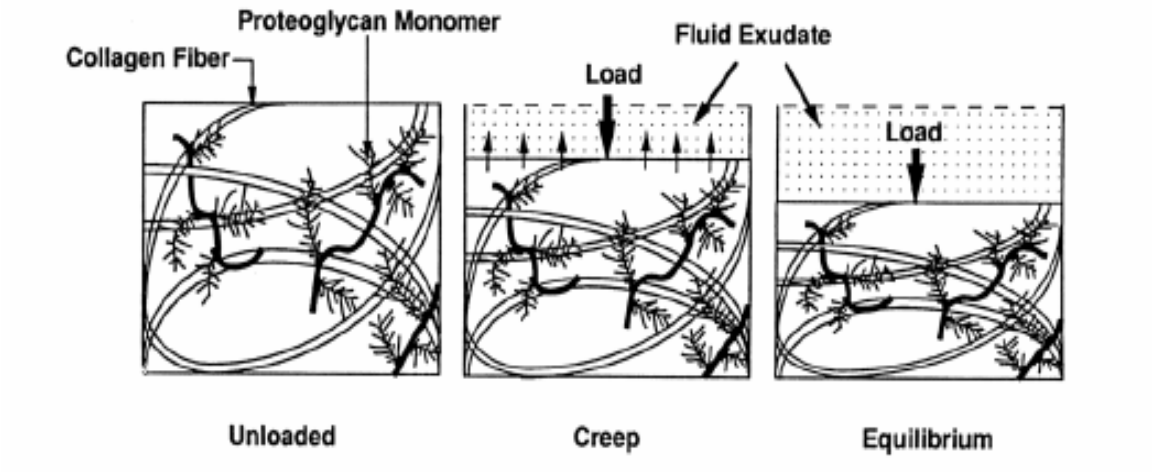

Figure 1.5. Biphasic Creep Behavior of Articular Cartilage During Compression. The rate of creep is controlled by the rate of fluid exudation from the tissue **[34].**

Typically, for normal cartilage, this equilibration process takes 2.5 to 6.0 hours to achieve. At equilibrium the fluid pressure subsides, and load support is provided entirely by the compressed collagen-aggrecan solid matrix **(Fig 1.5)**. However, because of the long equilibration time required for relaxation, articular cartilage is normally dynamically loaded under physiologic conditions, that is, no equilibrium state is reached. Thus, fluid pressurization will always exist within the tissue. Thus in normal articular cartilage, fluid pressurization is the dominant physiologic load-support mechanism in diarthrodial joints. This unique behavior of cartilage occurs only because the solid matrix has a very low permeability. Thus, one reason that articular cartilage is able to provide its unique and essential biomechanical function for eight decades or more is that nature has devised a material in which most of the destructive forces encountered are supported by water and not by the biological material itself. Obviously any artificial or synthetic matrix designed to reproduce the mechanical properties and longevity of articular cartilage must have a similar ability to deflect compressive loads to water **[7,33,39,50]**.

In designing biomaterials for cartilage replacement, a unique technology has been developed that chemically modifies the GAGs and collagen macromolecules, normally present in cartilage, as they are proven by nature to produce a mechanically functional cartilage tissue. The chemistry involved in this technology will be described next.

1.2 Tyramine-Based Hydrogels

Most of the chemical modification strategies for HA target the carboxyl or hydroxyl groups of the sugar moieties **[54].** In our laboratory, the focus is on chemical modification of the carboxyl groups of both HA and collagen with tyramine **[11]**. For the tyramine-based hyaluronan (TB-HA) hydrogels, hydrogel formation is produced in two stages involving two separate chemistries. **Step 1** involves substitution of carboxyl groups located on the glucuronic acid (glcA) residues of repeating disaccharides of HA **(box, Fig. 1.4)** with the amine group of tyramine **(Fig. 1.6)** through the formation of an amide bond using conventional carbodiimide chemistry. After purification of the tyramine-substituted HA (TS-HA), hydrogels are produced in **Step 2** by means of the enzymatic cross-linking of hydroxyphenyl groups on tyramine adducts on adjacent HA molecules.

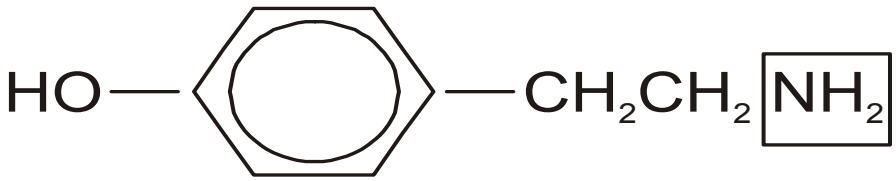

B. Tyramine

Figure 1.6. Chemical Structure of Tyramine.

Step 1: Carbodiimide Chemistry or Tyramine Substitution Reaction

HA is chemically substituted with tyramine through conventional carbodiimide chemistry, in which the carboxyl groups within the glucuronic acid (glcA) residues of the HA are reacted with the amine group of tyramine to form an amide bond **(Fig 1.7)**. The reaction consists of activating the carboxyl group with the carbodiimide, 1-ethyl-3-(3-dimethylaminopropyl)carbodiimide (EDC) to produce a reactive O-acylisourea intermediate. The desired amine bond, which covalently anchors tyramine to the HA molecule, is created by nucleophilic attack of the electron rich amine group of the now electron deficient carbonyl carbon of glcA. The EDC is converted to the unreactive acylurea, 1-ethyl-3-(3-dimethylaminopropyl)urea (EDU). The catalyst N-hydroxysuccinimide is introduced to improve the EDC reaction by formation of an active ester at more moderate pHs of 6 to 6.5, which diminishes the unproductive hydrolysis of EDC to EDU. Macromolecular TS-HA, produced through the carbodiimide reaction, is then dialyzed as a way of purifying from small molecular weight reagents and reaction products. After sterilization through filtration, the TS-HA is lyophilized and then resuspended at the desired concentrations in a proper sterile physiologic buffer.

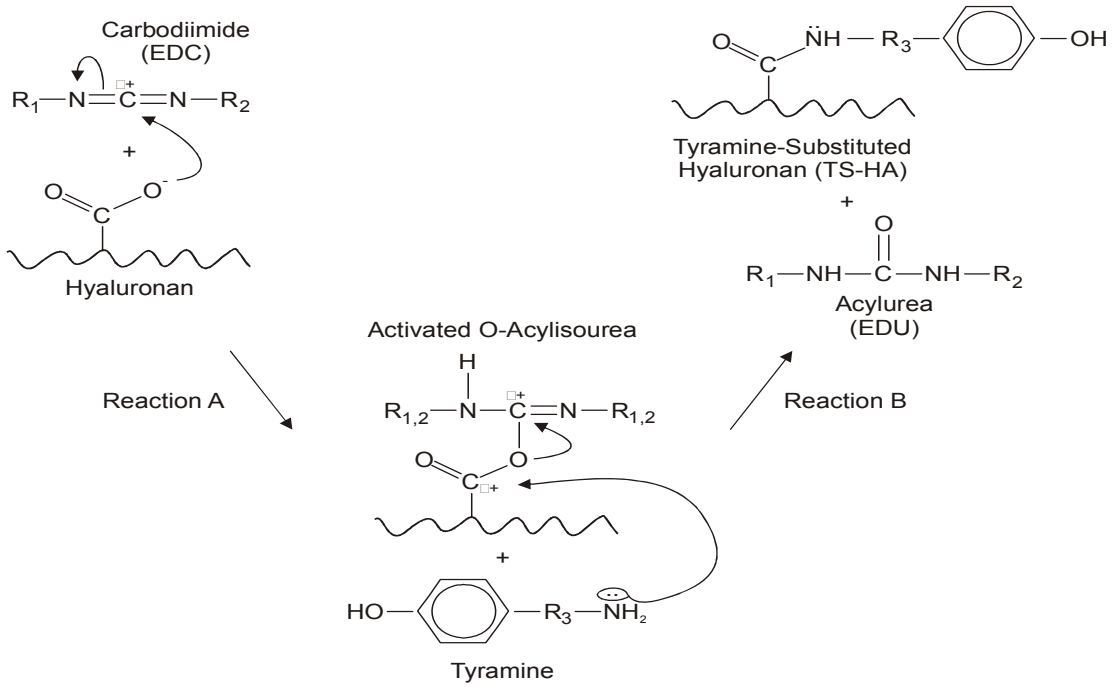

Figure 1.7. Schematic of Carbodiimide Chemistry. The carbodiimide-mediated formation of an amide bond from the primary amine of tyramine and a carboxyl group on a disaccharide of HA is shown, where R_1 = CH_2CH_3, R_2 = $CH_2CH_2CH_2NH^+(CH_3)_2Cl^-$ and R_3 = CH_2CH_2.**Reaction A:** activation of the carboxyl group with the carbodiimide, EDC, to create a reactive O-acylisourea intermediate. **Reaction B:** nucleophilic attack by the electron rich amine group of tyramine on the now electron deficient carbonyl carbon forming the desired amide bond between tyramine and HA.

Step 2: Peroxidase Catalyzed Oxidation of Tyramine to Dityramine

(Cross-linking Reaction)

Peroxidase in the presence of dilute hydrogen peroxide has the ability to preferentially remove the phenolic hydroxyl hydrogen atom from tyramine, leaving the phenolic hydroxyl oxygen with a single unshared atom acting as an extremely reactive free radical. The free radical isomerizes to one of the two equivalent ortho-position carbons, and afterward two such structures dimerize to create a covalent bond cross-linking the structures, which after enolizing, produces dityramine as show in **Fig 1.8**. The multiple formation of dityramine cross-links between adjacent HA molecules results in the formation of a three-dimensional network or hydrogel, which at the appropriate HA concentration functions as a biomimetic for cartilage ECM. It is important to note that the TS-HA is not the substrate for the peroxidase, but rather the peroxide. The cross-linking reaction is induced by the free radicals, produced from the reaction of the peroxide with the peroxidase, preferentially being accepted by the hydroxyphenyl group of tyramine.

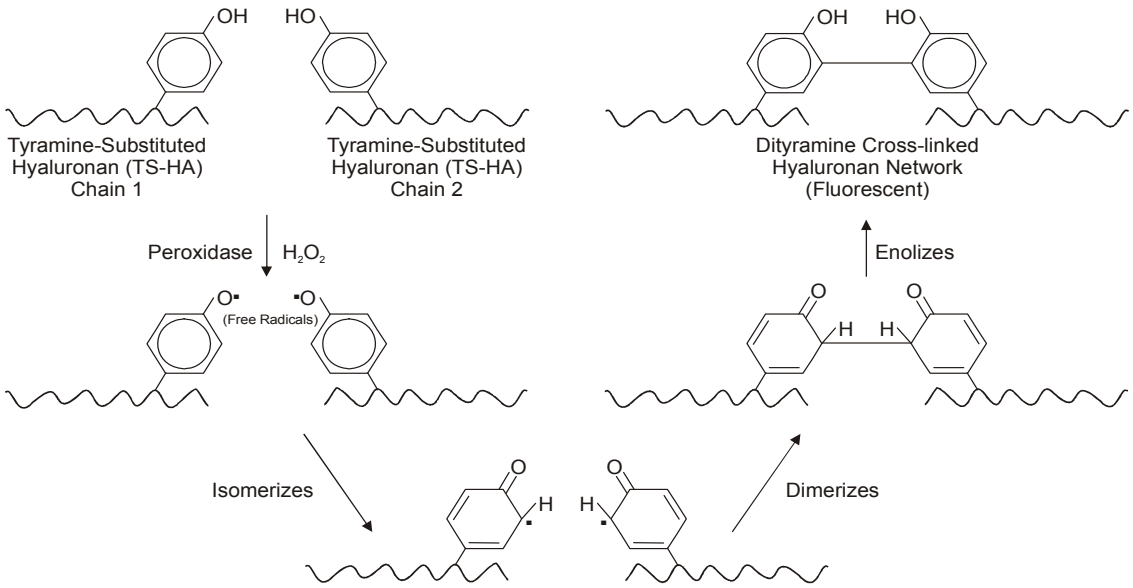

Figure 1.8. Schematic of the Proposed Mechanism for Peroxidase Catalyzed Oxidation of Tyramine on TS-HA to Form Dityramine Cross-links.

In producing TB-CO hydrogels, collagen in the commercial form of gelatin (GE) is utilized. GE is a mixture of water soluble, large polypeptides derived from denatured collagen. Traditionally, GE is produced by extraction from collagen-rich tissues, such as bovine or porcine skin or bone. Porcine skin GE was utilized for our experiments. The polypeptides have the same amino acid composition as the parent type I collagen, and they cover a very broad distribution range of molecular weights **[32]**. The tyramine substitution and hydrogel formation of TB-GE hydrogels follow the equivalent two step chemistry described above, except that the carboxyl groups involved in the tyramine substitution of Step 1 are on the side chains of the amino acids, aspartate and glutamate shown in **Fig 1.9**.

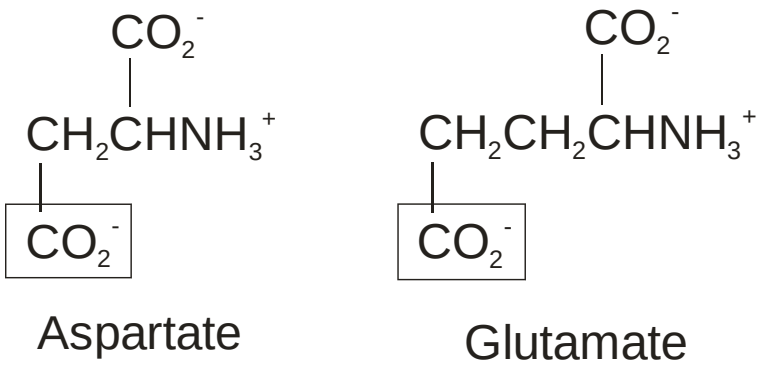

Figure 1.9. Aspartate and Glutamate Showing the Carboxyl Group Involved in Tyramine Substitution.

Table I displays the amino acid composition by residue and mole percent of the porcine GE material utilized for our experiments. During acid hydrolysis of the GE sample prior to derivatization, separation and detection of individual amino acids by HPLC, the amide side chains of asparagine and glutamine residues are hydrolyzed releasing ammonia and generating aspartate and glutamate, residues respectively. Thus the mole percents for aspartate (Asp) and glutamate (Glu) listed in **Table I** include the mole percents for both aspartate and asparagine (Asn), and glutamate and glutamine (Gln), respectively. It is therefore impossible to determine from amino acid analysis the actual number of available carboxyl groups on GE for tyramine substitution, however, the ratio of the moles of tyramine to the moles of Asp and Glu does allow for comparison of the effectiveness of the tyramine substitution reaction from one GE preparation to another.

Amino Acid Residue	Unsubstituted Gelatin Mole %	Tyramine-substituted Gelatin Mole %
Asp	5.21	5.13
Thr	1.83	1.8
Ser	3.66	3.6
Glu	8.02	7.9
Pro	13.91	13.71
Gly	38.72	38.15
Ala	12.40	12.22
Cys	0	0
Val	2.46	2.42
Met	0	0
Ile	1.04	1.03
Leu	2.62	2.58
Tyr	0.19	0.19
Phe	1.51	1.49
Lys	2.88	2.84
His	0.57	0.56
Arg	4.98	4.9
Tyramine	0	1.47

Table I. Amino acid composition as mole percent for type I gelatin (Sigma, St. Louis, MO; 300 bloom) both unsubstituted and tyramine substituted.

Figure 1.10 shows the amino acid sequence predicted for human type I collagen based on its DNA sequence. For comparison purposes, the human type I collagen and porcine GE sequences are expected to be highly conserved, and thus closely resemble the GE material used for our experiments. The human type I collagen sequence in **Figure 1.10** gives a predicted isoelectric point (pI) of 9.3 using both the scansite molecular weight and isoelectric point calculator and the protein calculator v3.3 programs **[42,40]**. This result is indicative of a basic or positively charged protein. We may assume this property for the gelatin used in our experiments. However, we also need to consider the fact that the chemistry for tyramine-substitution of GE neutralizes a portion of the negatively charged carboxyl groups on the aspartate and glutamate residues in GE by the mole percent of tyramine substitution, making the protein more positive after tyramine substitution.

G P M G P S G P R G L P G P P G A P G P Q G F Q G P P G E P
G E P G A S G P M G P P G P P G P P G K N G D D G E A G K P
G R P G E R G P P G P Q G A R G L P G T A G L P G M K G H R
G F S G L D G A K G D A G P A G P K G E P G S P G E N G A P
G Q M G P P G L P G E R G R P G A P G P A G A R G N D G A T
G A A G P P G P T G P A G P P G F P G A V G A K G E A G P Q
G P R G S E G P Q G V R G E P G P P G P A G A A G P A G N P
G A D G Q P G A K G A N G A P G I A G A P G F P G A R G P S
G P Q G P G G P P G P K G N S G E P G A P G S K G D T G A K
G E P G P V G V Q G P P G P A G E E G K R G A R G E P G P T
G L P G P P G E R G G P G S R G F P G A D G V A G P K G P A
G E R G S P G P A G P K G S P G E A G R P G E A G L P G A K
G L T G S P G S P G P D G K T G P P G P A G Q D G R P G P P
G P P G A R G Q A G V M G F P G P K G A A G E P G K A G E R
G V P G P P G A V G P A G K D G E A G A Q G P P G P A G P A
G E R G E Q G P A G S P G F Q G L P G P A G P P G E A G K P
G E Q G V P G D L G A P G P S G A R G E R G F P G E R G V Q
G P P G P A G P R G A N G A P G N D G A K G D A G A P G A P
G S Q G A P G L Q G M P G E R G A A G L P G P K G D R G D A
G P K G A D G S P G K D G V R G L T G P I G P P G P A G A P
G D K G E S G P S G P A G P T G A R G A P G D R G E P G P P
G P A G F A G P P G A D G Q P G A K G E P G D A G A K G D A
G P P G P A G P A G P P G P I G N V G A P G A K G A R G S A
G P P G A T G F P G A A G R V G P P G P S G N A G P P G P P
G P A G K E G G K G P R G E T G P A G R P G E V G P P G P P
G P A G E K G S P G A D G P A G A P G T P G P Q G I A G Q R
G V V G L P G Q R G E R G F P G L P G P S G E P G K Q G P S
G A S G E R G P P G P M G P P G L A G P P G E S G R E G A P
G A E G S P G R D G S P G A K G D R G E T G P A G P P G A P
G A P G A P G P V G P A G K S G D R G E T G P A G P A G P V
G P A G A R G P A G P Q G P R G D K G E T G E Q G D R G I K
G H R G F S G L Q G P P G P P G S P G E Q G P S G A S G P A
G P R G P P G S A G A P G K D G L N G L P G P I G P P G P R
G R T G D A G P V G P P G P P G P P G P P G P P G P P

Figure 1.10. Human Type I Collagen Sequence.

1.2.1 Measurement of Percent Substitution of Tyramine

The percent substitution of tyramine on HA can be calculated from the molar ratio of covalently bound tyramine residues to the total carboxyl groups on HA. Due to its hydroxyphenyl group, tyramine strongly absorbs UV light at a maximum of 275 nm. Thus, the molar concentration of tyramine associated with a TS-HA preparation can be easily determined by measuring its absorption at 275 nm relative to a tyramine standard curve as shown previously by our group **[11]**. Additionally, the molar concentration of total carboxyl groups in TB-HA is easily measured spectrophotometrically utilizing the standard hexuronic acid assay **[4]** routinely used for quantification of microgram quantities of GAG. The percent substitution of tyramine in TB-HA is consistently between 4 to 6%, which maintains the physiological properties of the native HA.

An estimate of the amount of tyramine covalently bound within a TS-GE and the molar concentration of total carboxyl groups in a given TS-GE preparation can be calculated through the recovery of nanomoles of amino acids obtained from Amino Acid Analysis (AAA) utilizing Cation Exchange Chromatography, as described in **Appendix A**. The percent substitution of tyramine in the TB-GE prepared for our experiments was consistently 11 to 13%. As mentioned above this is an underestimate of the actual tyramine substitution as the mole percent of Asp and Glu reported for GE upon its hydrolysis also contains Asn and Gln, respectively.

1.2.2 Detection of Dityramine Cross-links

Another advantageous spectrophotometric property is that the dityramine cross-links fluoresces blue-green upon exposure to UV light with an excitation maximum of 285 nm and an emission maximum of 415 nm. This property permits assessment of the degree of cross-linking within TB-HA hydrogels both qualitatively and quantitatively. Qualitatively, the fluorescence properties allow the visualization of hydrogels to assess both the initiation of the cross-linking reaction and its propagation all through the volume of a hydrogel form associated with peroxide diffusion. This is accomplished through the observation of hydrogels formation once placed on a UV light box. Quantitatively, the total fluorescence can be determined relative to a dityramine standard curve, and normalized to the total of hexuronic acid (carboxyl groups) content as described above for measurement of tyramine substitution **[11]**. This can be performed using either intact hydrogels, which are optically clear, or hydrogels that have been initially solubilized by hyaluronidase treatment.

Furthermore, our group has been able to identify methods for definitive characterization and quantification of the products of both the tyramine substitution (Step1) and cross-linking (Step 2) reactions involved in hydrogel formation, which includes NMR spectroscopy, Flourophore-Assisted Carbohydrate Electrophoresis (FACE) analysis and those based on spectrophotometric and fluorescent properties of the tyramine and dityramine adducts **[11]**. While *in vitro* methods of characterization have been identified, the identification of methods for characterization and quantification of these

chemically modified GAG and collagen macromolecules *in vivo* remain to be developed. The development of such methods is critical to facilitate the monitoring of these biomaterials in tissues. Hence, we focus on clinically established magnetic resonance imaging modalities already used to detect and analyze the macromolecular composition of cartilage so as to define and advance these methods.

1.3 Imaging Techniques for Cartilage Assessment

Evaluation of the ECM constituents of articular cartilage, GAG and collagen, is of particular interest to the study of degenerative joint disease such as osteoarthritis (OA). OA is a chronic degenerative disease characterized primarily by the loss of articular cartilage. Loss of articular cartilage may lead to inflammation, pain and associated pathology such as growth of new vasculature, osteophyte growth and joint space narrowing. Conventionally, OA has been diagnosed by these secondary indicators of cartilage loss via radiographic examination, in which a planar X-ray is used to assess the presence or absence of osteophytes and the width of the joint space. Determination of pathology is based on indirect measures of surrounding anatomical structures. While this is an effective approach, radiographs tend to be limited to the detection of OA only at later stages of disease progression because they lack the ability to directly image soft tissues **[51]**.

Furthermore, radiographs are relatively insensitive to biochemical changes, which are essential for early diagnosis and treatment of much pathology. For

instance, during the OA disease process, the PG content is reduced, the cells and collagen fibers are highly altered, and the collagen network is disrupted **[9].**

Noninvasive imaging techniques such as magnetic resonance imaging (MRI), computed tomography (CT), and ultrasound (UI) have demonstrated the potential to assess biochemical markers of cartilage integrity, each with its own intrinsic limitations.

The capabilities of MRI in the assessment of biochemical changes have prompted an increasing interest in employing this technique in the hopes of early diagnosis and treatments of OA. MRI has all of the distinct advantages conferred from being a non-invasive assessment technique. In addition, it can assess cartilage morphology directly and has shown promise for the detection of soft tissue changes. For instance, lesions found in T2-weighted images and T2 maps have been correlated with degradation of cartilage matrix (i.e. decreased collagen content, fibrillation, clefts), T1ρ relaxation times with PG depletion and T1 values using delayed-gadolinium enhanced MRI of cartilage (dGEMRIC) with PG content of cartilage **[51].**

Constrast-enhanced CT has also been proposed as an alternative to dGEMRIC. However, because detection of the contrast agent is accomplished directly via measurements of increased X-ray attenuation, this method requires increased amount of contrast agent to be injected into the patient prior to imaging and consequently an increased risk of complications related to contrast administration. Despite this limitation, CT methods are attractive because the

imaging procedure is quick and can generate images with hgh-resolution and isotropic voxel dimensions **[51]**.

Although MRI allows direct evaluation of cartilage, this technique can detect only major OA changes due to its low resolution. Hence, high-frequency ultrasound has been proposed as a method for detecting articular cartilage fibrillation that is characteristic of early signs of OA. The cartilage surface fibrillation is believed to originate from the breakdown of the collagen fibril network, and it can be detected from ultrasound images by means of qualitative evaluation or quantitative analysis. Qualitatively, fibrillation is assessed visually as a decrease in sharpness and echogenicity or increase in the irregularity of the cartilage surface. In quantitative analysis, the reflected ultrasound signal from the cartilage surface is typically analyzed in time or frequency domain and parameters such as signal amplitude or reflection coefficient are calculated **[45]**.

In the wake of the development of the current and new imaging methods for assessment of cartilage biochemistry, there is a need for a careful, systematic comparison of the proposed imaging methods to assess the sensitivity of each to the macromolecular content of cartilage (GAG and collagen). Although CT produces higher resolution images compared to MRI, MRI has the advantage of assessing changes in GAG and collagen within cartilage with no radiation exposure to patients and the use of less administered contrast agent, in the case of contrast-based imaging techniques. Hence, with the prospects of future clinical trials involving TB-hydrogels, MRI was preferred as the imaging technique to be utilized for this study. Furthermore, because we have the ability to formulate

synthetic GAG and collagen biomaterials, this investigation focused on the evaluation of T1 and T2 mapping, standard clinical contrast (T1-weighted, T2-weighted) imaging sequences, and contrast-enhanced dGEMRIC technique and their dependency and specificity to GAG and collagen concentrations.

1.4 Basis of Magnetic Resonance Imaging (MRI) [6]

The spinning proton or "*spin*" is classically considered to be like a bar magnet with north and south poles; nonetheless, the magnetic moment of a single proton is extremely small and not detectable by standard means. A vector representation (amplitude and direction) is helpful when contemplating the additive effects of many protons.

Thermal energy agitates and randomizes the direction of the spins in the tissue sample, and as a result there is no net tissue magnetization **(Fig 1.11 A)**. Under the influence of a strong magnetic field, B_o, however, the spins are more organized and can be generally characterized: alignment with (parallel to) the applied field at a low-energy level, and alignment against (antiparallel to) the field at slightly higher energy level **(Fig. 1.11 B)**.

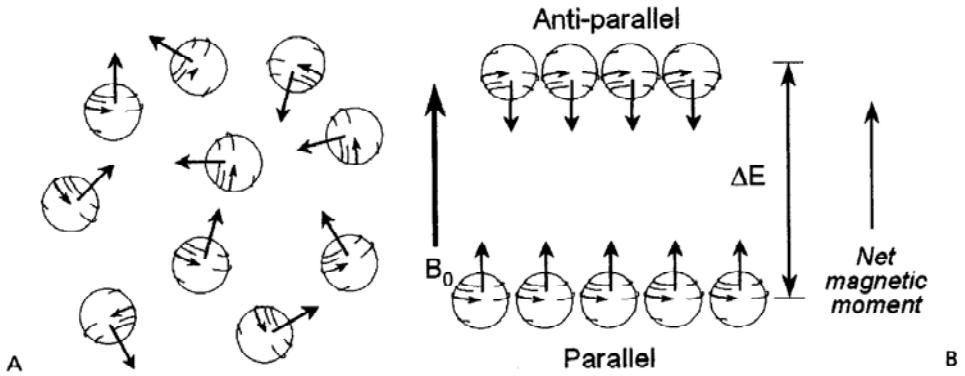

Fig 1.11. Simplified Distribution of "Free" Protons without and with External Magnetic Field. A: Without an external magnetic field, a group of protons assumes a random orientation of magnetic moments, producing an overall magnetic moment of zero. **B:** Under the influence of an applied external field, B_0, the protons assume a nonrandom alignment in tow possible orientations: parallel and antiparallel to the applied magnetic field. A slightly greater number of protons exist in the parallel direction, resulting in a measurable sample magnetic moment in the direction if B_0. **[6]**.

A slight majority of spins exist on the low-energy state, the number of which is determined by thermal energy of the sample (at absolute zero, 0 degrees Kelvin (K), all protons would be aligned in the low-energy state). For magnetic field at higher strength, the energy separation of the low and high energy levels is greater, as is the number of excess protons in the low-energy state. The number of excess protons in the low energy state at 1T is about 3 spins per million ($3x10^{-6}$) at physiologic temperatures and is proportional to the external magnetic field. Although this does not seem significant, for a typical voxel volume in MRI there are about 10^{21} protons, so there are $3 \times 10^{-6} \times 10^{21}$, or approximately 3×10^{15}, more spins in the low-energy state **[6]**. This number of protons produces an observable magnetic moment when summed.

In addition to energy separation of the spin states, the protons also experience a torque from the applied magnetic field that causes precession, in much the same way a spinning top wobbles due to the force of gravity **(Fig 1.12 A)**. The direction of the spin axis is perpendicular to the torque's twisting. This precession occurs at an angular frequency (number of rotations/sec about an axis of rotation) that is proportional to the magnetic field strength B_o.

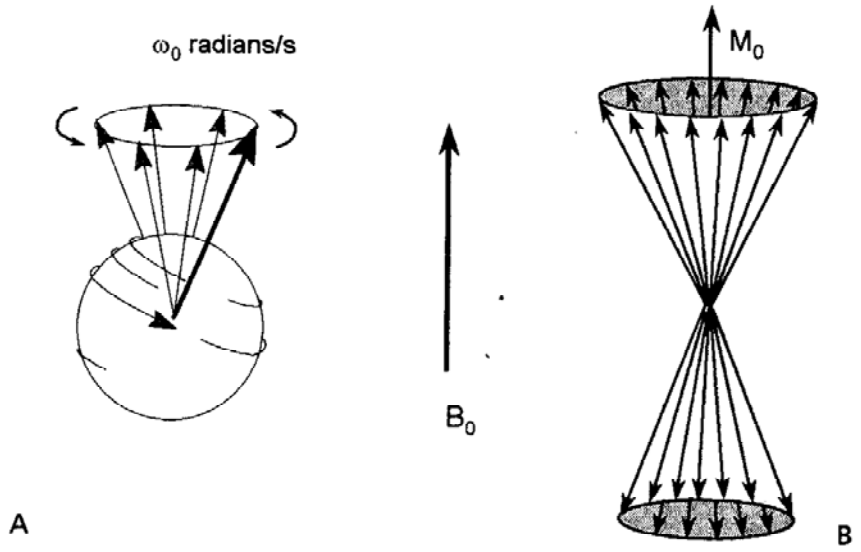

Figure 1.12. A: A single proton precesses about its axis with an angular frequency, ω, that is proportional to the externally applied magnetic field strength, according to the Larmor equation. **B:** A group of protons in the parallel and antiparallel energy states generates an equilibrium magnetization, M_0, in the direction of the applied magnetic field B_0. The protons are distributed randomly over the surface of the cone and produce no magnetization in the perpendicular direction **[6].**

The *Larmor equation* describes the dependence between the magnetic field, B_o, and the precessional angular frequency, ω_0:

$\omega_0 = \gamma B_o$

or, with respect to linear frequency:

$f_0 = (\gamma/ 2\pi) B_o$

where γ is the gyromagnetic ratio unique to each element, B_o is the magnetic field strength in tesla, *f* is the linear frequency in MHz (where $\omega = 2\pi f$: linear and angular frequency are related by 2π rotation about a circular path), and γ/ 2π is the gyromagnetic ratio expressed in MHz/T. Because energy is proportional to frequency, the energy separation, ΔE, between the parallel and antiparallel spins is proportional to the precessional frequency, and larger magnetic fields generate higher precessional frequencies. Each element has a unique gyromagnetic ratio that allows the discrimination of one element from another, based on the precessional frequency in a given magnetic field strength. In other words, the choice of frequency allows the resonance phenomenon to be tuned to a specific element **[6]**.

The millions of protons precessing in the parallel and antiparallel directions results in a distribution that can be represented by two cones with the net magnetic moment equal to the vector sum of all the protons in the sample in the direction of the applied magnetic field **(Fig 1.12 B)**. At equilibrium, no magnetic field exists perpendicular to the direction of the external magnetic field because the individual protons precess with a random distribution, which effectively

averages out any net magnetic moment. Energy (in the form of radiofrequency electromagnetic radiation) at the precessional frequency (related to ΔE) is absorbed and converts spins from the low-energy, parallel direction to the higher-energy, antiparallel direction. As the perturbed system goes back to its equilibrium state, the MRI signal is generated.

Typical magnetic field strengths for imaging range from 0.1 to 7T (1,000 to 70,000 G). For protons, the precessional or Larmor frequency is 127.74 MHz in a 3.0 T magnetic field (e.g. *f* = 42.58 MHz/T x 3T) **[6]**. This will also be the Larmor frequency for a proton in the imaging studies involved in this dissertation work as a 3T magnetic field was used. The frequency increases or decreases with increases or decreases of magnetic field strength. Accuracy and precision are crucial for the selective excitation of a given nucleus in a magnetic field of known strength. Spin precession frequency must be known to an extremely small fraction (10^{-12}) of the precessional frequency for modern imaging systems.

1.4.1 Generation and Detection of the Magnetic Resonance Signal

Application of radiofrequency (RF) energy synchronized to the precessional frequency of the protons causes displacement of the tissue magnetic moment from equilibrium conditions (e.g., more protons are in the antiparallel orientation). Return to equilibrium results in emission of MR signal proportional to the number of excited protons in the sample, with a rate that depends on the characteristics of the tissue. Excitation, detection, and acquisition of signals constitute the basic information necessary for MRI **[6]**.

The interactions of spins with their surroundings are modeled in the presence of external field effects by the phenomenological Bloch equation. In physics, specifically in MRI, the Bloch equations are a set of macroscopic equations that are used to calculate the nuclear magnetization **M** = (Mx, My, Mz) as a function of time when relaxation (T_1 and T_2) is present. These are phenomenological equations that were introduced by Felix Bloch in 1946 **[20]**.

Let **M**(*t*) = (M_x(t), M_y(t), M_z(t)) be the nuclear magnetization. Then the Bloch equations are given by **[20]:**

$$\frac{dM_x(t)}{dt} = \gamma(\mathbf{M}(t) \times \mathbf{B}(t))_x - \frac{M_x(t)}{T_2}$$

$$\frac{dM_y(t)}{dt} = \gamma(\mathbf{M}(t) \times \mathbf{B}(t))_y - \frac{M_y(t)}{T_2}$$

$$\frac{dM_z(t)}{dt} = \gamma(\mathbf{M}(t) \times \mathbf{B}(t))_z - \frac{M_z(t) - M_0}{T_1}$$

where γ is the gyromagnetic ratio and **B**(*t*) = (Bx(t), By(t), B_0 + ΔBz(t)) is the magnetic field experienced by the nuclei. In MRI, the magnetic field (**B**) is parallel to the z-axis, which makes the vector product of the last equation equal to zero. Therefore, integration of the last equation yields the formula for the z-magnetization (Mz) as a function of time (T1 relaxation):

Mz (t) = M_0 (1 – $e^{-t/T1}$)

The first and second equations are coupled differential equations and their solution is:

$$Mx(t) = e^{-t/T2}\ (M_x(0)\cos\omega_0 t + M_y(0)\sin\omega_0 t)$$

$$My(t) = e^{-t/T2}\ (M_y(0)\cos\omega_0 t - M_x(0)\sin\omega_0 t)$$

with ω being the Larmor frequency. This computation of the length of magnetization vector in the xy-plane yields the well known T2 relaxation relation:

$$Mxy(t) = M_0\, e^{-t/T2}$$

Thus the Bloch equations are simply a general formulation to describe spin behavior, which in the especial situation of MRI leads to the equations for T1 and T2 relaxation **[20].**

1.4.2 Free Induction Decay: T2 Relaxation [6]

The 90º RF pulse produces phase coherence of individual protons and generates the maximum possible transverse magnetization (Mxy) for a given sample volume. As Mxy rotates at the Larmor frequency, the receiver antenna coil is induced to produce a damped sinusoidal electronic signal known as the *free induction decay* (FID) signal.

The “decay” of the FID envelope is the result of the loss of phase coherence of the individual spins caused by a combo of spin-spin interactions and magnetic field variations. Micromagnetic inhomogeneities intrinsic to the structure of the sample cause a spin-spin interaction, whereby the individual spins precess at different frequencies due to slight changes in the local magnetic field strength caused by other spins. Some spins travel faster and some slower, resulting in the

loss of phase coherence. External magnetic field inhomogeneities arising from imperfections in the magnet or disruptions in the field by paramagnetic or ferromagnetic materials accelerate the dephasing process. Exponential relaxation decay, T2, represents the intrinsic *spin-spin interactions* that cause loss of phase coherence. The elapsed time between the peak transverse signal and 37% of the peak level (1/e) is the T2 decay constant **(Fig 1.13)**.

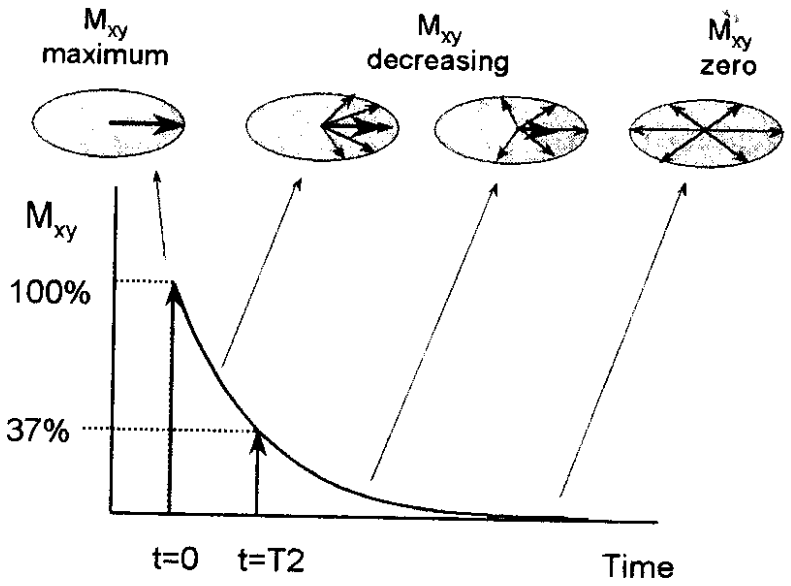

Figure 1.13. The loss of Mxy phase coherence occurs exponentially and is caused by intrinsic spin-spin interactions in the tissues, as well as extrinsic magnetic field inhomogeneities. The exponential decay constant, T2, is the time over which the signal decays to 37% of the maximal transverse magnetization (e.g. after a 90° pulse) **[6]**.

Mathematically, this exponential relationship is expressed as follows:

$$Mxy\ (t) = M_0\ e^{-t/T2}$$

Where Mxy is the transverse magnetic moment at time t for a sample that has M_0 transverse magnetization at t = 0. When t = T2, then $e^{-1} = 0.37$, and Mxy = 0.37 M_0. An analogous comparison to T2 decay is that of radioactive decay, with the exception that T2 is based on 1/e decay instead of half-life (1/2) decay. This means that the time for the FID to reach half of its original intensity is given by t = 0.693 x T2.

T2 decay mechanisms are determined by the molecular structure of the sample. Mobile molecules in amorphous liquids (e.g., cerebral spinal fluid [CSF]) exhibit a long T2, because a fast rapid molecular motion reduces or cancels intrinsic magnetic inhomogeneities. As the molecular size increases, constrained molecular motion causes the magnetic field variations to be more readily manifested and T2 decay to be more rapid. Hence, large nonmoving structures with stationary magnetic field have a very short T2.

1.4.3 Return to Equilibrium: T1 relaxation [6]

The loss of transverse magnetization (T2 decay) occurs relatively quickly, whereas the return of the excited magnetization to equilibrium (maximum longitudinal magnetization) takes a longer time. Individual excited spins must release their energy to the local tissue (the lattice). *Spin-lattice* relaxation is a term given for the exponential *regrowth* of Mz, and it depends on the

characteristics of the spin interaction with the *lattice* (the molecular arrangement and structure). The T1 relaxation is the time needed to *recover* 63% of the longitudinal magnetization, Mz, after 90º pulse (when Mz = 0). The recovery of Mz versus time after the 90º RF pulse is expressed mathematically as follows:

$$Mz\ (t) = M_0\ (1 - e^{-t/T1})$$

where Mz is the longitudinal magnetization that recovers after a time (t) in a material with a relation constant T1. **Figure 1.14** illustrates the recovery of Mz. When t = T1, then 1 – e-1 = 0.63, and Mz = 0.63 M_0. Full longitudinal recovery depends on the T1 time constant. For instance, at a time equal to 3 x T1 after a 90º pulse, 95% of the equilibrium magnetization is reestablished. After a period of 5 x T1, the sample is considered to be back to full longitudinal magnetization.

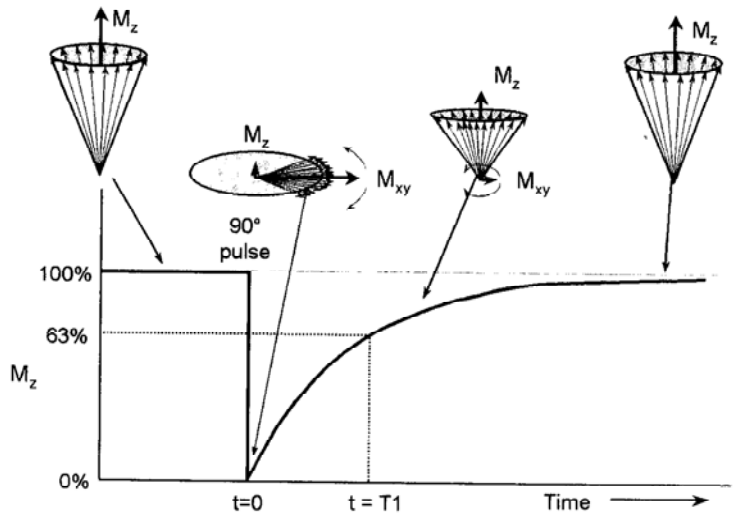

Figure 1.14. After a 90° pulse, longitudinal magnetization (Mz) is converted from a maximum value at equilibrium to zero. Return of Mz to equilibrium occurs exponentially and is characterized by the spin-lattice T1 relaxation constant. After an elapsed time equal to T1, 63% of the longitudinal magnetization is recovered. Spin-lattice recovery takes longer than spin-spin decay (T2) **[6]**.

T1 relaxation depends on the dissipation of absorbed energy into the surrounding molecular lattice. The relaxation time varies substantially for different tissue structures and pathologies. From a classical physics perspective, energy transfer is most efficient when the precessional frequency of the excited protons overlaps with the “vibrational” frequencies of the molecular lattice. Large, slowly moving molecules exhibit low vibrational frequencies that concentrate in the lowest part of the frequency spectrum. Moderately size molecules (e.g. proteins) and viscous fluids produce vibrations across an intermediate frequency range. Small molecules have vibrational frequencies with low, intermediate, and high-frequency components that span the widest frequency range. Hence, T1 relaxation is strongly dependent on the physical characteristics of the tissues.

As a result, for solid and slowly moving structures, low frequency variations exist and there is little spectral overlap with Larmor frequency. A small spectral overlap also occurs for unstructured tissue and fluids that exhibit a wide vibrational frequency spectrum but with low amplitude. In either situation, the inability to release energy to the lattice results in a relatively long T1 relaxation. One interesting case is that of water, which has an extremely long T1, but the addition of water-soluble proteins produces a hydration layer that slows the molecular vibrations and shifts the high frequencies in the spectrum to lower values that increase the amount of spectral overlap with the Larmor frequency and result in a dramatically shorter T1. Moderately sized molecules, such as lipids, proteins, and fats, have more structured lattice with a vibrational frequency spectrum that is most conductive to spin-lattice relaxation. For biologic tissues,

T1 ranges from 0.1 to 1 sec in soft tissues, and from 1 to 4 sec in aqueous tissues (e.g., CSF) and water.

T1 relaxation increases with higher field strengths. A corresponding increase in the Larmor precessional frequency reduces the spectral overlap of the molecular vibrational frequency spectrum, resulting in longer T1 times. Contrast agents, such as complex macromolecules containing gadolinium are effective in decreasing T1 relaxation time by allowing free protons to become bound and create a hydration layer, thus providing a spin-lattice energy sink and rapid return to equilibrium. Even a very small amount of gadolinium contrast in pure water has a dramatic effect on T1, decreasing the relaxation from a couple of seconds to tens of milliseconds.

1.4.4 Comparison of T1 and T2 [6]

T1 is always longer than T2. For instance, in a soft tissue, a T1 time of 500 msec has a corresponding T2 time that is typically 5 to 10 times shorter (i.e. approximately 50 msec). Molecular motion, size, and interactions influence T1 and T2 relaxation **(Fig 1.15)**. Molecules can be classified roughly into three size groups: small, medium, and large; with corresponding fast, medium, and slow vibrational frequencies. For reasons, described in the previous two sections, small molecules exhibit long T1 and long T2, and intermediate-sized molecules have short T1 and short T2; however, large, slowly moving or bound molecules have a long T1 and short T2 relaxation times. Because most tissues of interest in

MR imaging consist of intermediate to small-sized molecules, a long T1 usually infers a long T2, and a short T1 infers a short T2.

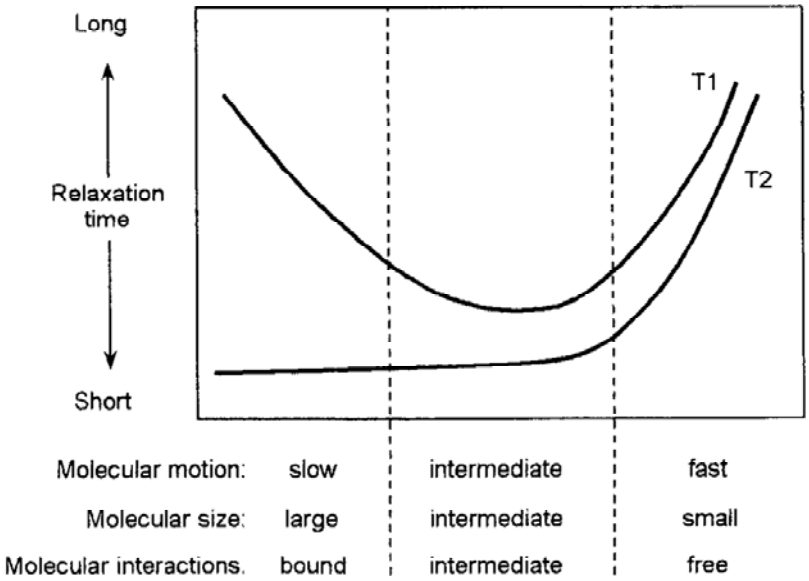

Figure 1.15. Factors affecting T1 and T2 relaxation times of different tissues are generally based on molecular motion, size and interactions. The relaxation times (vertical axis) are different for T1 and T2 **[6]**.

Magnetic field strength influences T1 relaxation but has an insignificant impact on T2 decay. This is related to the dependence of the Larmor frequency on the magnetic field strength and the degree of overlap with the molecular vibration spectrum. A higher magnetic field strength increases the Larmor frequency ($\omega_0 = \gamma B_o$), which reduces the amount of spectral overlap and produces a longer T1.

To summarize, T1 > T2, and the specific relaxation times are a function of the tissue characteristics. T1 and T2 decay constants are fundamental properties of tissues, and therefore, these tissue properties can be exploited by MRI to aid in the diagnosis of pathologic conditions such as cartilage degeneration in osteoarthritis.

1.5 Applied Magnetic Resonance Imaging (MRI) Techniques

This investigation employed delayed gadolinium-enhanced MRI of cartilage, T1 and T2 Mapping, and standard clinical contrast (T1-weighted, T2-weighted) imaging sequences to evaluate TB-hydrogels. These MRI methodologies are further explained below:

1.5.1 dGEMRIC

The major solid components in cartilage are proteoglycans (PG) and collagen. PGs consist of numerous GAG side chains that are negatively charged, providing the ECM with the majority of its fixed charge, the concentration of which is referred to as the tissue fixed charge density (FCD). This fixed charge density is relatively high in cartilage, on the order of – 200 mM or – 100 mg/ml **[22,15]**. An

early feature of OA is the loss of GAG, and hence FCD, from the tissue. Hence, dGEMRIC is an MRI method developed for monitoring the charge in the tissue as a means of detecting early cartilage degradation **[2].**

This approach follows a paradigm pioneered by Maroudas and colleagues **[37,35]**. It depends on the fact that GAG macromolecules contain numerous highly negatively charged ionized side groups. The principle is that a negatively charged ion is relatively excluded from normal cartilage containing a high concentration of (the highly negatively charged) GAG. This relative exclusion would not occur when GAGs are lost as part of degenerative processes, since the negative charge that they confer to cartilage also is lost. A measurement of concentration of the anionic contrast agent gadopentetate dimeglumine (Gd-$DTPA^{2-}$) should serve as a surrogate for measurement of GAG concentration as Gd-$DTPA^{2-}$ is expected to distribute proportionally into depleted areas of cartilage at a higher concentration than that in non-depleted areas. Since the concentration of gadolinium compounds can be determined from an MR measurement of T1, variations in tissue GAG concentration can be measured **[1]**.

Now, if absolute FCD is desired, a model must be used to calculate FCD from tissue/sample Gd-$DTPA^{2-}$ concentration. One model, that has been successfully used to quantify FCD from tissue Na+ concentration, is based on principles of electroneutrality within the cartilage tissue and electrochemical equilibrium between tissue and its surrounding tissue. Electroneutrality states that the total amount of negative charge in the tissue must equal the total amount of positive

charge. Electrochemical (Donnan) equilibrium relates the internal tissue ion concentrations to external bath concentrations **[36,41]**.

In the simplest model, the tissue is assumed to be a homogeneous composite containing electrolyte and an ionized solid matrix bathed in an electrolyte solution (e.g. saline, culture, medium, or synovial fluid). Assuming that the tissue/sample is equilibrated in a NaCl solution containing Gd-DTPA^{2-} (where the concentration of Gd-DTPA^{2-} and other minor constituents is negligible as compared with the NaCl concentration), electroneutrality is given by:

Bath : $[Na^+]_b - [Cl^-]_b = 0$ (1.1)

Tissue: $[Na^+]_t - [Cl^-]_t + FCD = 0$ (1.2)

Where subscript b stands for bath and subscript t stands for tissue.

Ideal electrochemical equilibrium requires that **[36,41]** (1.3):

$$\frac{[Na^+]_t}{[Na^+]_b} = \frac{[Cl^-]_b}{[Cl^-]_t} = \frac{[Gd\text{-}DTPA^{2-}]_b^{1/2}}{[Gd\text{-}DTPA^{2-}]_t^{1/2}}$$

Equations (1) through (3) can be solved to calculate FCD from either the measured tissue $[Na^+]_t$ or tissue $[Gd\text{-}DTPA^{2-}]_t$ and known bath ionic concentration:

Using measured Na+ concentration (1.4):

$$FCD = \frac{[Na^+]_b}{[Na^+]_t} - [Na^+]_t$$

Using measured Gd-DTPA $^{2-}$ concentration (1.5):

$$FCD = [Na^{+}]_b \left\{ \left[\frac{[Gd\text{-}DTPA^{2-}]_t}{[Gd\text{-}DTPA^{2-}]_b} \right]^{1/2} - \left[\frac{[Gd\text{-}DTPA^{2-}]_b}{[Gd\text{-}DTPA^{2-}]_t} \right]^{1/2} \right\}$$

The use of equations (1.4) and (1.5) to compute fixed charge density was first introduced by Maroudas **[36]** and has subsequently been used to compute FCD. The use of equation (5) required that $[Gd\text{-}DTPA^{2-}]_t$ be computed from tissue T1. The T1 values are converted to Gd-DTPA^{2-} concentration by calculating the difference between the relaxation rate of the sample with Gd-DTPA^{2-} ($1/T1_{post\text{-}Gd}$) and the relaxation rate of the sample without Gd-DTPA^{2-} ($1/T1_{pre\text{-}Gd}$) by using equation (1.6):

$$[Gd\text{-}DTPA]_{tissue} = \frac{1}{R1}\left[\frac{1}{T_{1post\text{-}Gd}} - \frac{1}{T_{1pre\text{-}Gd}}\right]$$

where R1 is the relaxivity of the Gd-DTPA^{2-} contrast agent in $(mM\text{-}sec)^{-1}$.

Furthermore, the T1-weighted images are obtained with an inversion-recovery turbo spin-echo acquisitions with inversion times (TI) systematically increased from 25 to 1600 msec to permit the calculation of T1 relaxation times. Subsequently, T1 maps are computed from the above image series and color-encoded to a standard scale to create the GAG index. The color-encoded T1

maps are then superimposed on morphological images for display, as seen in **Fig 1.16 [30].**

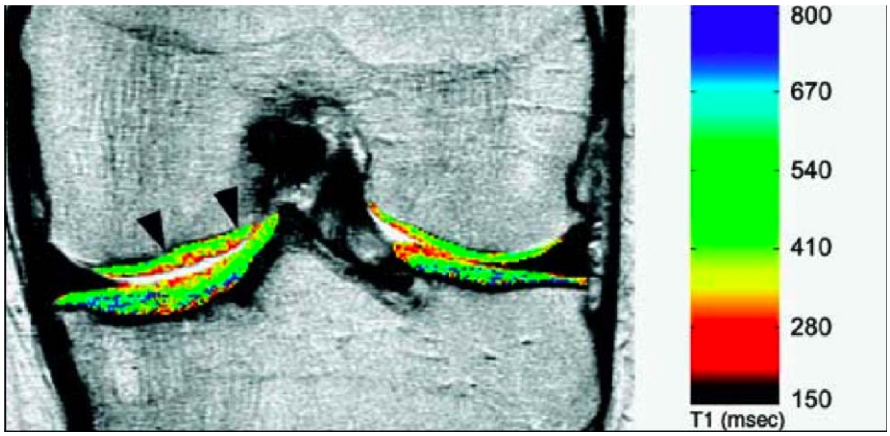

Figure 1.16. Color-Encoded T1 Map of Cartilage. This T1 map was obtained from a set of 7 STIR images with inversion times ranging from 50 to 1,650 msec superimposed on a gray-scale image of the knee. T1 values of repair tissue (arrowheads) in ACI site is 83% of that of adjacent, native articular cartilage of medial femoral condyle, indicating a slightly lower concentration of GAG within the repair tissue. Lower T1 values within superficial articular cartilage of medial femoral condyle and tibial plateaus indicate loss of GAG **[43].**

A strong correlation between T1 values obtained using dGEMRIC and PG concentration in *ex vivo* bovine cartilage specimens have been extensively reported in the literature **[2]**. The major drawback of this technique is the long equilibrium period between contrast agent administration and when imaging can start, which is required to allow diffusion of the contrast into the cartilage (usually 90 minutes). Another problem is the relatively long acquisition time needed to acquire sufficiently high spatial resolution images at multiple inversion times to create the T1 maps, during which time the subject must remain motionless **[30].**

1.5.2 T1 and T2 Mapping

T1 maps are generated with the same inversion recovery sequence used in the dGMERIC technique. T2 maps utilize a multisection, multiecho spin-echo sequence, and can be displayed as color-encoded images as are the T1 maps. An example of a T2 map of articular cartilage in **Fig 1.17** identified early OA as regions of increased T2 value. There has been dispute in the literature regarding sensitivity and specificity of T2 maps for the detection and quantitation of the early changes of OA in cartilage treated with enzymatic degradation. Most investigators have concluded that collagen rather than PGs is the major contributor to T2 in cartilage and that the earliest changes in OA are the loss of PGs. However, it is also well known that cartilage swelling occurs prior to loss of PGs. Thus increase in mobile water most likely is the cause of increased T2 relaxation times rather than the loss of PGs in the earliest stages of OA. Almost all commercial MRI systems include multisection, multiecho spin-echo

sequences suitable for measurement of *in vivo* T2 values. T2 maps can be acquired in a somewhat shorter period of time (<15 minutes) compared to measurement of T1 maps **[30].**

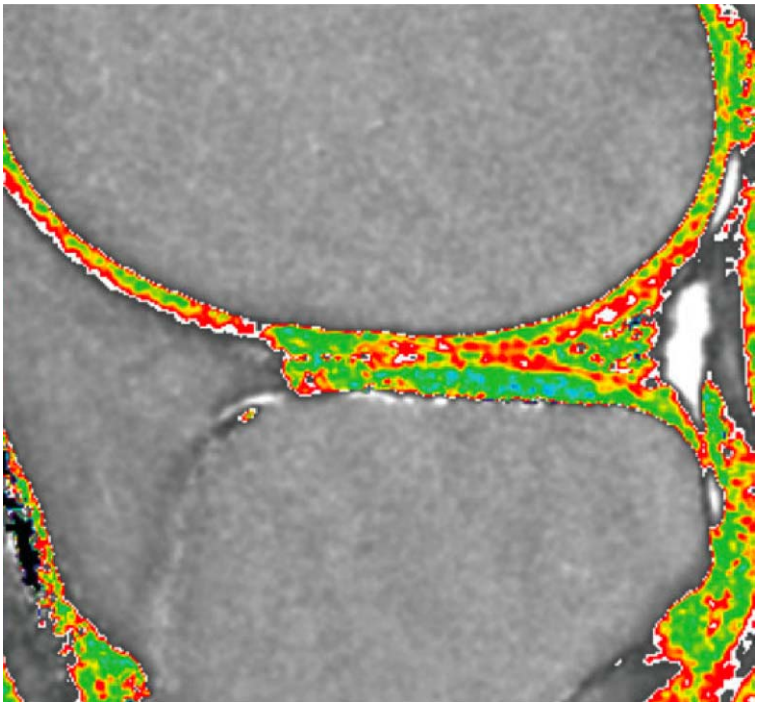

Figure 1.17. T2 Map of Articular Cartilage. The T2 map from a 53-year-old asymptomatic female demonstrates elevated T2 values near the articular surface of the femoral cartilage and increased heterogeneity in the spatial distribution of T2 values. This appearance is compatible with loss of structural organization of the cartilage collagen matrix seen with early OA. (Image courtesy of Timothy Mosher, MD, Hershey, PA, USA.) **[30]**.

The main drawback to T2 mapping is the lack of specificity in the relationship between T2 relaxation times and the changes in the macromolecular matrix than has been established for dGEMRIC. A recent publication presents a sequence that can produce both T1 and T2 maps that is intended to be used in conjunction with more contrast to enable the dGEMRIC technique **[52].**

1.5.3 MR Image Contrast

The signal intensity on the MR image is determined by the basic parameters of proton density, T1 relaxation time, and T2 relaxation time. Proton density is the concentration of protons in the tissue in the form of water and macromolecules (e.g. proteins and fat). The T1 and T2 relaxation time constants define the exponential recovery and decay curves of the longitudinal and transverse magnetization, respectively. The contrast on the MR image can be manipulated by changing the pulse sequence parameters. The most common image contrasts used clinically are proton density (PD), T1-weighted, and T2-weighted spin-echo or fast spin echo acquisitions. T1-weighted contrast uses a short TR and short TE (TR < 800 msec, TE < 20 msec). T2-weighted contrast uses a long TR and long TE (TR > 2000 msec, TE > 80 msec). T2-weighted contrast can be employed as a dual echo acquisition. The shorter echo (TE < 15 msec) being the proton density (PD) contrast **[6]**.

T1-weighted image contrast is based on emphasizing the T1 characteristics of tissues by de-emphasizing T2 contributions. The relatively short TR is used to maximize the differences in longitudinal magnetization during the return to

equilibrium, and a short TE to minimize T2 decay during signal acquisition. When TR is chosen to be 400 to 600 msec, the difference in longitudinal magnetization relaxation times (T1) between tissues is emphasized. For instance, fat, with a short T1, has a large signal, because the short T1 value allows rapid recovery of the Mz vector. The short T1 value means that the spins rapidly reassume their equilibrium conditions. White and gray matter have intermediate intensities or intermediate T1 values, and cerebrospinal fluid (CSF) has the lowest intensity or longest T1 value, **Fig 1.18 [6].**

Proton density image contrast relies mainly on differences in the number of protons per volume of tissue. At thermal equilibrium, those tissues with a greater proton density exhibit a larger longitudinal magnetization. Tissues such as lipids and fats have a high proton density compared with soft tissues; aqueous tissues such as CSF also have a high proton density. The long TR is used to minimize the T1 differences of the tissues, which allows longitudinal recovery so that the transverse magnetization differences result from variations in proton density (CSF>fat>gray matter<white matter). Since the TE is shorter (<15 msec) the amount of T2 decay signal acquisition is also minimized. In these conditions, fat and CSF display as relatively bright signal, and a light contrast inversion between white and gray matter occurs, **Fig 1.18 [6]**.

T2-weighted image contrast is achieved by reducing T1 effects with a long TR, and accentuating T2 differences with a long TE. The T2 weighted contrast is usually the second echo of a dual echo acquisition. Compared with T1-weighted contrast, T2-weighted image contrast inverts tissue contrast (CSF is brighter than

fat instead of darker), because short T1 tissues usually have a short T2 values, and long T1 tissues have a long T2 value. Tissues with a long T2 such as CSF maintain transverse magnetization longer than short T2 tissues, and subsequently result in higher signal intensity, **Fig 1.18**. A T2-weighted image demonstrates the contrast inversion and high tissue contrast features, compared with the T1-weighted image **[6]**.

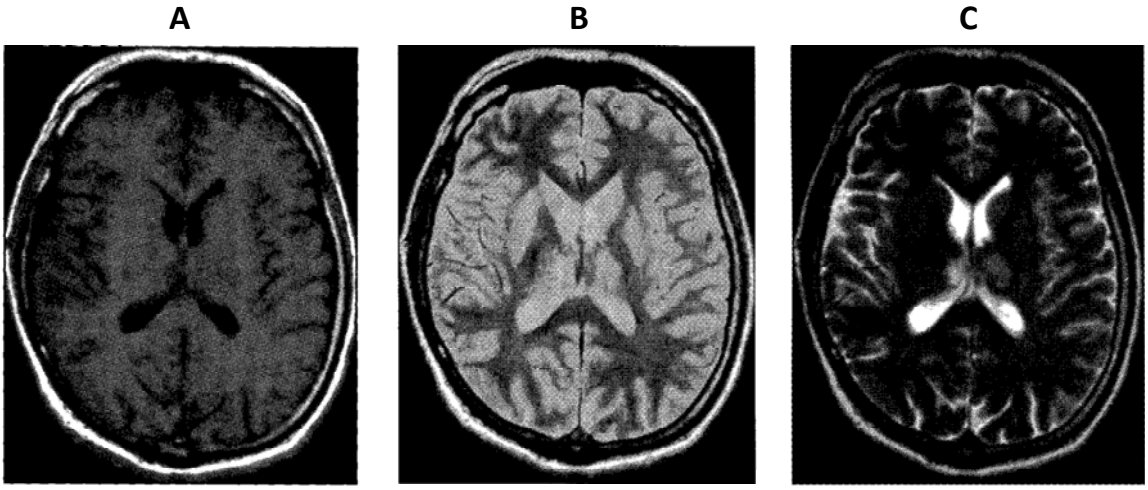

Figure 1.18. (A) T1-Weighted Axial Brain Image. Image obtained with TR = 549 msec and TE = 11 msec demonstrates bright image intensity for short-T1 tissues (white matter and fat) and dark intensity for long-T1 tissue (CFS). **(B)** Proton Density-Weighted Axial Brain Image. Image obtained with TR = 2,400 msec and TE = 30 msec, shoes reduced contrast compared with the T1-weighted image, but an overall higher signal amplitude. Tissues with higher proton concentration (e.g. fat, CSF) have higher image intensity. **(C)** T2-Weighted Axial Brain Image. Image obtained with TR = 2,400 msec and TE = 90 msec, has bright image intensity for long-T2 value tissues such as CSF and dark intensity for short T2 value tissues such as matter and fat **[6]**.

Cartilage contains a significant amount of water, approximately 80% in healthy tissue, with a relatively short transverse relaxation time, T2 (~40 msec) and intermediate T1 value (~700 -1000 msec). This water is the “observable” proton signal in an MR image of cartilage, **Fig 1.19 [5].** Thus, the most obvious and direct way to measure water content is with proton density images.

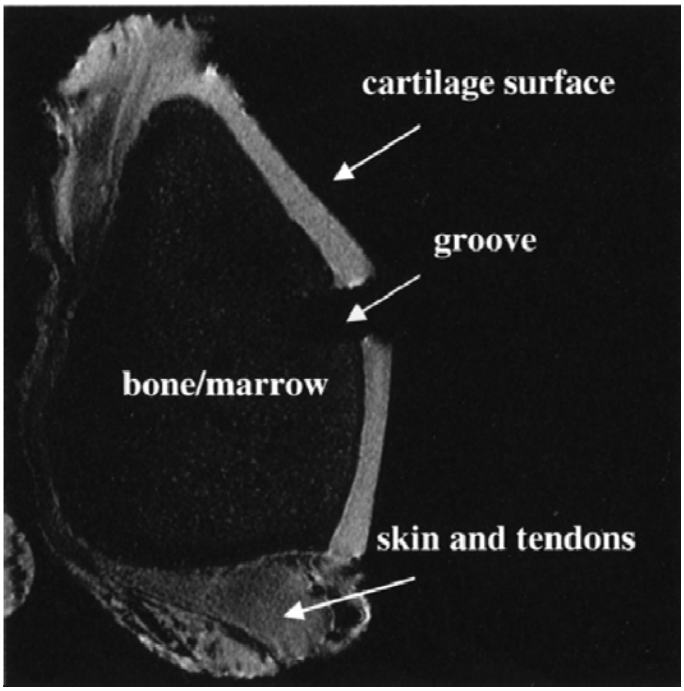

Figure 1.19. Axial Proton Density MR Image of a Specimen of Bovine Patella. A groove was cut into the articular surface to divide the cartilage in half **[5]**.

CHAPTER II

PRELIMINARY DATA

The experiments described in this chapter were previously performed in our laboratory. The results from these studies established the mechanical properties of TB-hydrogels by means of confined and unconfined compression tests; improved methods of cross-linking by means of the development of a dual syringe/needle injector device; and identified the need for alternative methods to evaluate the *in vivo* performance of the TB-hydrogels due to technical issues with histological analysis. This information has motivated and shaped the design of some of the experiments included in this dissertation work.

2.1 Mechanical Properties of TB-Hydrogels [10]

The mechanical properties of the TB-HA hydrogels have been measured through both confined and unconfined compression tests and using cylindrical plugs at concentrations of 6.25, 12.5, 25, 50, and 100 mg/ml of HA **(Fig 2.1)**. This concentration range was selected because the 6.25 mg/ml TB-Hydrogel was

the minimum concentration of hydrogel that could be mechanically tested. The concentration was doubled until reaching the maximum concentration of 100 mg/ml, which is the concentration of GAG in cartilage.

Five cylindrical plugs, approximately 7.1 mm in diameter and 3 mm in thickness, at each HA concentration were made for confined compression testing using a custom built polycarbonate confining chamber **(Fig. 2.2)**, and the freeze-thaw cross-linking technique.

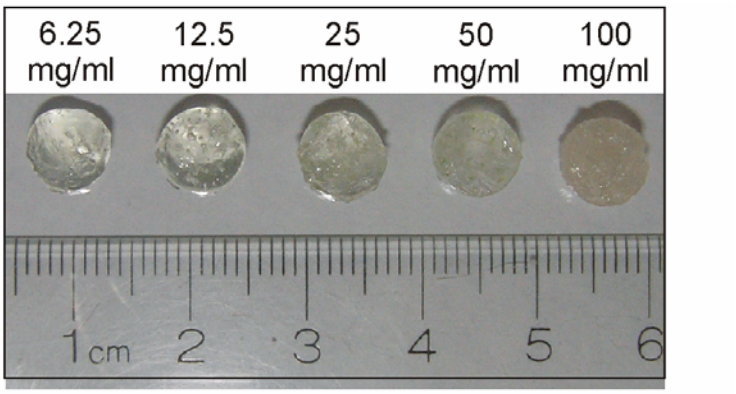

Figure 2.1. Photograph of TB-HA Hydrogels (6.25, 12.5, 25, 50, and 100 mg/ml).

Figure 2.2.Custom Built Confined Compression Testing Apparatus. Wells measured 7.1 mm in diameter and 3 mm in thickness.

Five of the six cylindrical cavities of the confining chamber were filled with replicate aliquots of the desired formulation containing 10 U/ml of horseradish peroxidase and frozen on dry ice. The chamber was then immersed in an excess (200 ml) of room temperature hydrogen peroxide solution (0.03%) to allow for thawing of the frozen hydrogel plugs and dityramine cross-linking throughout the plugs. Cross-linking was determined to be complete once the last visual evidence of ice had melted at the center of the forming hydrogel plugs (~5 minutes). The chamber was then removed and blotted dry prior to testing. For samples to be tested in unconfined compression, five cylindrical plugs (7.1 mm in diameter, and 3 mm in thickness) were cast using an unconfined sample mold (no bottom) and the same freeze-thaw technique as described above.

2.1.1 Confined Compression Test [10]

Confined compression testing was performed using a porous polypropylene filter platen (20 μm pores, 20% porosity). All testing was performed using an Instron 5543 (Instron Corp., Canton, MA) testing machine under computer control, which recorded the time-displacement-load data at a frequency of 10 Hz. A $\pm$5 N or $\pm$50 N load cell (Sensotec) was used as appropriate to monitor load throughout each test. A step of 30 μm (30 μm/sec), representing 1% strain, was applied and held until the sample reached equilibrium **[25]**. Equilibrium was defined as a relaxation rate that slowed to less than 10 mN min^{-1}, at which time the next step was automatically started, until 20 cycles (representing approximately 20% strain) were completed **(Fig 2.3.A) [25]**. The thickness of each sample tested in

both confined and unconfined compression was determined by measurement of the displacement at which the initial load was observed, relative to the bottom (zero displacement) of the single empty chamber **[25]**. The measured thickness was used to calculate the strain percentage for each step. Load data was normalized by sample cross-sectional area (39.6 mm^2) to compute stress. The equilibrium stress was plotted against the applied strain for each material formation **(Fig 2.3.B)**. For each material, the aggregate modulus was defined as the slope of the equilibrium stress-strain data in the linear range between 5% and 20% strain **[25]**.

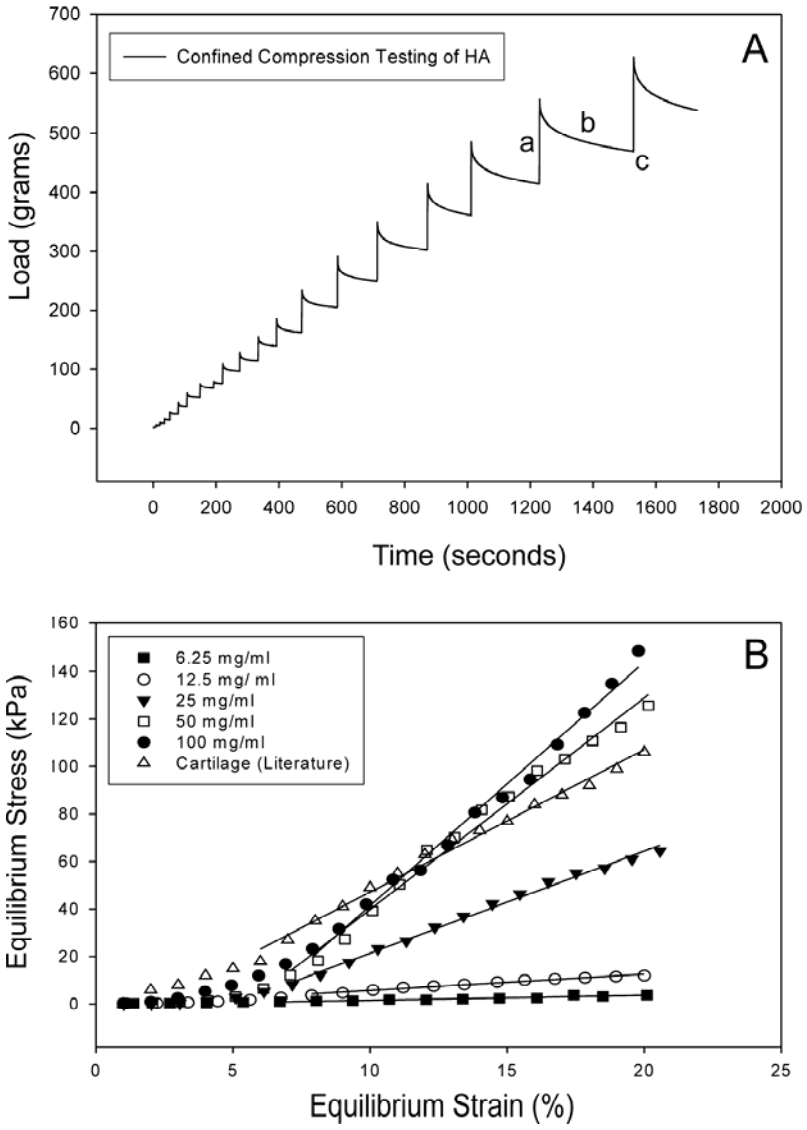

Figure 2.3. (A) Graph Showing Output Data of Load vs. Time. This data attained in confined compression over 20 cycles (approximately 20% strain) for the 25 mg/ml TB-HA hydrogel. This output data is representative of that obtained for all hydrogels tested in confined and unconfined compression. Each step is comprised of a 30 μm displacement to load (a), a period of stress relaxation (b), and finally equilibrium (c). **(B) Stress Strain Curves for TB-HA Hydrogel Plugs under Confined Compression.** The respective aggregate moduli were determined from the linear region, which is represented by the fitted lines for each individual material formulation and concentration **[25].** Unconfined stress-strain curves were similarly evaluated.

TB-HA Concentration (mg/ml)	Aggregate Modulus (Kpa)
6.25	24.1 ± 14.9
12.5	72.3 ± 24.4
25	482 ± 131
50	1020 ± 164
100	1240 ± 352

Table II. Aggregate modulus (KPa) values for each hydrogel formulation.

Table II shows that the hydrogels exhibited a range of aggregate moduli as result of varying GAG concentration as well as characteristic stress relaxation responses typical of viscoelastic materials. The aggregate moduli for the 25 – 100 mg/ml TB-HA samples were in the range of those previously reported for articular cartilage (470-1240 KPa) **[25,31,38,24]** with the 100 mg/ml and the 50 mg/ml TB-HA samples having moduli, which were equal to or exceeded those of previously reported values for articular cartilage in confined compression **[25,31,38,24].**

2.1.2 Unconfined Compression Test [10]

Unconfined compression testing was performed to determine the uniaxial unconfined compressive properties of hydrogel constructs. A similar protocol was followed for the unconfined compression stress relaxation tests as was followed for confined compression **[25]**. Concurrently, each sample was visualized (**Fig 2.4**) during the test at an image capture frequency of 1 Hz using a video system consisting of a 570 line black and white CCD camera (Model KP-M2U, Hitachi Denshi, Ltd., Tokyo, Japan) fitted with a 6.5X zoom lens with 12 mm fine focus and adjustable aperture, 1X short adapter and 0.5X auxiliary lens (Navitar, Inc., Rochester, NY). The camera and lens interfaced with a video capture board (DT3155 Frame Grabber, Data Translation, Inc., Marlboro, MA) and a standard microcomputer. A custom image capture software package interfaced with the microcomputer and the Instron 5543 testing system.

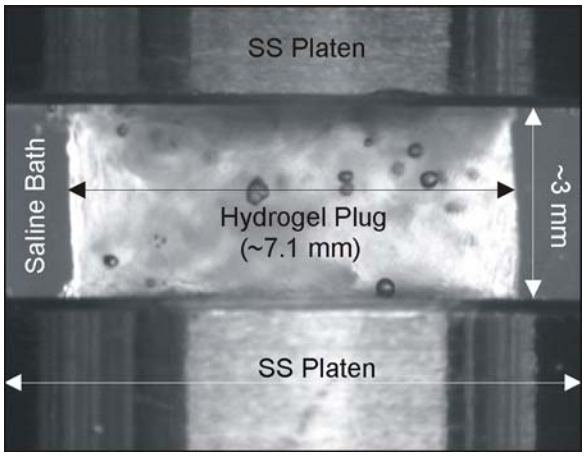

Figure 2.4. A Hydrogel Plug Visualized During Unconfined Compression as Used to Measure Poisson's Ratio.

Each sample was placed between two stainless steel loading platens, connected to the Instron testing machine **(Fig 2.4)**. A step of 30 μm (30 μm/sec), representing 1% strain, was applied until the sample reached equilibrium as defined previously. The temporal change in the lateral dimensions of each sample was determined from the optical image using the image capture software for each strain percentage step and used to determine Poisson's ratio at equilibrium **(Fig 2.4)**. The axial force was normalized by the sample cross-sectional area for each step to compute stress. The stress was plotted against the applied strain for each material formation, and Young's modulus was defined as the slope of the stress-strain data between 5% and 20% strain **[25].**

Shear modulus (G) was calculated using the measured values for Poisson's ration (υ) and Young's modulus (E) and equation 7 **[25]**. Quantitative agreement between the two different testing methods was determined by using the values directly measured of aggregate modulus (H) and Young's modulus to calculate the value for Poisson's ratio from equation 8 **[25]**, and then comparing this calculated value of Poisson's ratio to the value measured optically during unconfined compression testing **[25].**

$$G = \frac{E}{2(1+\upsilon)} \qquad (7)$$

$$H = \frac{(1-\upsilon)}{(1+\upsilon)(1-2\upsilon)} E \qquad (8)$$

TB-HA Conc. (mg/ml)	Young's Modulus (Kpa)	Shear Modulus (Kpa)	Poisson's Ratio (unconfined test)	Poisson's Ratio (Eq)
6.25	9.53 ± 4.14	3.68 ± 1.94	0.29 ± 0.077	0.42 ± 0.11
12.5	28.2 ± 6.23	10.5 ± 3.02	0.34 ± 0.031	0.42 ± 0.059
25	81.7 ± 26.6	30.3 ± 12.9	0.35 ± 0.029	0.47 ± 0.072
50	178 ± 44.2	65.1 ± 19.9	0.37 ± 0.11	0.47 ± 0.049
100	549 ± 129	202 ± 60.4	0.37 ± 0.077	0.41 ± 0.053

Table III. Young's modulus, shear modulus, and poisson's ratio values for each material formulation.

The values for Young's modulus, shear modulus, the measured Poisson's ratio and calculated Poisson's ratio are seen in **Tables III**. In contrast to the confined compression testing, only the 100 mg/ml TB-HA hydrogel displayed a Young's modulus in the range of those values previously reported for articular cartilage (445-800 KPa) **[25,44,26].** While the shear moduli of all hydrogels tested were below the range of those values previously reported for articular cartilage (370-1100 KPa) **[23,14]**, the 100 mg/ml TB-HA hydrogel had the highest shear modulus of the hydrogels tested. The measured values for Poisson's ratio were in the range of those previously reported for articular cartilage (0.15 – 0.62) **[25,44,26,29].** There was no significant difference found between the measured and calculated values of Poisson's ratio for the 100 mg/ml TB-HA hydrogel. Differences were seen between the measured and calculated values at lower concentrations. This is probably due to the difficulty in measuring values of Poisson's ratio in hydrogels of low polymer concentration due to increasingly non-uniform deformation at the lateral edges of these samples.

At concentrations similar to those in cartilage, the data presented here support preservation of sufficient negative charge on the tyramine-substituted GAGs to produce the high charge density required to recreate the swelling pressure and low matrix porosity characteristic of articular cartilage, but in an artificial cartilage substitute. The dityramine cross-links between GAG chains in the TB-HA constructs are designed to serve a similar function to those normally found in the collagen meshwork, while the use of HA chains provides the Donnan and stress shielding effects needed for cartilage function and durability. From the confined

and unconfined mechanical testing data, it was determined that the 100 mg/ml TB-HA sample exhibited the values of aggregate modulus, Young's modulus and Poisson's ratio, which were in the range of those previously reported for articular cartilage.

2.2 Dual Syringe/Needle Injector Device [10]

A porcine cartilage repair model had been previously used by our laboratory to test in a live surgical venue the concept of *in situ* (in vivo) cross-linking of the TB-hydrogel using the 100 mg/ml TB-HA formulation, the optimal formulation based on the results of the mechanical testing described above. These experiments used a compress applied to the repair site surface to diffuse hydrogen peroxide through the TS-HA plug and cause cross-linking. While these experiments confirmed the in vivo tolerance of the cross-linking reagents and TS-HA materials on the joint, the primary observation form these experiments was that reliance on hydrogen peroxide diffusion for cross-linking of the TS-HA plug was unreliable, and mainly responsible for the resulting poor fixation and longevity seen in the porcine study. The viscous nature of the 100 mg/ml TS-HA did not allow for complete diffusion, resulting in incomplete cross-linking using the procedure described above. Furthermore, blood flow from the subchondral bone at the repair site, while not interfering with filling of the defect, may also have interfered with the ability of the hydrogen peroxide to completely cross-link the TS-HA. The development of a methodology to ensure complete cross-linking and fixation within the *in vivo* repair site was a preferred solution. In order to insure complete

cross-linking and ensure fixation, a dual syringe/needle injection device was developed to simultaneously deliver controlled volumes of TS-HA and hydrogen peroxide. In addition, an adhesive strength test was developed in order to quantify the fixation between the TB-HA hydrogel and the surrounding cartilage matrix when using various defect treatment protocols that take advantage of the unique chemistry of the cross-linking reaction to optimize fixation.

The injector device was designed and developed to take advantage of the chemistry behind the tyramine-based hydrogels. The device consists of two syringe barrels (10 ml and 1 ml volumes), a 16 gauge outer diameter dual needle, and a delivery system to drive both syringe plungers simultaneously **(Fig 2.5)**.

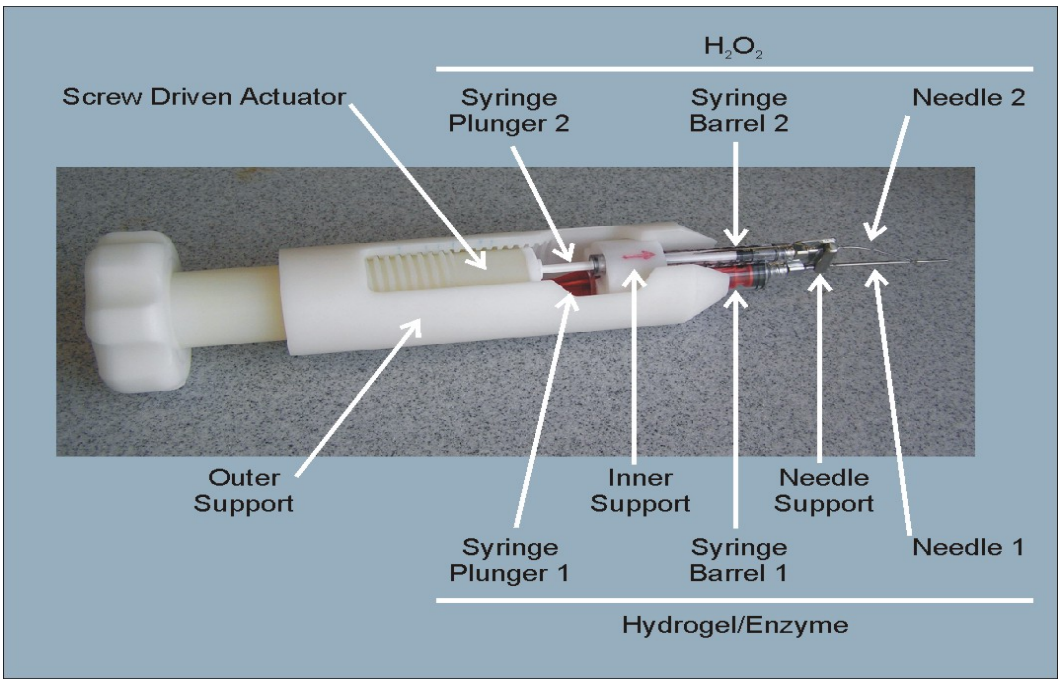

Figure 2.5. Dual Syringe/Needle Device Assembly. This includes actuator, barrels, plungers and dual needle.

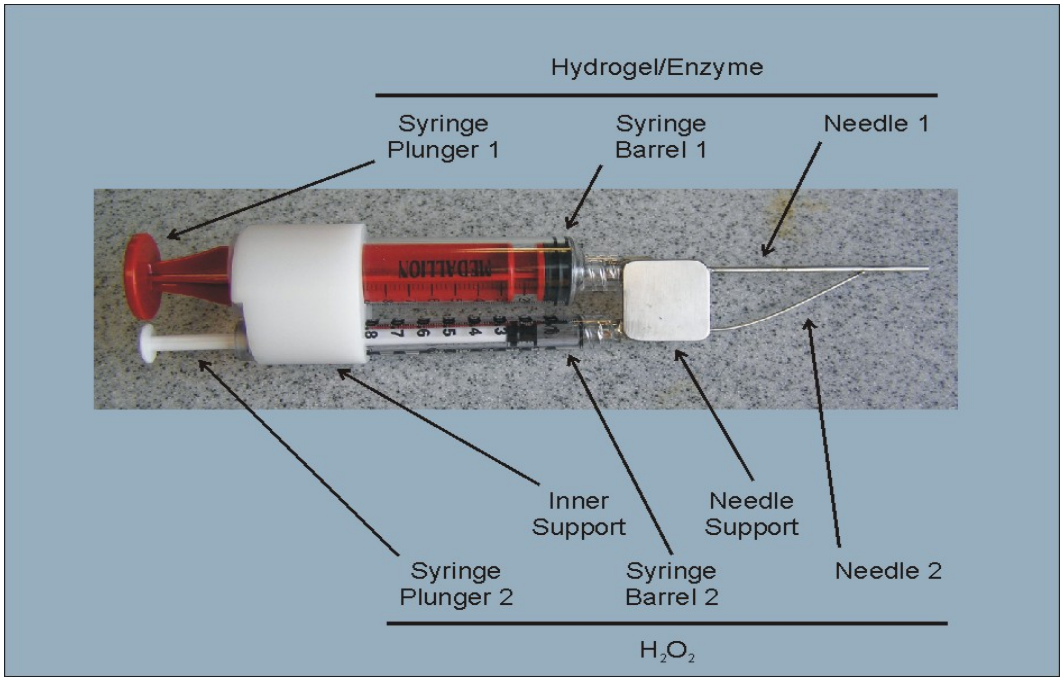

Figure 2.6. Alternative View. Syringe barrels, plungers and dual needle assembly without the actuator.

The 10 ml syringe (barrel 1) is filled with the desired solution of TS-HA, thoroughly mixed with HRP, while the 1 ml syringe (barrel 2) contains a solution of hydrogel peroxide. The diameter of the TS-HA containing syringe has an internal radial area 12.5 times greater the internal radial area of the hydrogen peroxide containing syringe. A single actuator is used to drive two corresponding plungers at the same longitudinal rate through both barrels, and results in the constant proportional extrusion of 12.5 volumes of the TS-HA solution from barrel 1, compared to one volume of hydrogen peroxide from barrel 2. This ratio was chosen to deliver a minimum volume of hydrogen peroxide that would ensure cross-linking of TS-HA. Attached to the ends of both barrels is a needle-inside-a-needle device designed to accept the extruded solutions from barrels 1 and 2 **(Fig 2.6)**. The internal radial areas of the needles were designed to maintain the proportional extrusion of the two solutions created by the syringe barrels as the solutions are extruded from the end of the dual needle. The TS-HA solution within the lumen of the larger needle (needle 1) is directed to the outside of smaller needle (needle 2) that contains hydrogen peroxide, while keeping both solutions separate **(Fig 2.7)** until final extrusion from the needle device. This is necessary due to the extremely fast rate of cross-linking time for the TS-HA hydrogel, which results in clogging of the needle lumen if allowed to mix prior to extrusion at the needle tip.

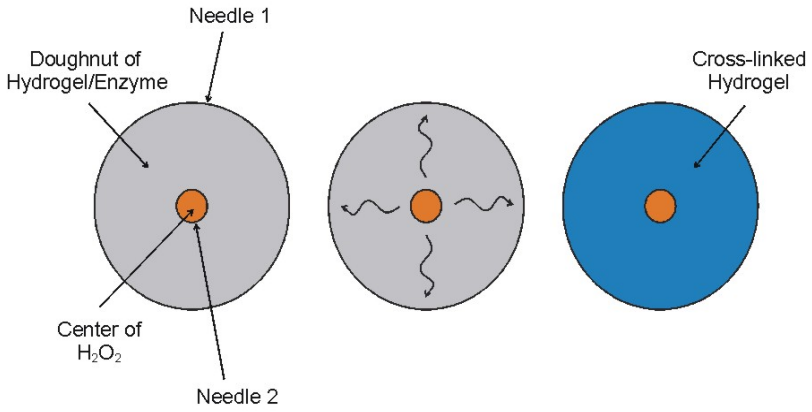

Figure 2.7. Schematic of the Extrusion of Solutions from Dual Needles. Orientation of needle 1 (contains TS-HA/HRP) and needle 2 (contains hydrogen peroxide) within dual needle device.

A screw driven actuator was chosen in order to attain the mechanical advantage required to deliver highly viscous TS-HA solutions, such as the 100 mg/ml used for cartilage repair, while allowing for a single control mechanism to deliver the contents of both syringes **(Fig 2.5)**. The materials used in the design of the entire assembly including actuator, barrels, plungers and needle, were chosen from commercially available supplies, which could tolerate pressures generated due to the viscous nature of the TS-HA, and to allow for easy sterilization. It was determined from *in vitro* testing and observation that the dual syringe/needle design resulted in the easy delivery of cross-linked TB-HA hydrogel.

2.3 In Vivo Validation of Dual Syringe/Needle Injector Device [10]

Both *ex vivo* cross-linked press fit plugs and in situ cross-linked plugs formed using the dual syringe/needle injection device described above were evaluated in a rabbit defect repair model for 1 week and 1 one month to test initial fixation. Press fit plugs were chosen as this is the standard used in current clinical cartilage repair procedures involving implantation of cartilage plugs. Two rabbits were used for each treatment condition, and for each time point, for a total of 8 animals. The goals of the rabbit repair model were to evaluate the two strategies for initial fixation, their effect on longevity and wear characteristics within the joint, and the ease of use of the dual syringe/needle injection device in a live surgical setting. Dual osteochondral defects were created in the medial trochlear facet using a 2.8 mm (1/8 inch) drill bit which had been pre-sterilized. The depth of drill insertion was 5 mm. The defects were then filled by either insertion of the pre-

formed press fit plugs into the defects, or filling of the defects using the dual syringe/needle injection device.

All of the rabbits used in this study returned to full weight bearing immediately following surgery and showed no ill effects from the surgical procedure. Significant bleeding was encountered during surgery, but this did not interfere with the ability to fill the defect space with TS-HA using the delivery device. The entire procedure for filling each defect with both the press fit plugs and the device was determined to be relatively quick and simple by the surgeons involved in the study. Following euthanization, macroscopic inspection of the surgical repaired knees and joint space for both the press fit defect group **(Fig 2.8 A)** and the device filled group **(Fig 2.8 B)** revealed no evidence of inflammatory reaction, or any chronic reaction to the biomaterial and cross-linking agents used. For both groups both the proximal and distal lesions were completely filled with a transparent material, indicating the presence of the TB-HA. The surrounding articular cartilage and opposing articular surface did not show any evidence of abnormal wear for both one week and one month animals. Upon physical examination, both the press fit and the device filled group, exhibited repairs that contoured grossly with the surrounding articular surface. Furthermore, the only distinction that could be made between the repair surface and the surrounding cartilage was the fact that the repair site displayed a qualitatively more slippery surface texture to the surgeon. No distinction could be made between the one week and one month time points based on the gross examination described above.

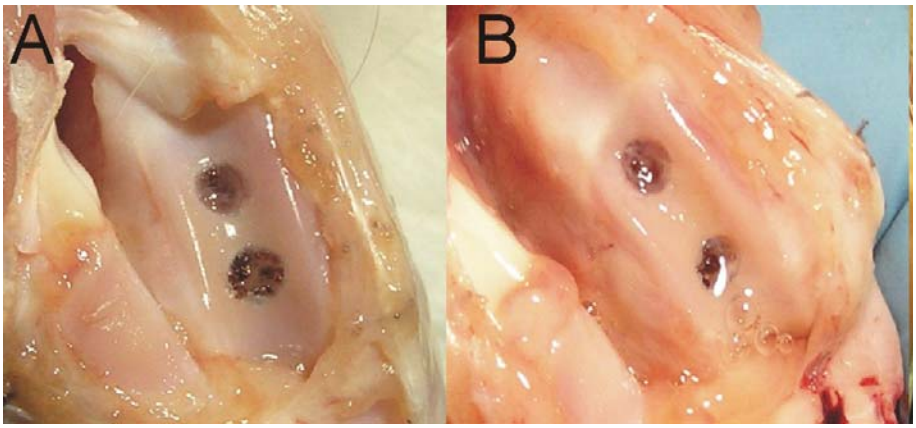

Figure 2.8. Repaired Cartilage Sites. Representative photographs following sacrifice at one month for: (A) the press fit group; (B) the device filled group.

Thus, from the results of the gross examination of the rabbit model it was determined that the press fit and device filled treatment strategies appeared stable after one month. These results indicate that the single most important factor in determining success may be complete cross-linking of the TB-HA hydrogel, since both the press fit and device filled plugs did not appear to perform differently at one month of time. Additional differences between time points may be revealed through histological examination of the repair sites. Unfortunately, histological evaluation of the defects has been wrought with challenges due to the difficulties that occur when using conventional histological processing techniques on hydrogel samples. An example of the poor histological results is shown in **Figure 2.9** for a repair site which has been treated with a preformed press fit plug at one month following surgery, with similarly poor results seen independent for the device filled cross-linking method.

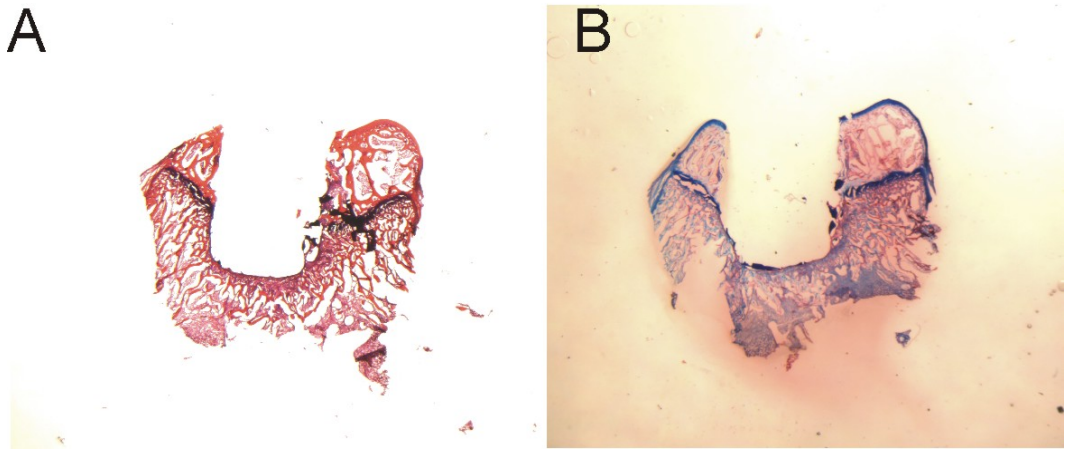

Figure 2.9. Histological Evaluation. Representative histological photographs (12x magnification) of a press fit plug repair site at one month stained with: A) H&E or B) or alcian blue.

Upon visualization under low magnification (12x), following staining with either H&E **(Fig 2.9 A)** or alcian blue **(Fig 2.9 B)**, a void can be seen where the TB-HA hydrogel plug is expected to appear. Increased magnification (40x) shows fragments of hydrogel remaining at or near the defect borders (not shown). Gross dissection of the same sample confirms the presence of the TB-HA, as seen in **Figure 2.10**, and demonstrates that the hydrogel portion of the repair site is being lost following sectioning, during the dehydration steps of the staining process, in which the hydrogel with its exceptionally high water content shrinks disproportional to the surrounding tissue.

Figure 2.10. Photograph of Cartilage Repair Site. Following gross dissection of the press fit plug repair site seen in Figure 2.9.

These results highlight the need for methods that allow for visualization of the TB-hydrogels that is representative of their *in vivo* orientation to surrounding tissues. Hence, this study to utilize noninvasive imaging techniques such as MRI that permits to evaluation of the efficacy of TB-hydrogels in large animal models as it is required for FDA approval and clinical trial testing.

CHAPTER III

CHALLENGES IN SAMPLE PREPARATION

This chapter explains some of the issues encountered during this investigation in terms of sample preparation, and how they were addressed in order to meet the objectives of this dissertation work.

3.1 Shrinking and Swelling of TB-hydrogels

When the TB-hydrogels are cross-linked in water, they form solid, stable hydrogels in the absence of measurable shrinking or swelling. However, when the TB-hydrogels are either cross-linked directly in PBS, or are equilibrated with PBS following cross-linking in water shrinking or swelling of the hydrogel mass occurs depending on the initial HA or GE concentration. For the experiments described in this thesis, all TB-hydrogels were cross-linked first in water followed by equilibration in PBS as described in **Appendix A**. Initial cross-linking of the TB-hydrogels in water allowed for formation of homogeneous solid hydrogel

masses that were not always obtained when cross-linking directly in PBS. Subsequent equilibration of the TB-hydrogels in PBS allowed for acquisition imaging data under conditions of ionic strength, pH, etc. similar to those of the human body.

When cross-linking in water then equilibrating in PBS, it was noticed that the TB-HA hydrogels at 6.25, 12.5, and 25 mg/ml of HA shrank about 30-35 % of their original volumes; while the TB-HA hydrogels at 50 and 100 mg/ml of HA swelled about 10% or less of their original volumes. Shrinking of the TB-GE hydrogels was even more dramatic as the hydrogels were reduced to 70 to 90 % of their original volumes. The hydrogels formed from equal concentration of HA and GE or TB-CO shrank or swelled similar to the TB-HA. This shrinking or swelling effect in PBS induces significant changes in the concentrations of the material. Hence, correlation curves of initial versus final concentrations for all the materials were made. These curves allowed for preparation of TB-hydrogels of predictable final concentrations after PBS equilibration **(Fig 3.1 A, B, C)**. Because the 50 and 100 mg/ml were swelling rather than shrinking, they were simply adjusted to 50 and 100 mg/ml concentration by addition of the appropriate fluid volume following concentration on vacuum concentrator.

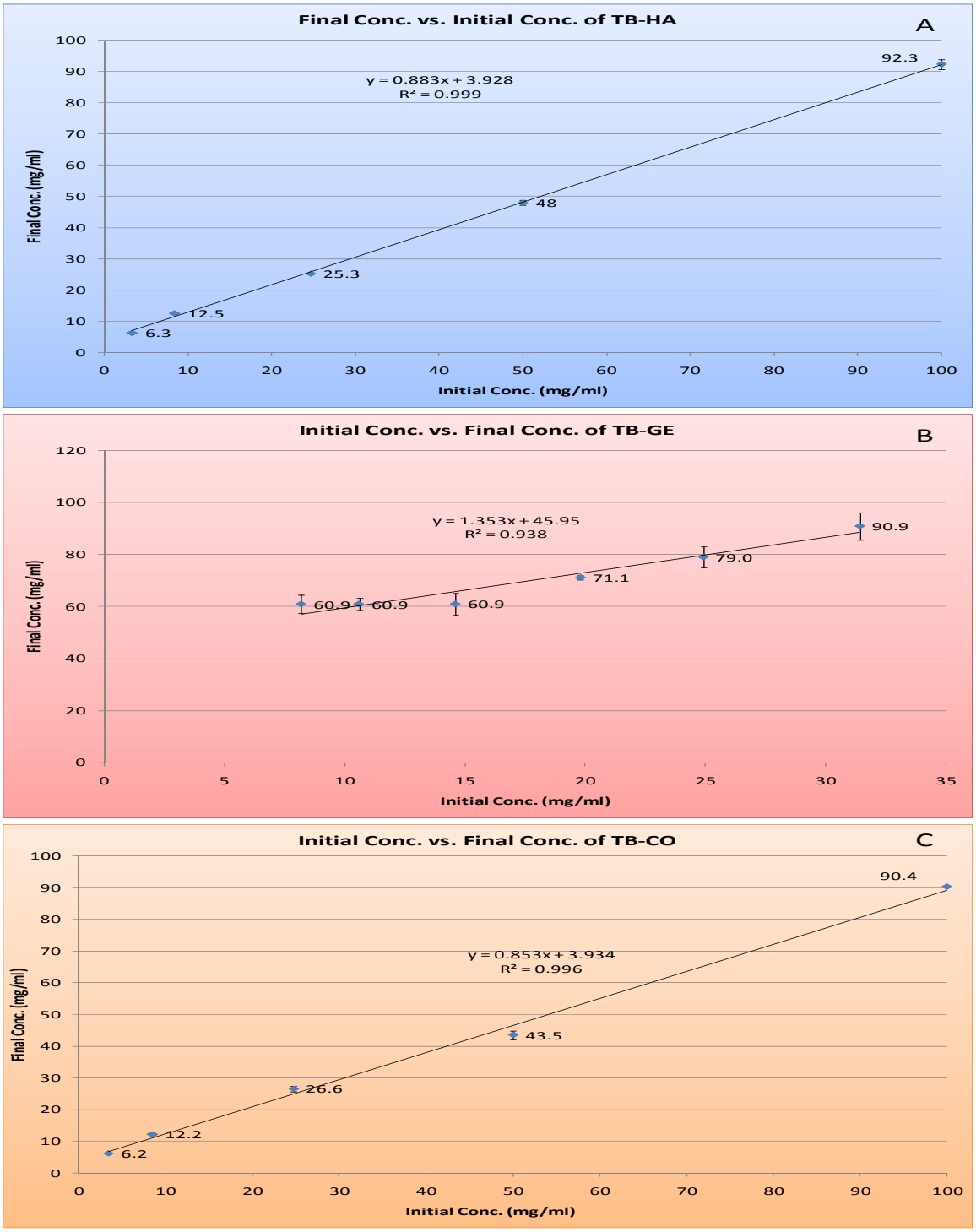

Figure 3.1. Correlation Curve of Initial Versus Final Concentrations for TB-HA (Panel A), TB-GE (Panel B), and TB-CO (Panel C). The correlation of initial versus final concentration is much higher for the TB-HA and TB-CO samples, than for the TB-GE samples.The standard deviations in each plot (**A, B, C**) are an average of 4 samples per concentration of TB-HA, TB-GE, and TB-CO that were used for the experiments involved in this study.

As seen in **Figure 3.1 A**, the TB-HA hydrogels displayed a nice linear correlation between the initial and final concentrations. The small standard deviations in TB-HA hydrogels are indicative of the high reproducibility of formation of these materials. In the case of the TB-GE **(Fig 3.1 B)**, the final concentration as a function of the initial concentration is far less linear with much wider standard deviations indicative of a lower reproducibility of formation compared to the TB-HA. This effect on TB-GE mirrors the properties of collagen and its function in cartilage. The cartilage matrix collapses in the absence of sufficient PG concentration, as the PGs are responsible for maintaining the swelling pressure that expands the collagen network. On the other hand as seen in **Figure 3.1 C**, the TB-CO composed of both HA and GE (collagen) similar to that of cartilage ECM behaved more like the TB-HA with a linear fit and a high coefficient of correlation (0.99). Once again, because the HA or GAG content is incorporated into these materials with the HA having similar strong charge-to-charge repulsive forces as PGs, the matrix integrity is preserved. Based on these results, TB-HA and TB-CO hydrogels cross-linked in water, and then equilibrated in PBS were formed at the desired concentrations of 6.25, 12.5, 25, 50 and 100 mg/ml; while only TB-GE hydrogels cross-linked in water could be formed at 6.25, 12.5, 25, 50 and 100 mg/ml. TB-GE hydrogels cross-linked in water and then equilibrated in PBS could only be formed at 60, 70, 80 and 90 mg/ml.

3.2 Diffusion of Hydrogen Peroxide

Diffusion of hydrogen peroxide through the entire material volume is required to obtain fully cross-linked hydrogels. This was restricted when the concentration and volume of the samples increased. This is explained by a decrease in the porosity of the material with increasing concentration of HA or GE, which reduces matrix porosity slowing the diffusion of the hydrogen peroxide to the point that the embedded enzyme (HRP II) can deplete the hydrogen peroxide before it fully diffuses throughout the hydrogel mass.

Di-tyramine cross-links fluoresce blue-green upon exposure to UV light. **Figure 3.2** shows an example of the limited diffusion of hydrogen peroxide in the presence of higher concentrations of TS-HA and increased volumes of the materials. This figure shows how the hydrogen peroxide diffused through most of the volume of 12.5 mg/ml TB-HA hydrogels that were made at increasing volumes of 200, 400, 600, 800 and 1000 µl. On the other hand, the hydrogen peroxide hardly diffused through TB-HA hydrogels at 25 mg/ml, cross-linking only the top surface of the material.

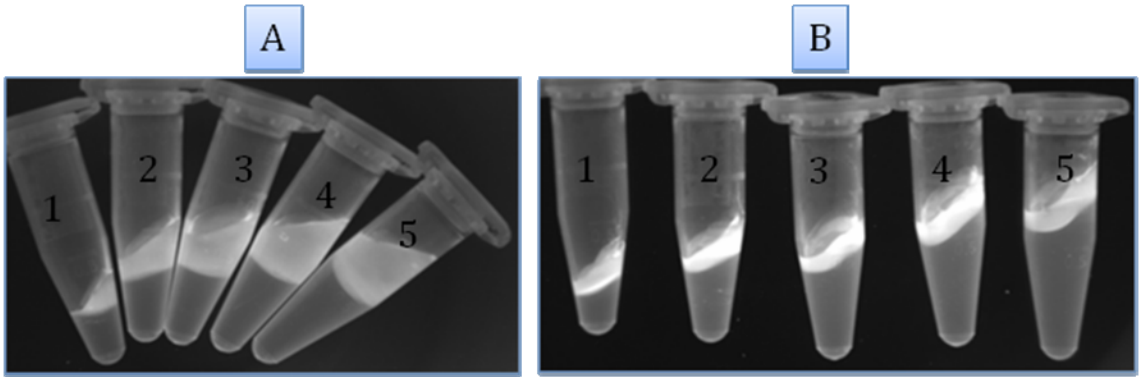

Figure 3.2. Hydrogen Peroxide Diffusion. The photos were taken under UV-light immediately after adding hydrogen peroxide to initiate cross-linking. **A:** TB-HA at 12.5 mg/ml prepared in 5 different volumes (1-5) of 200, 400, 600, 800, 1000 μl, respectively. The 5 samples were spiked with a 0.3 % hydrogen peroxide solution that diffused quickly through the hydrogel volume. **B:** The same as panel A, except that the TB-HA is at 25 mg/ml concentration. The 0.3 % hydrogen peroxide solution diffused through only about 5% of the hydrogel volume.

Hence, a hydrogel was determined to be fully cross-linked after adding the hydrogen peroxide, if it fluoresced uniformly blue-green throughout its entire volume when exposed to UV-light. Otherwise, the hydrogel was considered partially cross-linked and inadequate for our studies.

This dependence of hydrogel cross-linking on diffusion of hydrogen peroxide at concentrations of 25 mg/ml or higher correlates well with previous results for mechanical testing. **Figure 2.3 B** in **Chapter II** showed the equilibrium stress plotted against the applied strain for TB-HA hydrogels at various HA concentrations, with the slope of the lines the aggregate moduli or compressive strength of the materials. The slope of the line for the 6.25 and 12.5 mg/ml TB-HA hydrogels are similarly low. However, when the concentration is increased to 25 mg/ml, the slope becomes much steeper, and this steepness increases even further with the 50 and 100 mg/ml concentrations. This increase in aggregate modulus or the ability of the materials to absorb energy is dependent upon the matrices ability to influence the flow of water through its pores, which occurs between the 12.5 and 25 mg/ml HA concentration as with the hydrogen peroxide.

The difficulty with partial cross-linking was overcome by using the dual/syringe needle injector device described in **Chapter II**. The injector device was determined to be the best method suited for attaining fully cross-linked TB-HA and TB-GE hydrogels at 25, 50 and 100 mg/ml concentrations as well as for the composite materials (TB-CO) from 6.25, 12.5, 25 and 50 mg/ml). The exception to this was the TB-CO hydrogel composed of both the 100 mg/ml TB-HA and 100mg/ml TB-GE concentration. The viscosity of this composite material

exceeded the maximum pressure that the injector device could generate to extrude the cross-linked hydrogel. Hence, the composite materials at this particular concentration were cross-linked by mechanically mixing the combined TS-HA and TS-GE containing the enzyme with the hydrogen peroxide in increments of 100 µl up to 1 ml volumes.

CHAPTER IV

DETERMINATION OF T1 AND T2 MAGNETIC RESONANCE IMAGING (MRI) PROPERTIES OF TYRAMINE-BASED HYALURONAN AND COLLAGEN HYDROGELS

4.1 Introduction

Tyramine-based (TB) HA and collagen hydrogels are new biomaterials in the process of commercial development for a variety of clinical applications **[45].** Collagen and glycosaminoglycans (GAGs) such as HA are major components of most tissue extracellular matrices (ECMs), and MRI techniques have been developed for non-invasive imaging and assessment of these two macromolecular constituents. Many MRI imaging sequences are known to be influenced by matrix composition, in particular collagen and GAG content. Many of these approaches claim more specificity for a particular molecular species over that of others, for example: T2 mapping sequences correspond to collagen content, and T1 mapping sequences and charge-based imaging techniques such as Gadolinium Enhanced MRI of Cartilage **(**dGEMRIC) correspond to GAG

content **[46]**. While these measurements have been validated in cartilage, the sensitivities of these MRI techniques to collagen and GAG content within cartilage are not generally independent **[46]**. The objective of this study was to apply these MRI methods to a controlled system of synthetic ECM composed of TB-HA and TB-collagen molecules and evaluate their sensitivity and specificity, as well as their qualitative and quantitative accuracy for measuring matrix composition. This work provides a scientific basis to better understand the relationship between these MRI methods and tissue composition, and to detect, distinguish, characterize and quantify the TB-hydrogels.

4.2 Experimental Design

T1 and T2 acquisitions were employed in these experiments. HA and collagen (as gelatin, GE) equilibrated in PBS were imaged independently at concentrations of 0, 6.25, 12.5, 25, 50 and 100 mg/ml and 0, 60, 70, 80 and 90 mg/ml, respectively. Additionally, GE in water was imaged at 0, 6.25, 12.5, 25, 50 and 100 mg/ml. Composite materials, a combination of HA and GE, equilibrated in PBS were imaged at 0, 6.25, 12.5, 25, 50 and 100 mg/ml of both HA and GE. These materials were prepared in 1 ml volumes, and under 3 different formulations: 1) unsubstituted; 2) tyramine-substituted; and 3) tyramine-substituted plus enzyme and hydrogen peroxide (cross-linked). The series of 15 samples under the 3 different conditions (45 samples) were imaged 2 to 5 times using each MRI technique at different time points (test-retest measurement reproducibility) using a clinical 3T MRI system. The mean T1 and T2 values

were compared first as a function of concentration, then as a function of the three different formulations.

Initially the contribution of the HRP enzyme to the MRI signal of TB-HA and TB-GE hydrogels was thought potentially significant, as the iron containing porphyrin ring of the HRP was predicted to have some measurable magnetic properties. However, T1 and T2 values of HRP in PBS alone at 5, 10 and 20 u/ml, which bracketed the 10 u/ml of HRP used to prepare all the cross-linked hydrogels used in this dissertation, were found to be the same as for PBS control samples **(Fig 4.1)**. Therefore it was concluded that the addition of HRP would have no effect on the imaging properties of the TB-hydrogels, and hence, the imaging of tyramine-substituted samples with HRP only was eliminated from our studies.

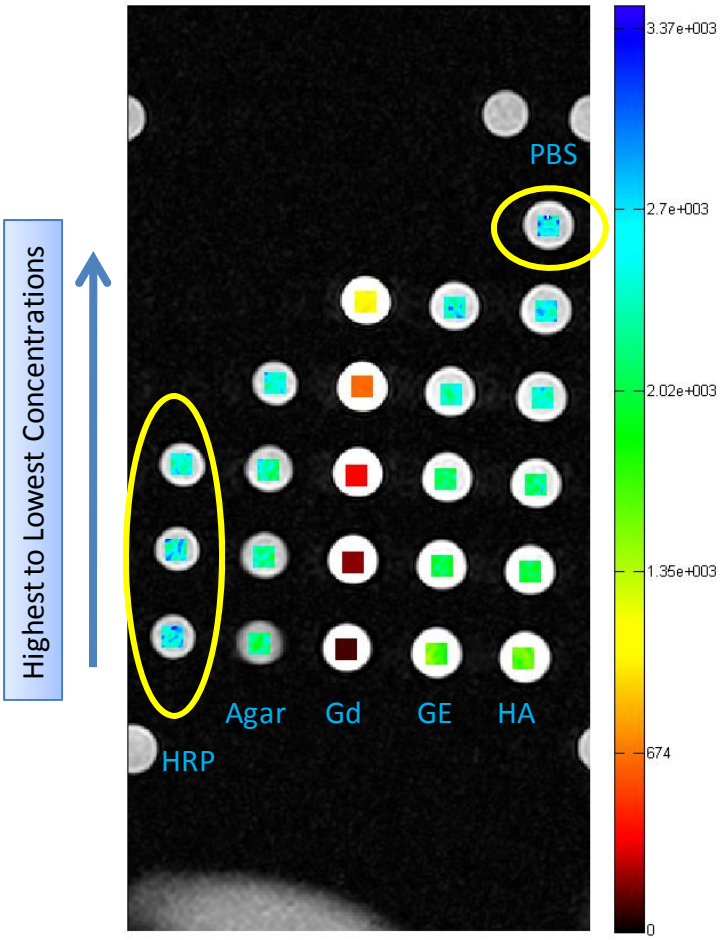

Figure 4.1. T1 Map of Horse Radish Peroxidase (HRP) Solutions. HRP at 5, 10, and 20 u/ml, agar at 0.5, 1, 2, and 4 weight percent, Magnevist (Gd-DTPA) at 0.125, 0.25, 0.5, 1 and 2 mM, unsubstituted gelatin (GE) and unsubstituted hyaluronan (HA) at 6.25, 12.5, 25, 50, and 100 mg/ml and PBS controls. The HRP alone (yellow circle on the left) imaged similar to the PBS control (yellow circle on top right). HRP at 5, 10 and 20 u/ml had T1 values of 2,456, 2,552, and 2,628 msec while PBS had a T1 value of 2,642 msec.

The materials and methods for the synthesis of TS-HA and TS-GE and their hydrogel formation or cross-linking are described in **Appendix A**. **Table IV** represents the hydrogel biomaterials that were prepared for these experiments. In addition to these samples, calibration curves of agar and Magnevist (Gd-DTPA^{-2}) contrast agent were prepared along with a second concentration curve of cross-linked GE without saline equilibration (in water).

Samples & controls	Description	Concentrations (mg/ml)	Total N° of samples
HA	Unsubstituted Hyaluronan	6.25, 12.5, 25, 50, 100	5
GE	Unsubstituted Gelatin	6.25, 12.5, 25, 50, 100	5
TS-HA	Tyramine-Substituted Hyaluronan	6.25, 12.5, 25, 50, 100	5
TS-GE	Tyramine-Substituted Gelatin	6.25, 12.5, 25, 50, 100	5
TB-HA	Tyramine-Based Hyaluronan (Cross-linked)	6.25, 12.5, 25, 50, 100	5
TB-GE/ TB-Gew	Tyramine-Based Gelatin (Cross-linked)/ Tyramine-Based Gelatin (Cross-linked) in Water	60, 70, 80, 90 (PBS)/6.25, 12.5, 25, 50, 100 (Water)	4 (PBS)/5 (Water)
CO	Unsubstituted Hyaluronan/Gelatin (Composite)	6.25, 12.5, 25, 50, 100	5
TS-CO	Tyramine-Substituted Hyaluronan/Gelatin (Composite)	6.25, 12.5, 25, 50, 100	5
TB-CO	Tyramine-Based Hyaluronan/Gelatin (Cross-linked Composite)	6.25, 12.5, 25, 50, 100	5
Ag	Agar (Calibration Curve)	0.5, 1, 2, 4 (weight %)	4
Gd-DTPA^{-2}	Gadolinium (Calibration Curve)	0.125, 0.25, 0.5, 1, 2 (mM)	5
			58

Table IV: Description of the hydrogel biomaterial compositions used for imaging. All samples were prepared in PBS unless otherwise indicated.

After material formulation, 1 ml of each material was transferred to a 1.5 ml cryotube, and all tubes arranged in a rack to form a grid. The pattern of the grid is composed of the 58 samples described in **Table IV** plus 5 control samples (4 of PBS and 1 of water), for a total of 63 samples (**Figs 4.2 and 4.3)**.

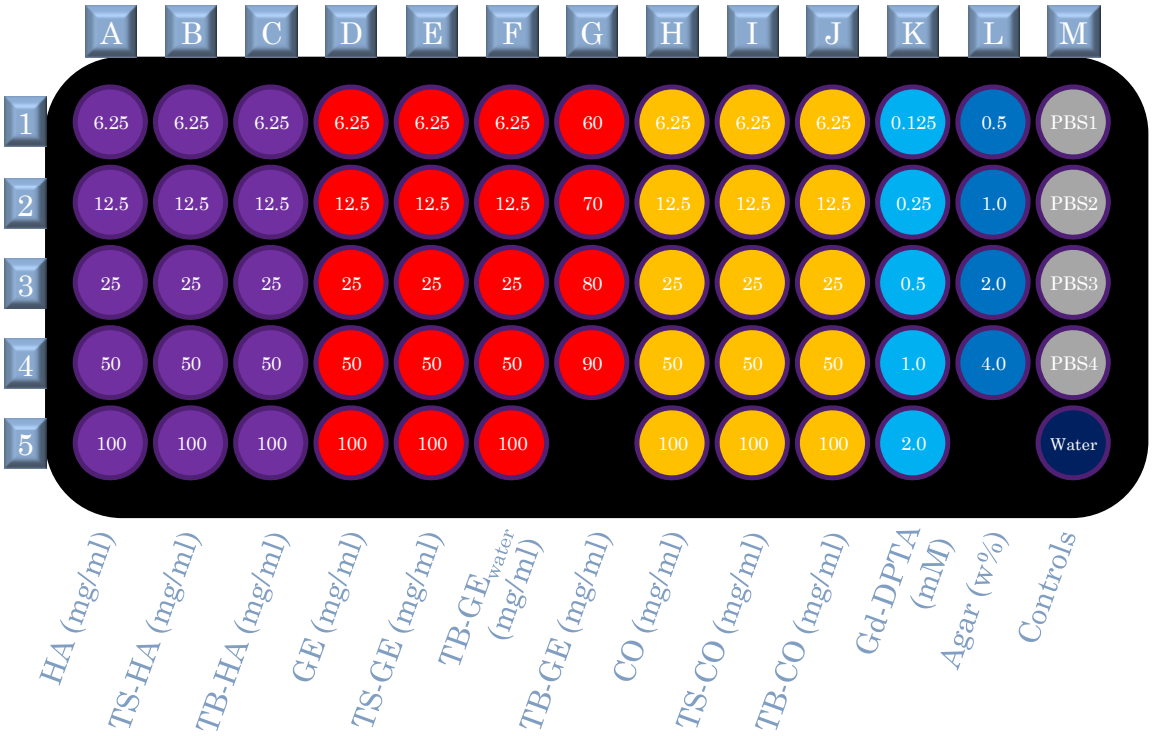

Figure 4.2 Schematic of the Grid for Imaged Samples. From left to right, columns A - J contain: unsubstituted hyaluronan (HA), tyramine-substituted HA (TS-HA), cross-linked HA (TB-HA), unsubstituted gelatin (GE), tyramine-substituted GE (TS-GE), cross-linked GE in water (TB-GE$_{water}$), cross-linked GE in PBS (TB-GE), unsubstituted HA/GE composite (CO), tyramine-substituted HA/GE CO (TS-CO), cross-linked HA/GE CO (TB-CO). Controls included: PBS (column M), water (column M), agar (column L), and Magnevist (Gd-DPTA, column K). All samples were at the concentrations indicated.

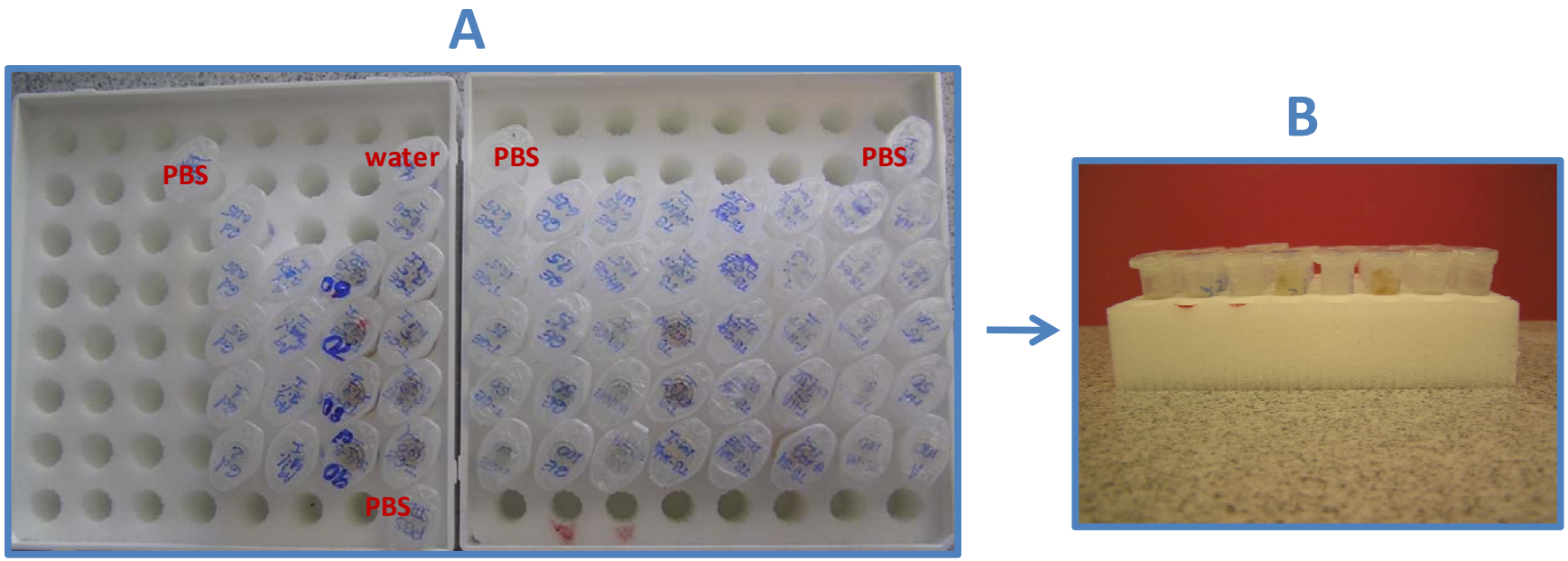

Figure 4.3 Actual Grid of Imaged Samples. A: Samples contained in padded boxes used for imaging. The controls were positioned outside the sample set to create asymmetry used in sample identification/validation. **B:** Shows the samples properly leveled allowing imaging of a single circumferential cross-section of all samples in one single MRI slice for subsequent analysis.

Figure 4.3 shows the samples and controls contained in the boxes used for imaging. This arrangement allowed all the samples to be placed at the same level **(Fig 4.3 B)**, which facilitated localizing all the samples in a single T1 or T2 acquisition slice. Additionally, each set of samples was imaged between 2 and 5 times on different days for test-retest reproducibility as shown in **Table V**.

Sample Set	May 14 '09	Aug 21 '09	Sept 13 '09	Oct 01 '09	Oct 07 '09	Total N° of Imaging
HA	x	x	x	x	x	5
GE	x	x	x	x	x	5
TS-HA		x	x	x	x	4
TS-GE		x	x	x	x	4
TB-HA		x	x	x	x	4
TB-GE		x	x	xx	xx	4/2
CO		x	x	x	x	4
TS-CO				x	x	2
TB-CO				x	x	2
Ag	x	x	x	x	x	5
Gd	x	x	x	x	x	5

Table V: Frequency of re-imaging for the different hydrogel sample sets.

4.3 T1 and T2 Mapping

All of the MRI evaluations described in this dissertation were performed at room temperature using a standard quadrature head coil in a 3 T MRI system (Tim TRIO; Siemens Medical Solutions, Erlangen, Germany).

First, gradient echo localizer images were used to identify a coronal slice that included all samples within the grid enabling them to be imaged simultaneously. The spatial resolution for the grid MRI acquisitions was provided; the specimen spatial resolution was sized proportional. Next, T1 and T2 image series were acquired using the following parameters:

T1 sequence: An inversion recovery fast (turbo) spin echo sequence was used to measure T1 with a repetition time (TR) = 6000 msec; inversion time (TI) = 23 msec, 75 msec, 150 msec, 300 msec, 750 msec, 1,400 msec, 2,000 msec and 2,800 msec; echo time (TE) = 10 msec; field of view (FOV) = 260 x 130 mm; slice thickness = 1.9 mm; matrix = 256 x 128, and 1 average. The inversion recovery imaging sequence produced 8 images from a single slice location, each with a different TI.

T2 sequence: T2 relaxation time of the samples was measured using a spin echo based Carr-Purcell-Meiboom-Gill (CPMG) imaging sequence with a TR = 6,000 msec and 32 echoes **[47]**. Two spin echo sequences were performed to be able to cover both the materials with very short T2 values and the materials with very long T2 values. The first spin echo started at TE: 15 msec with a maximum of 480 msec, followed by a second one started at TE = 30 msec with a maximum of 960 msec. All images were obtained from a single slice with a FOV

= 260 x 130 mm; slice thickness = 1.9 mm; matrix size = 256 X 128, and 1 average. The CPMG imaging sequence produced 32 images from a single slice location, each with a different TE.

Post-Processing Image: The images were reviewed and exported using DicomWorks. Then, T1 and T2 maps were computed using MRIMapper (MIT, Cambridge, MA) and MATLAB (Mathworks, Natick, MA). For both the T1 and T2 maps, this process began by loading the images into the MRIMapper with the appropriate parameters. The MRIMapper produced a T1 or a T2 image that could be analyzed by drawing regions of interest **(Fig 4.4)**.

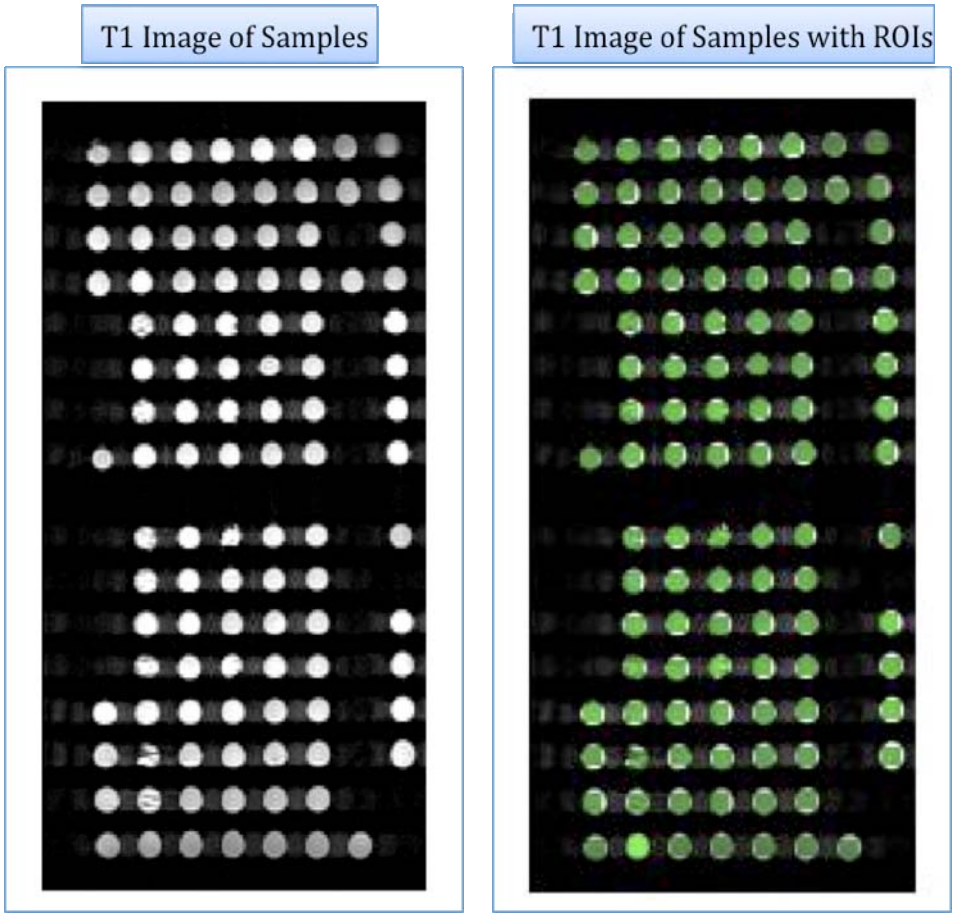

Figure 4.4. Example of T1 Image Produced by the MRIMapper. Left: Inversion recovery image at TI = 23 msec displayed by the MRIMapper. This image is used to draw regions of interest (ROI) for analysis. **Right:** T1 image with 4x4 ROIs superimposed. The artifact between samples observed was caused by the foam in which the samples were contained (see Fig 3.1), and does not interfere with analysis.

Regions of interest (ROI) for analysis were selected as a 4x4 to 6x6 set of pixels from the center of each hydrogel sample as shown in **Fig 4.4**. Then, the MRIMapper generated T1 maps by curve-fitting to a three-parameter exponential fit $Mxy = M_o (1–2Ae–TI/T1 + e–TR/T1)$, where Mxy is the pixel signal intensity from the image obtained as a function of TI, M_o is the signal intensity that would be obtained from the sample in the fully relaxed state, and $A = 1\text{-}\cos\theta$ is the flip angle of the inversion pulse. T2 maps are generated by fitting logarithmically to $My = M_o \exp(-TE/T2)$, where My is the pixel signal intensity from the image obtained as a function of TE, and M_o is as defined above. The calculated T1 or T2 value was an average of the pixels from the ROI of each sample. The T1 or T2 map was displayed superimposed onto the corresponding inversion recovery or spin echo images, as shown in the results section.

The T1 and T2 mean values were utilized to calculate material relaxivity R1 and R2, respectively. R1 and R2 values were calculated, using a least-squares fit, as the slope of [1/T1 (or 1/T2) – $1/T1_{pbs}$ (or $1/T2_{pbs}$)] vs. concentration of each sample, where T1 or T2 is the T1 or T2 of the sample and $T1_{pbs}$ or $T2_{pbs}$ is the T1 or T2 of PBS. For instance, the R1 of unsubstituted HA was computed by determining the 1/T1 – $1/T1_{pbs}$ for each concentration of HA as shown in **Table VI**. After these values are calculated, the R1 is calculated by plotting the 1/T1 – $1/T1_{pbs}$ values against the sample concentrations as shown in **Fig 4.5**.

Sample	[mg/ml]	T1	1/T1- 1/T1$_{PBS}$
PBS		2469 ± 178.8	0
HA 6.25	6.25	2219 ± 112	0.00005
HA 12.5	12.5	2183± 132	0.00005
HA 25	25	2051 ± 158	0.00008
HA 50	50	1835 ± 133	0.00014
HA 100	100	1482 ± 48	0.00027

Table VI. Calculation of 1/T1-1/T1$_{pbs}$ for HA.

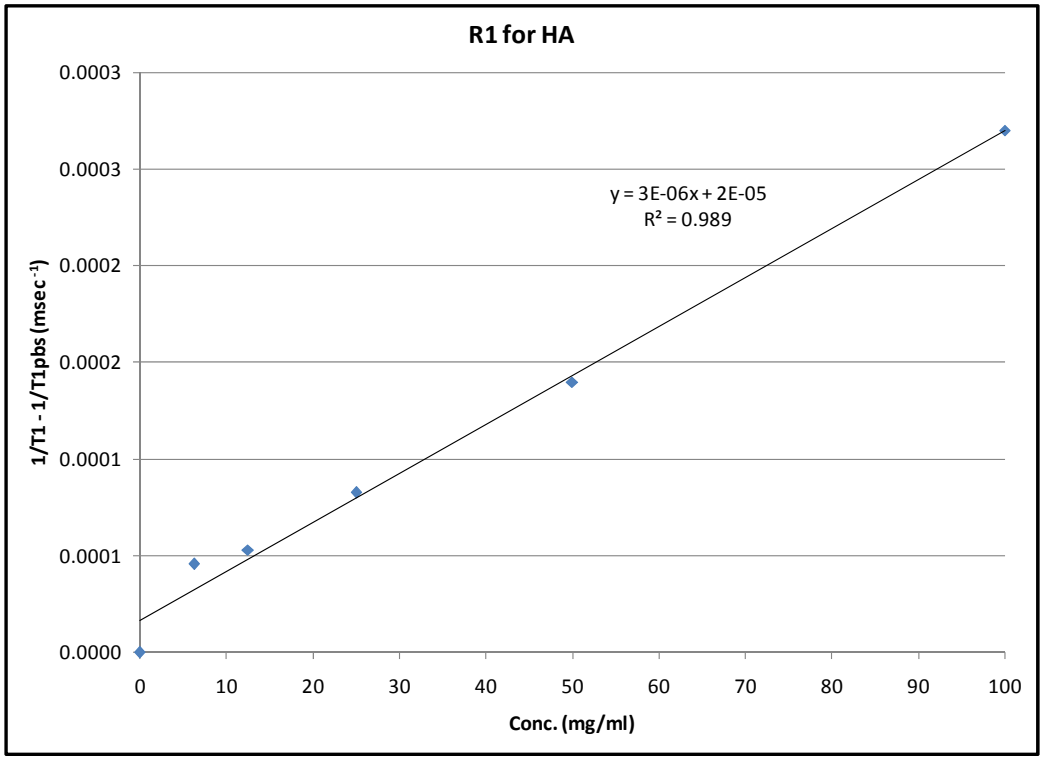

Figure 4.5. Relaxivity of T1 (R1) for HA. Slope (R1) of the linear relationship of 1/T1 – 1/T1$_{pbs}$ vs. HA concentration.

4.4 Results and Discussion

For the purpose of describing the results for these experiments, the T1 and T2 data acquired from the last imaging day (11/07/09) is used as example. This was necessary due to a drift observed in the magnet values from day to day **(Fig B–I. in Appendix B)**. The T1 and T2 data collected for all 5 days is shown in **Appendix B**.

4.4.1. T1 and T2 Mapping

As anticipated, the T1 and T2 maps differentiated changes in HA and GE concentration that could be represented both qualitatively and quantatively. Qualitatively, the T1 and T2 color-coded maps resulted in a color gradient that differentiated the various concentrations of either HA or GE as shown in **Fig 4.6**. Both T1 and T2 decreased with increasing concentrations of the materials. T1 values for unsubstituted HA (HA), tyramine-substituted HA (TS-HA), and cross-linked HA (TB-HA) hydrogels were within a range of 1,370 to 2,730 msec (green to light blue). T1 values for the unsubstituted composite (CO), tyramine-substituted composite (TS-CO) and cross-linked composite (TB-CO) hydrogels were within a range of 684 to 2,730 msec (orange to light blue). The T1 values for the unsubstituted GE (GE), tyramine-substituted GE (TS-GE) and cross-linked GE (TB-GE) hydrogels in water were in the same range as the HA materials or from 1,370 to 2,730 msec (green to light blue). As expected, the Gd control samples had short T1 values, while the agar, PBS and water control samples all had long T1 values.

T2 values for unsubstituted HA (HA), tyramine-substituted HA (TS-HA) and cross-linked HA (TB-HA) hydrogels were within a range of 200 to 1,170 msec (light red to green). T2 values for unsubstituted composite (CO), tyramine-substituted composite (TS-CO) and cross-linked composite (TB-CO) hydrogels were within a range of 100 to 1,170 msec (dark red to green). The T2 values for unsubstituted GE (GE), tyramine-substituted GE (TS-GE) and cross-linked GE (TB-GE) hydrogels in water were within a range of 391 to 1,560 msec (orange to light blue). As expected, the Gd and agar control samples had short T2 values, and the PBS and water contol samples had long T2 values.

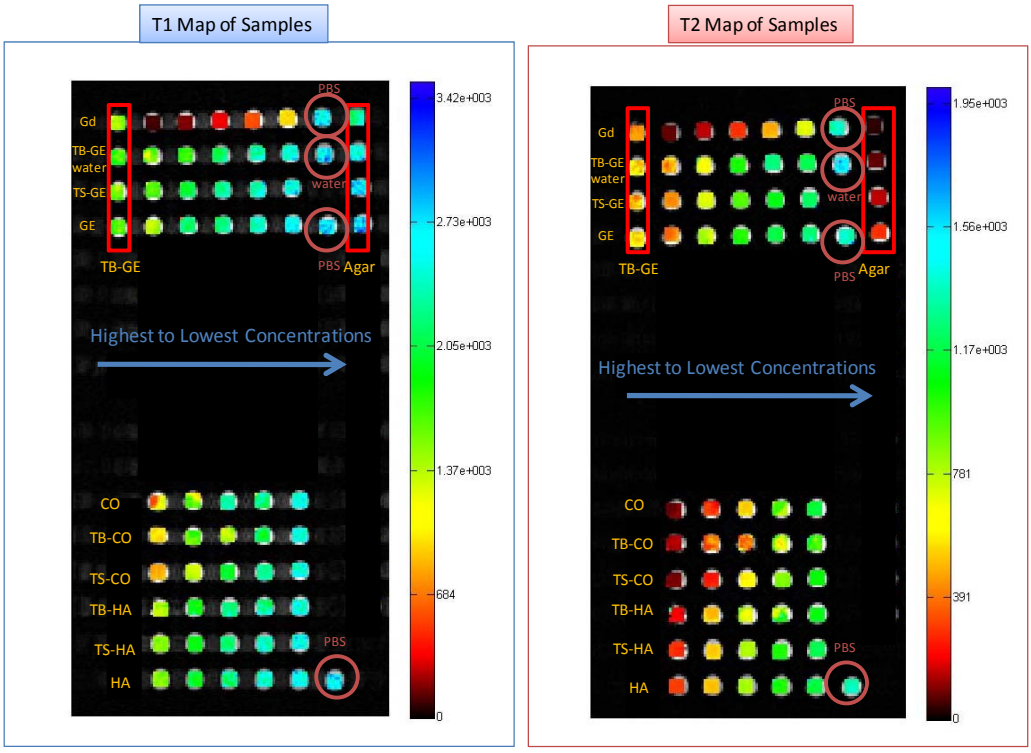

Fig 4.6. T1 and T2 Maps. Left Panel: T1 map with a mapping range of 0 to 3,500 msec (colored bar on right). T1 decreases with increasing concentration for all the samples. The unsubstituted hyaluronan (HA), tyramine-substituted HA (TS-HA), and cross-linked HA (TB-HA) samples are located at the bottom in decreasing concentration from left to right. The unsubstituted composite (CO), tyramine-substituted CO (TS-CO), and cross-linked CO (TB-CO) samples are also located at the bottom in decreasing concentration from left to right. The unsubstituted gelatin (GE), tyramine-substituted GE (TS-GE), and cross-linked GE in water (TB-GE water) samples are located at the top with decreasing concentration from left to right starting with the second column (right of red box). The cross-linked GE (TB-GE) in PBS is at the top left in the red box with decreasing concentration from top to bottom. The gadolinium (Gd) samples are located at the top with decreasing concentration from left to right starting with the second column (right of red box). The agar (Agar) samples are located at the top right in the red box with decreasing concentration from top to bottom. PBS and water control samples are circled in red. **Right Panel:** T2 map with a mapping range of 0 to 2,000 msec (colored bar on right). T2 decreases with increasing concentration for all the samples. Samples are as indicated for the left panel.

4.4.2. Relationship of Materials and Magnetic Properties

Quantitatively, the T1 and T2 values and their respective R1 and R2 values were measured for each material. First, the magnetic properties of gadolinium (Gd) controls used in this study were consistent with those found in the literature **(48,49)**. The T1 and T2 values **(Table VII)** and respective R1 and R2 values **(Table VIII)** for Gd are within the range of values typical for this contrast agent at a 3T field strength **[48,49]**. The T1 and T2 values **(Table VII)** and respective R1 and R2 values **(Table VIII)** for Agar are within the range of values expected for this material at 3T. However, direct comparison with the literature could not be performed for agar because this material has been imaged at concentrations and conditions different from our experiments. Furthermore, these results validate the T1, T2, R1 and R2 values concurrently obtained for the hydrogel materials descibed below.

Control	Weight %	T1 (msec)	T2 (15 msec)	T2 (30 msec)
Agar 0.5	0.5	2173±177	288±5	283±5
Agar 1	1	2033±105	162±3	157±4
Agar 2	2	1942±191	85±2	82±3
Agar 4	4	1646±78	44±3	44±6
	mM			
Gd 0.125	0.125	1036 ± 30	661±15	708±10
Gd 0.25	0.25	634 ± 13	441±8	459±10
Gd 0.5	0.5	352 ± 7	260±4	268±6
Gd 1	1	189 ± 4	142±3	146±5
Gd 2	2	98 ± 3	76±3	78±4

[1] $T1_{PBS}$ value on this imaging day was 2,469±178.8 msec

Table VII. T1 and T2 values for agar and Gd-DTPA^{-2} controls. These T1 and T2 values are comparable to previously reported literature values for Gd-DTPA^{-2} at 3T [48, 49].

Controls	R1 (mM^{-1} s^{-1})	r^2	R2 (mM^{-1} s^{-1})	r^2	R2 (mM^{-1} s^{-1})	r^2
Agar	0.05	0.98	5.50	1	5.52	1
Gd-DTPA^{-2}	5.31	1	6.22	1	6.09	1

Table VIII. R1 and R2 (15 and 30 msec echo spacing) values for agar and Gd-DTPA^{-2} calculated using units of concentration previously reported in the literature. R1 and R2 values of Gd-DTPA^{-2} at 3.0 T are comparable to the values found in the literature of 4.5 and 5.0 mM^{-1} s^{-1}, respectively, using a wider range of Gd-DTPA^{-2} concentrations than previously reported. [48, 49].

As explained in **Chapter I**, the *longitudinal relaxation time* or *spin-lattice relaxation time* T1 is influenced by the characteristics of the spin interaction with the *lattice*, the molecular arrangement and structure. Whereas the transverse relaxation time or spin-spin relaxation time is influenced by the intrinsic *spin-spin interactions* that cause loss of phase coherence due to the intrinsic magnetic properties of the sample. Even though the rate of exponential recovery and decay of T1 and T2 respectively is affected by different factors, both T1 and T2 decreased with increasing concentrations as shown in **Table IX**. For the purpose of explaining the impact of T1 and T2 in the various materials independent of the hydrogel chemistry, **Table IX** only includes values for the unsubstituted HA, GE and CO materials. The same pattern is observed in the tyramine-substituted and cross-linked samples.

Based on those characteristics (i.e. molecular size, motion and molecular interaction) that affect the length of T1 and T2 **(see Figure 1.14)**, agar is considered a large, slow, bound molecule, and as predicted for a compound with these characteristics, exhibits a long T1 (>1,500 msec) and a short T2 (<700 msec). The Magnevist (Gd) control showed T1 and T2 values characteristic of an intermediate molecule according to **Figure 1.14** with a short T1 and a short T2, even though this compound is a small molecule expected to have a fast molecular motion and free molecular interactions. This incongruity contributes to the utility of Magnevist as an MRI contrast agent. Conventionally, HA and GE are regarded as slow moving, large, bound structural molecules, and therefore based on **Figure 1.14** would be expected to exhibit a long T1 and short T2 similar to

agar. However, at lower concentrations they exhibit a long T1 and T2 characteristic of fast moving, small, free molecules. However, with increasing concentration and at the same concentration (~25 mg/ml) that these materials transition in terms of their ability to influence the flow of water (see effect on aggregate modulus, **Figure 2.3B**), or hydrogen peroxide (see effect on cross-linking efficiency, **Figure 3.2**) through their pores, they also transition to short T1 and T2 values characteristic of more intermediate molecules. This maybe due to the free mobile water that decreases with increasing concentration of these materials with the 100 mg/ml CO samples having T1 and T2 values characteristic of cartilage.

Sample	[g/L]	T1 (msec)	T2 (15 msec)	T2 (30 msec)
HA 6.25	6.25	2219±112	1144±26	1195±35
HA 12.5	12.5	2183±132	1008±22	1057±20
HA 25	25	2051±158	821±13	816±14
HA 50	50	1835±133	536±7	516±8
HA 100	100	1482±48	309±5	294±5
Sample				
GE 6.25	6.25	2332±126	1169±33	1247±26
GE 12.5	12.5	2305±195	1075±27	1146±15
GE 25	25	2177±218	976±17	980±15
GE 50	50	1751±84	607±24	584±27
GE 100	100	1122±49	264±9	249±12
Sample				
CO 6.25	12.5	2311±204	1079±20	1182±25
CO 12.5	25	2137±138	855±67	879±71
CO 25	50	2257±107	474±6	468±7
CO 50	100	1371±135	287±31	274±26
CO 100	200	760±279	77±10	76±10
Control				
Agar 0.5	5	2173±177	288±5	283±5
Agar 1	10	2033±105	162±3	157±4
Agar 2	20	1942±191	85±2	82±3
Agar 4	40	1646±78	44±3	44±6
Control				
Gd 0.125	0.12	1036 ± 30	661±15	708±10
Gd 0.25	0.23	634 ± 13	441±8	459±10
Gd 0.5	0.47	352 ± 7	260±4	268±6
Gd 1	0.94	189 ± 4	142±3	146±5
Gd 2	1.88	98 ± 3	76±3	78±4

[1] $T1_{PBS}$ value on this imaging day was 2,469±178.8

Table IX. T1 and T2 values for unsubstituted hyaluronan (HA), gelatin (GE) and HA/GE composite (CO) materials as well as agar (Agar) and gadolinium (Gd) controls. T1 and T2 values for the Agar and Gd controls are the same as in Table VII, but the concentrations have been converted to g/L.

The relationship between the T1 values and material concentration in **Table IX** is best illustrated graphically in **Fig 4.7** along with the calculated relaxivity values (R1) or slopes calculated using linear regression. For instance, Magnevist (Gd) has the highest impact on T1 using a small range of concentrations, as expected for an effective MRI contrast agent. It exhibits a linear relationship with an extremely high coefficient of correlation ($r^2 = 1$) **(Fig. 4.7 A)**. Agar also results in high linearity and coefficient of correlation **(Fig 4.7 B)**; however with a much lesser impact on T1 compared to the Magnevist. When the R1 of the unsubstituted HA, GE and CO materials are compared **(Fig 4.7 C)**, HA has the smallest R1 value; while GE and CO have similar R1, which may indicate that the collagen present in the GE and CO materials plays a more prominent role in their magnetic properties than HA.

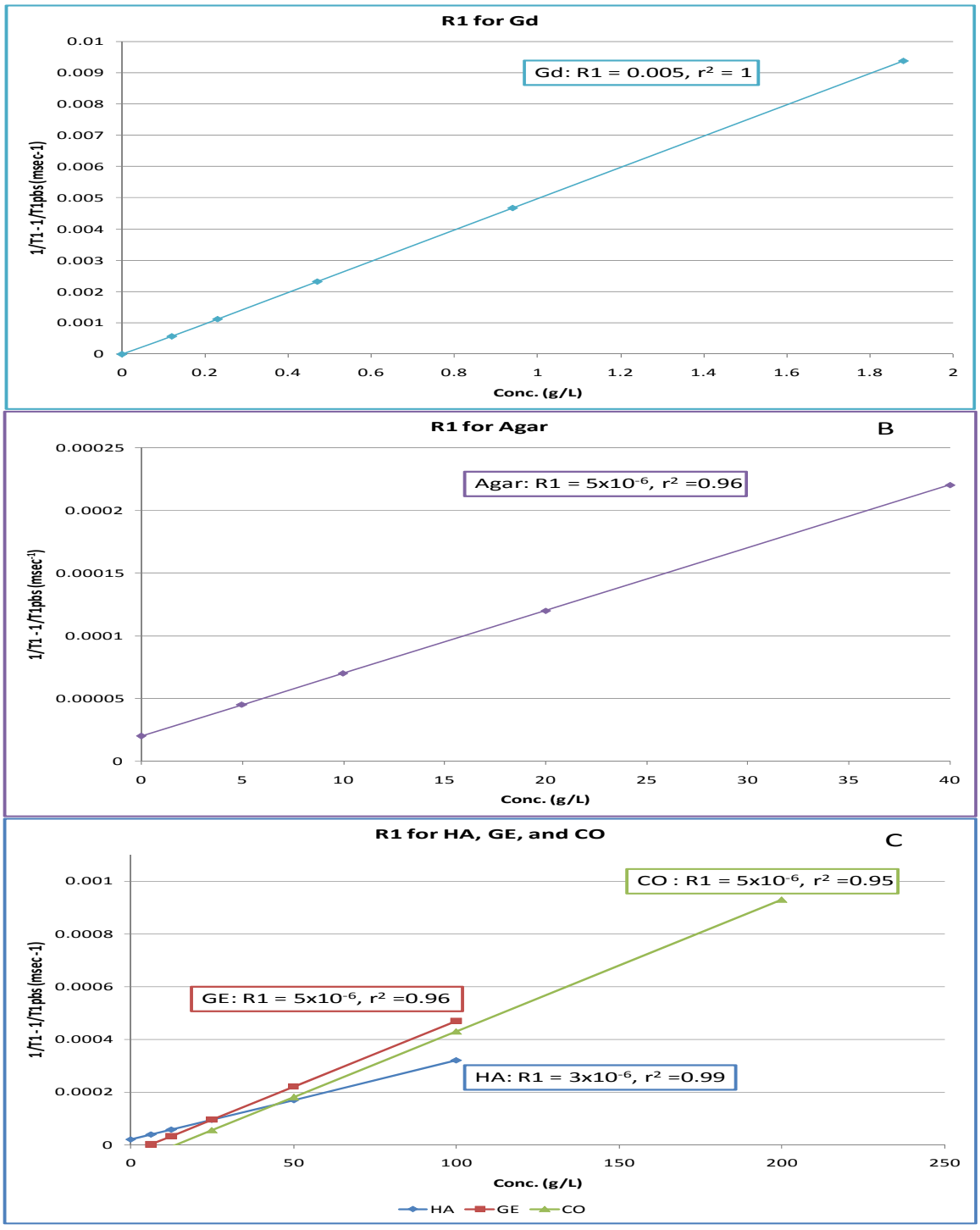

Figure 4.7. Relationship of T1 versus Concentration (g/L) for Unsubstituted Hyaluronan (HA), Gelatin (GE) and HA/GE Composite (CO) Materials as Well as Agar and Gadolinium (Gd) Controls. The relaxivity of T1 values (R1) and coefficients of correlation (r^2) for each relationship are provided (boxes). **A:** Linear relationship between Gd-DTPA^{-2} concentration and T1 values with a high coefficient of correlation ($r^2 = 1$). **B:** Linear relationship between Agar concentration and T1 values with a high coefficient of correlation ($r^2 = 0.96$). **C:** Linear relationship between HA, GE and CO material concentration and T1 values with a high coefficients of correlation ($r^2 > 0.95$). Note the differences in the y-axis scales.

When the T1 values of HA, GE, CO, Agar and Magnevist are plotted versus concentration together on the same scale, the significant effect of incremental increases in concentration on T1 produced by the Magnevist MRI contrast agent is clearly noticeable **(Fig 4.8)**. For ease of comparison, **Fig 4.8** includes a table of the calculated minimum concentration required for each material to generate a significant impact on T1. Since PBS produces the longest T1 value (2,469 msec), the concentration of each material was calculated assuming a T1 value of half the $T1_{pbs}$ value (1,234.5 msec) and using the linear relation between $1/T1 - 1/T1_{pbs}$ vs. concentration of the material represented by each of the plots in **Figs. 4.7** and **4.8**. As shown in the table in **Fig 4.8**, Magnevist (Gd) required a material concentration three orders of magnitude less than that required for the other material tested in order to reduce the T1 to half the $T1_{PBS}$. This is consistent with its role as an MRI contrast agent. Agar, GE, CO or HA all had values of the same order of magnitude with the HA value greater than the GE value greater than the CO value greater than the Agar value These results clearly show that the differences in magnetic properties represented by the various effects of each material on the relaxation time, T1, are commanded by the intrinsic properties of each material.

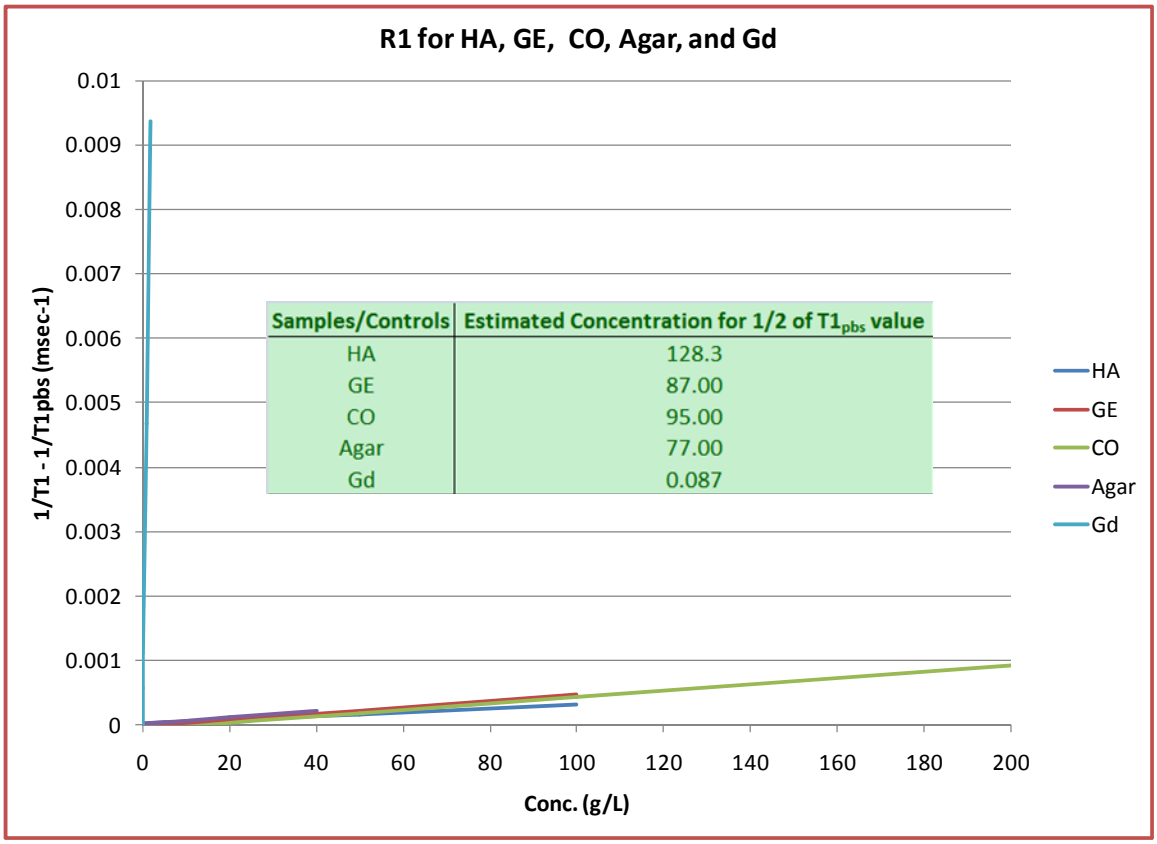

Figure 4.8. Comparison of Relaxivity of T1 Values (R1) for Unsubstituted Hyaluronan (HA), Gelatin (GE) and HA/GE Composite (CO) Materials as Well as Agar and Gadolinium (Gd) Controls Using the Same Y-Axis Scale. Gd (Gd-DTPA^{-2}), as a MR contrast agent, has the largest R1 value, and thus the highest impact on T1 with each incremental increase of its concentration. The HA, GE, CO and Agar materials all having similar R1 values, and thus similar impacts on T1 with each incremental increase of their concentrations. The inset table shows the calculated concentration of each material required to achieve half the T1 value of PBS. As a MR contrast agent, the concentration of Gd required is three orders of magnitude lower than the concentration of Agar, GE, CO or HA, which are all of the same order of magnitude with the HA value greater than the GE value greater than the CO value greater than the Agar value.

4.4.3. Relaxivity of T1 (R1) and Relaxivity of T2 (R2)

In order to determine whether or not the low tyramine substitution and di-tyramine cross-linking used in our chemistry had an effect on the imaging properties of the HA, GE and CO materials, the values for R1, R2 measured using echo spacing 15 msec, and R2 measured using echo spacing 30 msec were calculated for HA, GE, and CO unsubstituted, tyramine-substituted, and di-tyramine cross-linked.

Table X shows the R1 and R2 values obtained for unsubstituted HA, GE and CO materials. As described before, R1 or R2 is the slope of a best fit line relating T1 or T2, respectively, to the concentration of the materials. The results indicate that the unsubstituted GE had the highest R1 value, followed by unsubstituted CO, and then unsubstituted HA; while the unsubstituted CO material, a combination of HA and GE, had the highest R2 value, followed by unsubstituted GE, and then unsubstituted HA. The high coefficients of correlation ($r^2 > 0.95$) for the fits of unsubstituted HA, GE and CO materials are indicative of the high correlation between both T1 and T2 and material concentration.

Sample	R1	r^2	R2 (15 ms)	r^2	R2 (30 ms)	r^2
HA	0.0025	0.99	0.025	1	0.027	1
GE	0.0049	0.98	0.030	0.97	0.033	0.98
CO	0.0046	0.98	0.060	0.96	0.062	0.97

Table X. R1 and R2 (15 msec and 30 msec) values for unsubstituted hyaluronan (HA), gelatin (GE), and HA/GE composite (CO) materials.

To verify whether or not tyramine-substitution had an effect on the imaging properties of the HA, GE and CO materials, **Tables XI– XIII** and **Figs 4.9 – 4.11**, respectively, provide direct comparison of the relaxivities of unsubstituted and tyramine-substituted materials. For HA, the slope or R1 and R2 (15 and 30 msec echo spacing) values increased with tyramine-substitution of HA (TS-HA) **(Table XI** , **Fig 4.9)**. In the case of GE, tyramine-substitution decreased R1 and R2 (15 and 30 msec) values **(Table XII, Fig 4.10)**. This is presumably due to the fact that GE intrinsically gels in its unsubstituted form, and tyramine substitution disrupts this intrinsic gelling with an associated decrease in R1 and R2 values. Tyramine substitution also decreased R1 and R2 (15 and 30 msec) in the CO materials **(Table XIII, Fig 4.11)** presumably for a similar reason.

Another objective of this study was to determine whether the second step of our chemistry that involves di-tyramine cross-linking had any consequence to the imaging properties of the materials. Hence, **Tables XI - XIII** and **Figs 4.9 – 4.11** also include the R1 and R2 values of the cross-linked materials (TB-HA, TB-GE and TB-CO, respectively) for comparison to unsubstituted and tyramine-substituted materials. **Table XI** and **Fig 4.9** shows that the R1 and R2 values increase further upon cross-linking (TB-HA) of the TS-HA. These changes in relaxivity are actually more pronounced in the R2 values. **Table XII** and **Fig 4.10** demonstrate a recovery (increase) in R1 and R2 values for the GE material upon cross-linking (TB-GE) of the TS-GE as the loss in ability to intrinsically gel is partially overcome by the gelling caused by dityramine cross-linking; although it could not fully recover to that of the unsubstituted GE material. Also, high

coefficients of correlation (r^2 > 0.95) were obtained for the HA, GE and CO materials under the three conditions of unsubstituted, tyramine-substituted, and cross-linked, which is indicative of a high correlation between T1 and T2 and concentration of these materials. This was not the case for the post PBS equilibrated TB-GE material (r^2 = 0.65), which was not an unexpected result due to the inconsistency observed in the final concentrations observed for the TB-GE when equilibrated in PBS as described in **Chapter III**. The relaxivity values further decreased with cross-linking (TB-CO) of the TS-CO material as illustrated in **Table XIII** and **Fig 4.11**. Additionally, the CO, TS-CO and TB-CO materials at 100 mg/ml **(Appendix B)**, which all contain GAG and collagen concentrations found in cartilage, had T1 values in the ~700 to 1,000 msec range typical of cartilage **[50]**. Therefore, these biomaterials replicate both the mechanical and imaging properties of cartilage.

Sample	R1	r^2	R2 (15 ms)	r^2	R2 (30 ms)	r^2
HA	0.0025	0.99	0.025	1	0.027	1
TS-HA	0.0028	1	0.028	0.99	0.033	0.99
TB-HA	0.0031	1	0.039	0.98	0.049	0.97

Table XI. R1 and R2 (15 msec and 30 msec) values for unsubstituted hyaluronan (HA), tyramine-substituted hyaluronan (TS-HA), and cross-linked hyaluronan (TB-HA) materials.

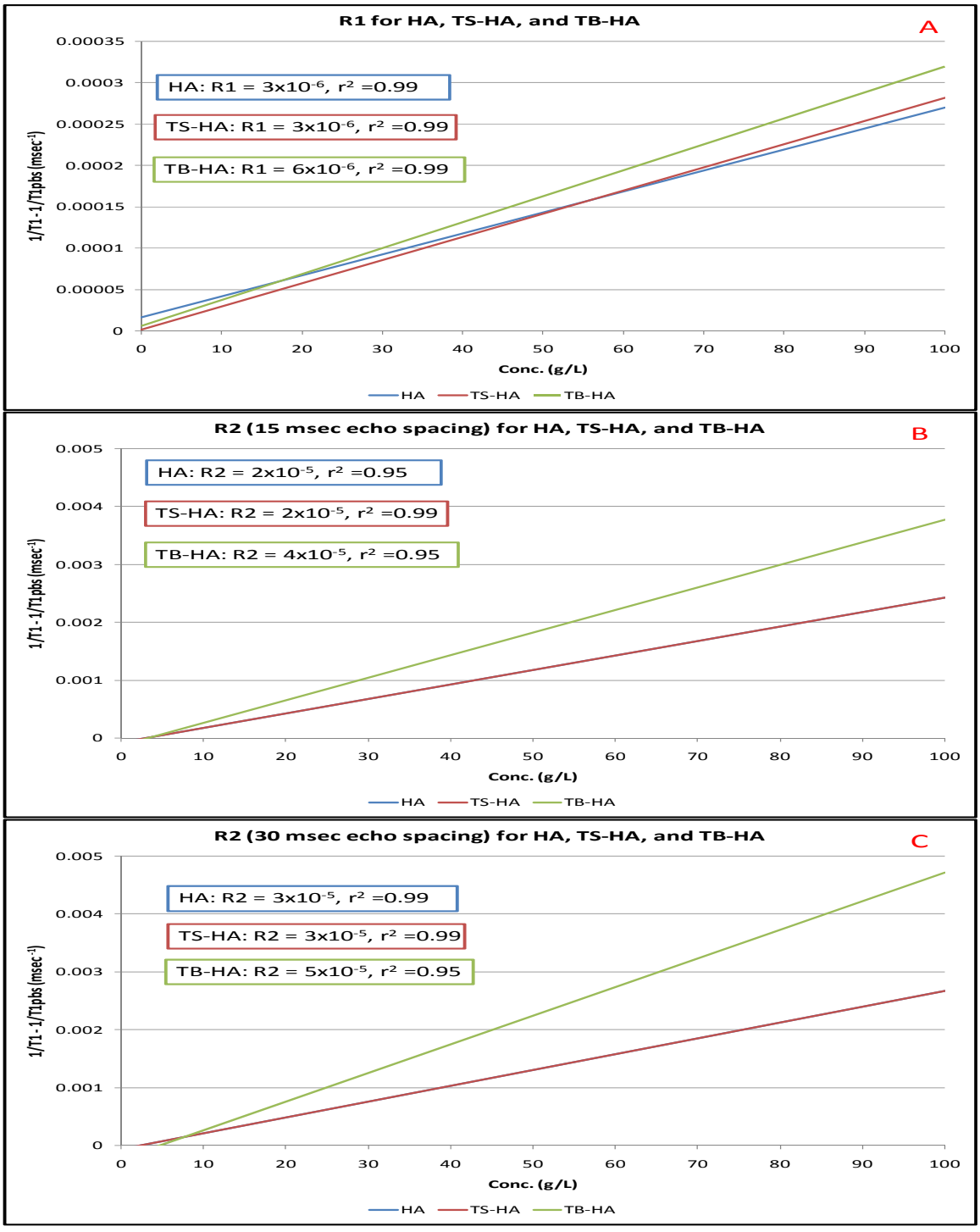

Figure 4.9. R1 (panel A), R2 at 15 msec (panel B) and R2 at 30 msec (panel C) Values for HA (blue), TS-HA (red), and TB-HA (yellow). In panel B and C, HA and TS-HA had similar slopes (R2 values); therefore, the TS-HA curves overlay the HA curves.

Sample	R1	r^2	R2 (15 ms)	r^2	R2 (30 ms)	r^2
GE	0.0049	0.98	0.030	0.97	0.033	0.98
TS-GE	0.0021	0.99	0.017	1	0.017	1
TB-GEw	0.0033	1	0.018	0.99	0.019	1
TB-GE	0.0024	0.65	0.018	0.97	0.018	0.97

Table XII. R1 and R2 (15 msec and 30 msec) for unsubstituted gelatin (GE), tyramine-tubstituted gelatin (TS-GE), and cross-linked gelatin in PBS (TB-GE) and water (TB-GEw) materials.

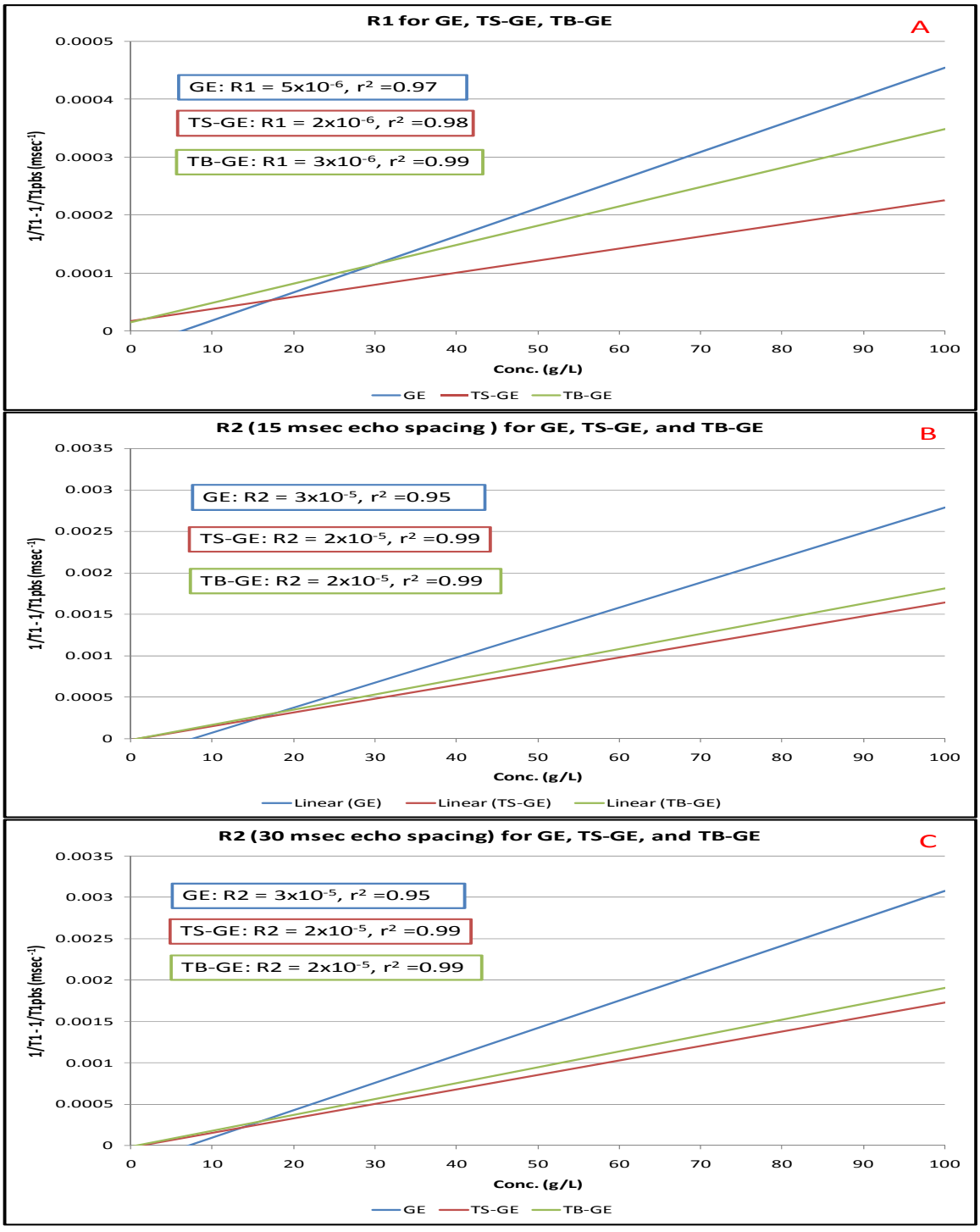

Figure 4.10. R1 (panel A), R2 at 15 msec (panel B) and R2 at 30 msec (panel C) Values for GE (blue), TS-GE (red), and TB-GE (yellow).

Sample	R1	r^2	R2 (15 ms)	r^2	R2 (30 ms)	r^2
CO	0.0046	0.98	0.060	0.96	0.062	0.97
TS-CO	0.0043	1	0.049	0.98	0.054	0.99
TB-CO	0.0031	0.99	0.030	0.97	0.034	0.97

Table XIII. R1 and R2 (15 msec and 30 msec) values for unsubstituted HA/GE composite (CO), tyramine-substituted HA/GE composite (TS-CO), and cross-linked HA/GE composite (TB-CO) materials.

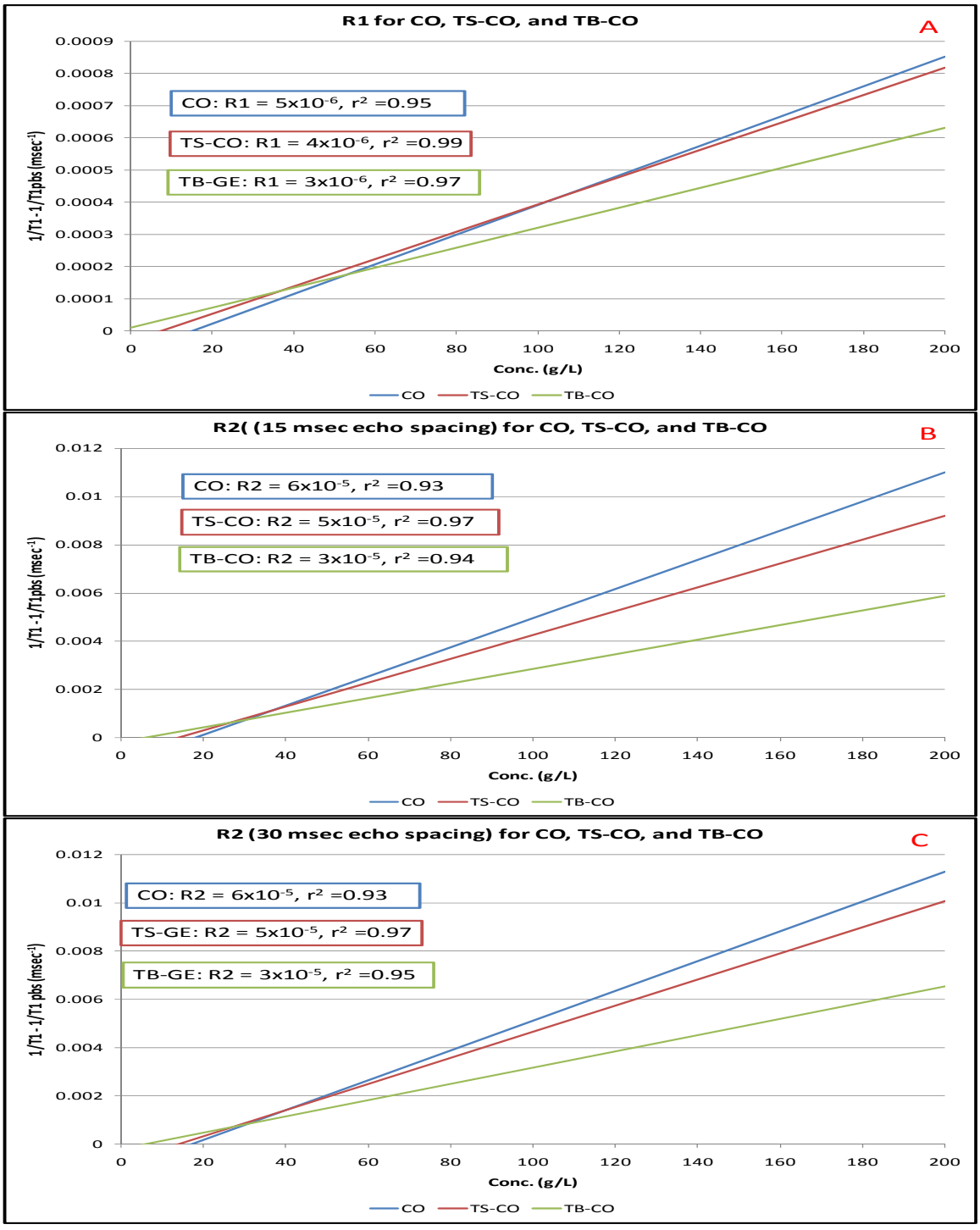

Figure 4.11. R1 (panel A), R2 at 15 msec (panel B) and R2 at 30 msec (panel C) Values for CO (blue), TS-CO (red), and TB-CO (yellow).

As mentioned before, the 3.0 T MR that we used to image the various materials was inconsistent from day to day. To illustrate this variability, the R1 and R2 (15 msec and 30 msec) values obtained from the acquired T1 and T2 values on the different days have been averaged for each material formulation and provided with their standard deviations in **Tables XIV – XVI**, respectively. This inconsistency was brought to the attention of Siemens Corporation, which is in the process of trying to identify the source of this issue.

R1							
Sample	May 14' 09	Agu 21' 09	Sep 13 '09	Oct 1' 09	Oct 7 '09	Average R1	SD (±)
HA	0.0025	0.0023	0.0031	0.0029	0.0025	0.0027	0.0003
TS-HA		0.0026	0.0035	0.0030	0.0028	0.0030	0.0004
TB-HA		0.0029	0.0037	0.0034	0.0031	0.0033	0.0003
GE	0.0023	0.0026	0.0027	0.0034	0.0049	0.0032	0.0010
TS-GE		0.0016	0.0024	0.0023	0.0021	0.0021	0.0004
TB-GE				0.0028	0.0024	0.0026	0.0003
TB-Gew		0.0020	0.0030	0.0034	0.0033	0.0029	0.0006
CO		0.0053	0.0056	0.0070	0.0092	0.0068	0.0018
TS-CO				0.0085	0.0085	0.0085	0.0000
TB-CO				0.0061	0.0062	0.0062	0.0001
Agar	0.018	0.016	0.029	0.021	0.046	0.026	0.012
Gd-DTPA^{-2}	4.92	5.23	5.82	5.31	5.31	5.32	0.32

Table XIV. Average of R1 values for all materials imaged on the different days.

R2 (15 msec echo spacing)							
Sample	May 14' 09	Agu 21' 09	Sep 13 '09	Oct 1' 09	Oct 7 '09	Average R2	SD (±)
HA	0.028	0.026	0.021	0.027	0.025	0.025	0.003
TS-HA		0.028	0.024	0.029	0.028	0.027	0.003
TB-HA		0.044	0.033	0.030	0.039	0.036	0.006
GE	0.016	0.020	0.016	0.018	0.030	0.020	0.006
TS-GE		0.014	0.016	0.016	0.017	0.016	0.001
TB-GE				0.016	0.018	0.017	0.001
TB-Gew		0.014	0.014	0.014	0.018	0.015	0.002
CO		0.093	0.089	0.103	0.121	0.101	0.014
TS-CO				0.098	0.099	0.099	0.000
TB-CO				0.062	0.061	0.062	0.001
Agar	6.23	5.93	5.26	6.62	5.50	5.91	0.55
Gd-DTPA^{-2}	5.49	5.84	6.62	6.09	6.22	6.05	0.42

Table XV. Average of R2 (15 msec echo spacing) values for all materials imaged on the different days.

R2 (30 msec echo spacing)							
Sample	**May 14' 09**	**Agu 21' 09**	**Sep 13 '09**	**Oct 1' 09**	**Oct 7 '09**	**Average R2**	**SD (±)**
HA	0.029	0.028	0.023	0.026	0.027	0.027	0.002
TS-HA		0.031	0.026	0.031	0.033	0.030	0.003
TB-HA		0.048	0.036	0.034	0.049	0.042	0.008
GE	0.015	0.020	0.016	0.019	0.033	0.021	0.007
TS-GE		0.014	0.016	0.017	0.017	0.016	0.002
TB-GE				0.016	0.018	0.017	0.002
TB-Gew		0.015	0.015	0.015	0.019	0.016	0.002
CO		0.095	0.090	0.105	0.124	0.104	0.015
TS-CO				0.100	0.108	0.104	0.006
TB-CO				0.053	0.067	0.060	0.010
Agar	6.06	6.25	5.27	6.62	5.52	5.94	0.55
Gd-DTPA^{-2}	5.14	5.78	6.53	6.19	6.09	5.95	0.53

Table XVI. Average of R2 (30 msec echo spacing) values for all materials imaged on the different days.

In summary, the outcome of this study suggests that both T1 and T2 were equally sensitive to incremental changes in both HA and collagen concentration. HA was expected to have a larger impact than collagen on T1. However, they showed a similar impact on T1. Collagen was expected to have a larger impact than HA on T2. Yet, GE and HA showed a comparable impact on T2. The greatest impact on both T1 and T2 was produced by the combination of HA and collagen or the composite (CO) materials. Molecular motion, size and interaction are factors affecting T1 and T2 relaxation times. It has been previously stated that slow, large, bound molecules have a long T1 and short T2; fast, small, free molecules have a long T1 and T2; and intermediate molecules have a short T1 and T2 (see **Chapter I**). Nonetheless, this study implies that this criterion is not always followed. It seems as if molecular interaction has the greatest effect on T1 and T2, regardless of the molecular size and motion. Tyramine substitution and di-tyramine cross-linking produced some effects on R1 and R2 compared to the unsubstituted materials. The relaxivity of HA slightly increased with tyramine-substitution and then again with cross-linking. By contrast for GE, the relaxivity decreased upon tyramine-substitution of GE, and then increased with subsequent cross-linking, as a result of first disruption of intrinsic gelation of the GE, and then synthetic gelation of the GE through formation of dityramine bridges during the HRP catalyzed cross-linking reaction.

Additionally, this study demonstrated the differences in magnetic properties of Magnevist (Gd), as an MRI contrast agent, compared to agar and the HA, GE and CO hydrogel biomaterials. Magnevist had the ability to generate a significant

effect on T1 with a concentration as small as 0.087 g/L compared to the other materials (HA, GE, CO and Agar), which required from 800 to 1,500 times the concentration of Magnevist to have a similar effect.

The T1 and T2 values decreased with increasing concentration of all materials. The T1 or T2 value differences between 6.25 and 12.5 mg/ml concentrations were about 30-90 msec. However, once the concentration reached 25, 50 and 100 mg/ml the T1 or T2 values dropped by 200-900 msec **(Appendix B)**. These substantial differences in the imaging properties between the low and high concentration materials correspond with the results seen in the mechanical testing data for these biomaterials. The aggregate modulus for the 6.25 and 12.5 mg/ml hydrogels is between 20-70 Kpa, while the 25, 50 and 100 mg/ml have modulus of 400-1,200 Kpa, as shown in **Table I**. Hence, a pronounced change in the mechanical properties of these materials is noticed when reaching the 25 mg/ml concentration, and this can also be observed through the imaging properties of these materials.

The T1 and T2 values of TB-hydrogels are much longer than those of native articular cartilage, thus they could be readily distinguished from the surrounding tissue. The composite materials at 100 mg/ml, which have T1 value in the ~ 700 to 1,000 msec range that is representative of cartilage **[50]**, could also be distinguished as its T2 values are higher than native articular cartilage (T2 of cartilage 20 – 40 msec) **[50]**. Lastly, this study has successfully applied MRI methods to a controlled system of synthetic ECM composed of TB-HA and TB-collagen molecules and evaluated their sensitivity and specificity for measuring

matrix composition. This work has provided a better understanding of the relationship between these MRI methods and tissue composition that can now be used to improve these MRI techniques for detection and measurement of GAG and collagen content in cartilage. Additionally, we now have the ability to detect, distinguish, and characterize the TB-hydrogels through MRI. We have identified the T1 and T2 values of TB-hydrogels at various concentrations, hence any *in vivo* changes in HA or collagen content in the materials can be easily detected through MRI. This is certainly a valuable tool that will allow evaluation of the performance of TB-hydrogels *in vivo* with time, which could not be achieved through histological procedures due to hydrogel dehydration, as explained in **Chapter II**.

CHAPTER V

GLYCOSAMINOGLYCAN (GAG) MEASUREMENT IN TYRAMINE-BASED HYDROGELS THROUGH DELAYED GADOLINIUM ENHANCED MRI OF CARTILAGE (dGEMRIC) TECHNIQUE

5.1 Introduction

The theory behind the dGEMRIC technique for measurement of GAG content in articular cartilage is based on a negatively charged contrast agent such as Gd-DTPA (Magnevist, Bayer Healthcare Pharmaceuticals, Park Ridge, NJ) distributing within cartilage inversely to the concentration of negatively charged GAG molecules **[52].** It is expected that this same charge-based imaging technique should also distinguish and quantify the GAG content in the TB-hydrogels. The equation used in this charge-based imaging technique to calculate the Gd-DTPA concentration in a sample, and hence the GAG index requires knowledge of the spin-lattice relaxivity (R1) of the contrast agent in the tissue or material being analyzed. The R1 for Gd-DTPA in intact cartilage and in solution have been previously determined at 8.45 T and shown to be independent of GAG concentration **[53].** Nevertheless, recent work by Stanisz

[52] has suggested that relaxivity is sensitive to macromolecular content at lower (e.g. clinical) field strengths. The objective of this investigation was to use the dGEMRIC technique to quantify GAG concentration in TB-hydrogels as well as to verify the dependency of Gd-DTPA relaxivity on the environmental macromolecular content using a defined-system of TB-hydrogels at lower field strengths.

5.2 Experimental Design

dGEMRIC uses T1 inversion recovery images measured before (pre) and after (post) equilibration in defined solutions of Gd-DTPA to compute the GAG index. The T1 inversion recovery sequences have already been described in **Chapter IV.** The MRI acquisition method was similar to that used clinically to probe the macromolecular composition of cartilage. Imaging of TB-HA at concentrations of 6.25, 12.5, 25, 50 and 100 mg/ml, TB-GE at concentrations of 60, 70, 80 and 90 mg/ml, and HA/GE composites of equal ratios (6.25:6.25, 12.5:12.5, 25:25, 50:50 and 100:100 HA to GE, respectively) were performed. The samples were all formulated in 1.5 ml cryotubes at 1 ml volumes, and the $T1_{pre\text{-}Gd}$ values of this series of samples measured. Then the samples placed in individual dialysis bags and equilibrated in one of three Gd-DTPA bath s in PBS of 0.5, 1 or 2 mM ($[Gd\text{-}DTPA]_{bath}$) for approximately 48 h while stirring at 4ºC. Once the samples reached equilibrium with the bath solution, the samples were removed from the dialysis bags, blotted dry, weighed, and subjected to another set of T1 measurements to obtain $T1_{post\text{-}Gd}$ values. The gadolinium concentration of each

sample after bath equilibration ($[Gd\text{-}DTPA]_{material}$) was then calculated using **Equation 5.1** and the measured $T1_{pre\text{-}Gd}$, and $T1_{post\text{-}Gd}$ values and the R1 for Gd-DTPA in each material determined through a separate series of experiments described below. A theoretical GAG concentration for each sample was calculated using **Equation 5.2**, and the $[Gd\text{-}DTPA]_{bath}$ and $[Gd\text{-}DTPA]_{material}$ values. A comparison of R1 among the samples was made, and a comparison of the actual and theoretical GAG concentrations for each sample was performed.

5.3 Materials and Methods

5.3.1 Samples Preparation and Gd-DTPA Equilibration

The materials and methods for the synthesis of TS-HA, TS-GE and TS-CO samples, and their formation into TB-hydrogels are described in **Appendix A**. After post cross-linking equilibration of the materials in PBS, the TB-hydrogels were arranged in a rack to form a grid composed of 3 groups of 14 samples (5 TB-HA only, 4 TB-GE only, and 5 HA/GE composites) plus 5 Gd-DPTA and 3 PBS controls for a total of 45 samples **(Fig 5.1)** with each group representing one of the three Gd-DTPA bath concentrations to be used (A = 2 mM, B = 1 mM and C = 0.5 mM).

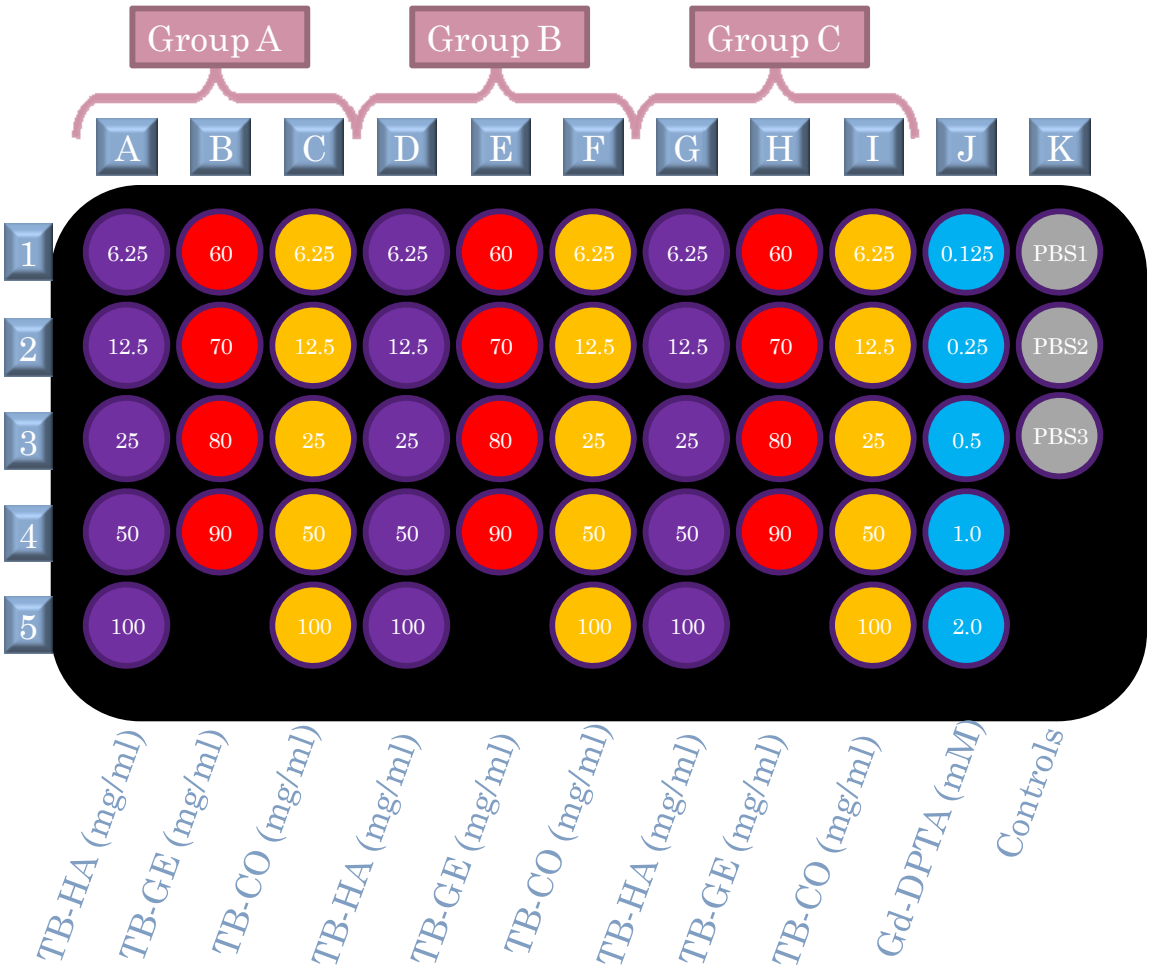

Figure 5.1. Grid of Samples Imaged for dGEMRIC. In the grid, columns A, D and G contain the cross-linked hyaluronan (TB-HA) samples, columns B, E and H contain the cross-linked gelatin (TB-GE) samples, and columns C, F and I contain the cross-linked HA/GE composite (TB-CO) samples arranged into three replicate groups (A, B and C). Five Gd-DPTA (column J), and three PBS (column K) samples were also included as internal controls. All samples were at the initial concentrations indicated.

Two liters of Gd-DTPA bath in PBS at concentrations of 0.5, 1 and 2 mM were made from a stock solution of Gd-DTPA (Magnevisit, Bayer Healthcare Pharmaceuticals, Park Ridge, NJ) at 522.495 mM, and cooled to 4°C. Each cross-linked hydrogel was removed from its container and transferred to a 4 cm long piece of dialysis membrane tubing of MWCO = 6-8,000 daltons, 3.3 ml/cm of volume/length, and 32 mm diameter (Spectrum Laboratories, Inc) as shown in **Figure 5.2**. Next, each sample group (A, B and C in **Figure 5.1**) was immersed in its corresponding Gd-DTPA bath (2, 1 and 0.5 mM, respectively). Equilibration occurred with constant mixing at 4°C over 48h.

Figure 5.2. TB-Hydrogel Plug in Dialysis Tubing Prior to Gd-DTPA^{-2} Bath Equilibration.

To corroborate that the samples reached equilibrium in the 3 different Gd baths (0.5, 1 and 2 mM), the $[Gd\text{-}DTPA]_{bath}$ values were plotted versus the pre- and post-Gd T1 values to confirm a linear relationship with the slope or R1 of Gd-DTPA for each sample **(Figure 5.3)**.

5.3.2 Measurement of Gadolinium (Gd) Concentration using Inductively Coupled Plasma – Mass Spectroscopy (ICP-MS)

To calculate the R1 for the Gd-DTPA for each sample the equilibrium concentration of Gd-DTPA in the biopolymers ($[Gd\text{-}DTPA]_{material}$) must be determined. Therefore, once the samples were imaged for the second time or after equilibration in the Gd baths, an aliquot of 200 µl out of the 1 ml volume of the samples was sent to the Trace Element Research Laboratory at Ohio State University for ICP-MS analysis.

A Perkin Elmer Optima 3000DV Inductively Coupled Optical Emission Spectrometer was used with the following settings: power: 1300w, plasma gas: 15 L/min, auxillary gas: 0.5 L/min, nebulizer gas: 0.6 L/min, sample uptake: 0.5 ml/min pumped via peristaltic pump.

Sample preparation:

The samples were treated by adding 0.2 ml concentrated Certified ACS+ nitric acid to each 0.2 ml sample (as submitted to TERL) and allowed to sit undisturbed for ~40 h. The samples were then quantitatively transferred to 8 ml LDPE bottles (bottles were rinsed 3x with deionized water before use) and diluted to 5 ml total

with deionized water (Millipore Milli-Q deionizer). The samples were 4% v/v nitric acid after the dilution.

All sample and standard preparation performed in a HEPA filtered class 10 laminar flow exhausting hood. Calibration standards were made by diluting a 1000 ug/ml (ppm) Gd standard stock solution purchased from Inorganic Ventures (IVStandards.com) via serial dilutions to the intended concentration. The standards were all prepared in 4% v/v Certified ACS+ nitric acid to match the 25x diluted samples. A calibration blank of 4% v/v Certified ACS+ nitric acid in deionized water was used.

5.3.3 Pre and Post Gd-DTPA MRI Measurements

For each sample, or series of samples, the T1 was mapped twice, first before equilibration with Gd-DTPA ($T1_{pre\text{-}Gd}$) and then after equilibration with Gd-DTPA ($T1_{post\text{-}Gd}$). An inversion recovery fast (turbo) spin echo sequence was used to measure T1 with TR = 6000 msec; TI = 23 msec, 75 msec, 150 msec, 300 msec, 750 msec, 1,400 msec, 2,000 msec and 2,800 msec; TE = 10 msec; FOV = 270 x 130 mm; slice thickness = 1.9 mm; matrix = 256 x 128. As described in **Chapter IV**, the eight images were curve-fit to generate T1 maps using a three-parameter exponential fit $SI = M_0 (1–2Ae–TI/T1 + e–TR/T1)$ with MRIMapper (MIT, Cambridge, MA) and MATLAB (MathWorks, Natick, MA) **[47].** The regions of interests (ROI) to be mapped were selected as 4x4 set of pixels from the center of each hydrogel sample. The calculated $T1_{pre\text{-}Gd}$ and $T1_{post\text{-}Gd}$ values were

an average of the pixels from the ROI from each sample. The color-coded T1 maps were displayed superimposed on the TI = 23 msec image.

5.3.4 Fixed Charge Density (FCD) and Glycosaminoglycan (GAG) content Computation

As described below in **Results and Discussion**, the $[\text{Gd-DTPA}]_{material}$ values obtained using ICP-MS were not reliable. Therefore, in order to determine the $[\text{Gd-DTPA}]_{material}$ values necessary to calculate the matrix fixed charge density (FCD) per **Equation 5.2**, we used **Equation 5.1**. In addition to the $T1_{pre\text{-}Gd}$ and $T1_{post\text{-}Gd}$ values acquired as described above, **Equation 5.1** requires determination of the R1 value for Gd-DTPA in the materials composition of interest. Therefore, T1 values were obtained for HA and GE samples at concentrations of 100 mg/ml containing Gd-DTPA at concentrations of 0.125, 0.25, 0.5, 1 and 2 mM. These T1 values were then used to calculate the R1 for Gd in the HA and GE at 100 mg/ml as previously described in **Chapter 4**. These R1 values together with the $T1_{pre\text{-}Gd}$ and $T1_{post\text{-}Gd}$ values were then used to calculate the Gd concentration inside the 100 mg/ml samples ($\text{Gd-DTPA}_{material}$) through **Equation 5.1**, the derivation of which was explained in **Chapter I**.

Equation 5.1:

$$[\text{Gd-DTPA}]_{material} = \frac{1}{R1}\left[\frac{1}{T_{1post\text{-}Gd}} - \frac{1}{T_{1pre\text{-}Gd}}\right]$$

Once the $[Gd\text{-}DTPA]_{material}$ values had been calculated through **Equation 5.1**, they were used to calculate the fixed charge density (FCD) for each sample using the "quasi-theoretical" model **Equation 5.2** the derivation of which is also explained in **Chapter I [54]**.

Equation 5.2:

$$FCD = [Na^{+}]_{bath} \left\{ \left[\frac{[Gd\text{-}DTPA]_{material}}{[Gd\text{-}DTPA]_{bath}} \right]^{1/2} - \left[\frac{[Gd\text{-}DTPA]_{bath}}{[Gd\text{-}DTPA]_{material}} \right]^{1/2} \right\}$$

After the FCD were calculated, they were converted to a theoretical GAG concentration by assuming a molecular weight of 400 g/mole, the molecular weight of the HA disaccharide, and also similar to those of the chondroitin sulfate disaccharide in cartilage.

5.4 Results and Discussion

The $T1_{pre\text{-}Gd}$ and $T1_{post\text{-}Gd}$ values as $1/T1_{pre} - 1/T1_{post}$ for all of the samples imaged in Figure 5.1 is shown in **Table XVII**. Plots of $T1_{pre\text{-}Gd}$ and $T1_{post\text{-}Gd}$ values versus Gd-DTPA bath concentration verified that the TB-HA, TB-GE and TB-CO had reached equilibrium by virtue of a linear relationship with coefficients of correlation >0.9 as shown in **Figs 5.3 – 5.5**.

TB-HA (mg/ml)					
	100	50	25	12.5	6.25
Gd(M)	1/T1pre - 1/T1post	1/T1pre - 1/T1post	1/T1pre - 1/T1post	1/T1pre - 1/T1post	1/T1pre - 1/T1post
0.002	0.0051	0.0042	0.0068	0.0083	0.0100
0.001	0.0021	0.0035	0.0042	0.0046	0.0050
0.0005	0.0011	0.0013	0.0024	0.0026	0.0027
TB-CO (mg/ml)					
	100	50	25	12.5	6.25
Gd(M)	1/T1pre - 1/T1post	1/T1pre - 1/T1post	1/T1pre - 1/T1post	1/T1pre - 1/T1post	1/T1pre - 1/T1post
0.002	0.0038	0.0076	0.0081	0.0093	0.0098
0.001	0.0027	0.0043	0.0038	0.0050	0.0052
0.0005	0.0014	0.0022	0.0021	0.0026	0.0028
TB-GE (mg/ml)					
	90	80	70	60	
Gd(M)	1/T1pre - 1/T1post	1/T1pre - 1/T1post	1/T1pre - 1/T1post	1/T1pre - 1/T1post	
0.002	0.0138	0.0143	0.0143	0.0117	
0.001	0.0068	0.0078	0.0078	0.0070	
0.0005	0.0038	0.0045	0.0041	0.0047	

Table XVII. The $T1_{pre\text{-}Gd}$ and $T1_{post\text{-}Gd}$ values as $1/T1_{pre} - 1/T1_{post}$ for each Gd-DTPA Bath Concentration (0.5, 1 and 2 mM) for TB-HA, TB-GE and TB-CO samples described in Figure 5.1.

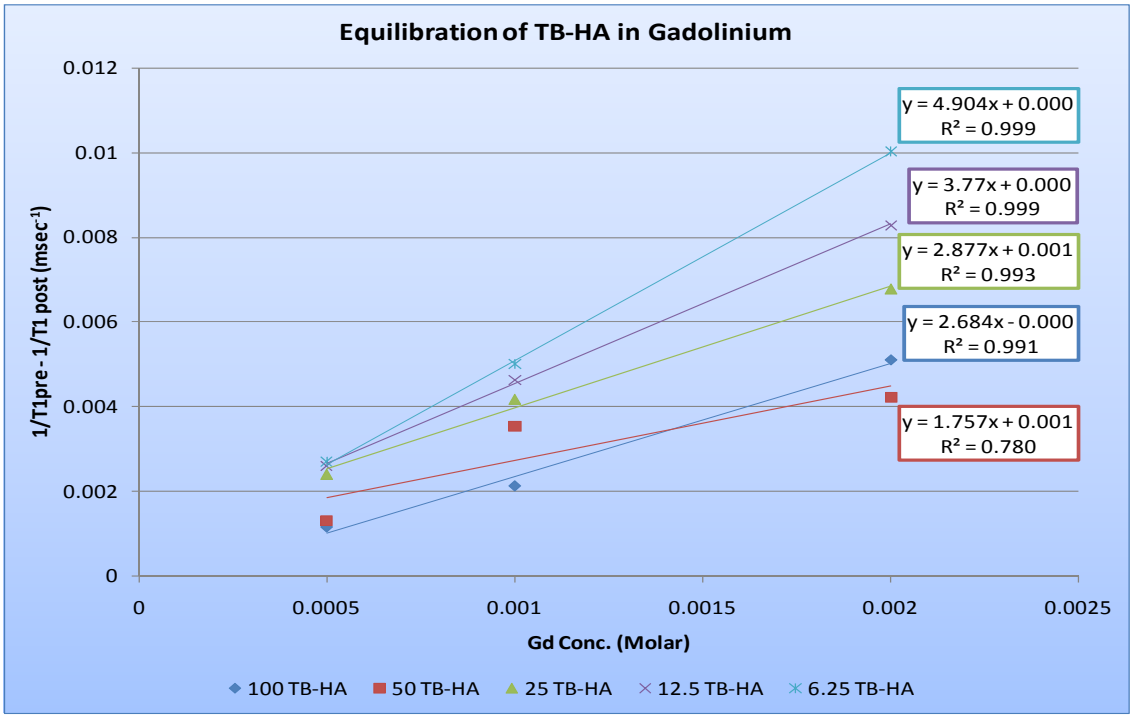

Figure 5.3. TB-HA Samples Equilibrated in Gd-DTPA Baths. $T1_{pre\text{-}Gd}$ and $T1_{post\text{-}Gd}$ values as $1/T1_{pre} - 1/T1_{post}$ plotted versus the Gd-DTPA bath concentrations (0.5, 1 and 2 mM) for TB-HA concentrations of 6.25, 12.5, 25, 50 and 100 mg/ml.

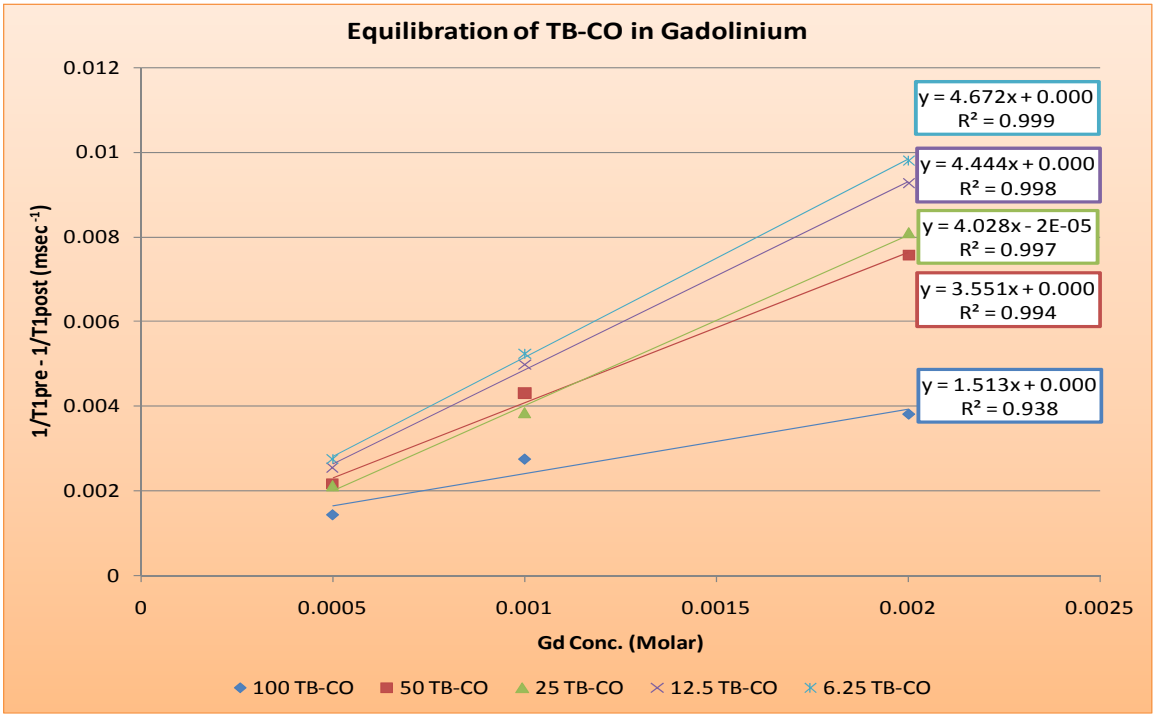

Figure 5.4. TB-CO Samples Equilibrated in Gd-DTPA. $T1_{pre\text{-}Gd}$ and $T1_{post\text{-}Gd}$ values as $1/T1_{pre} - 1/T1_{post}$ plotted versus the Gd-DTPA bath concentrations (0.5, 1 and 2 mM) for TB-CO concentrations of 6.25, 12.5, 25, 50 and 100 mg/ml.

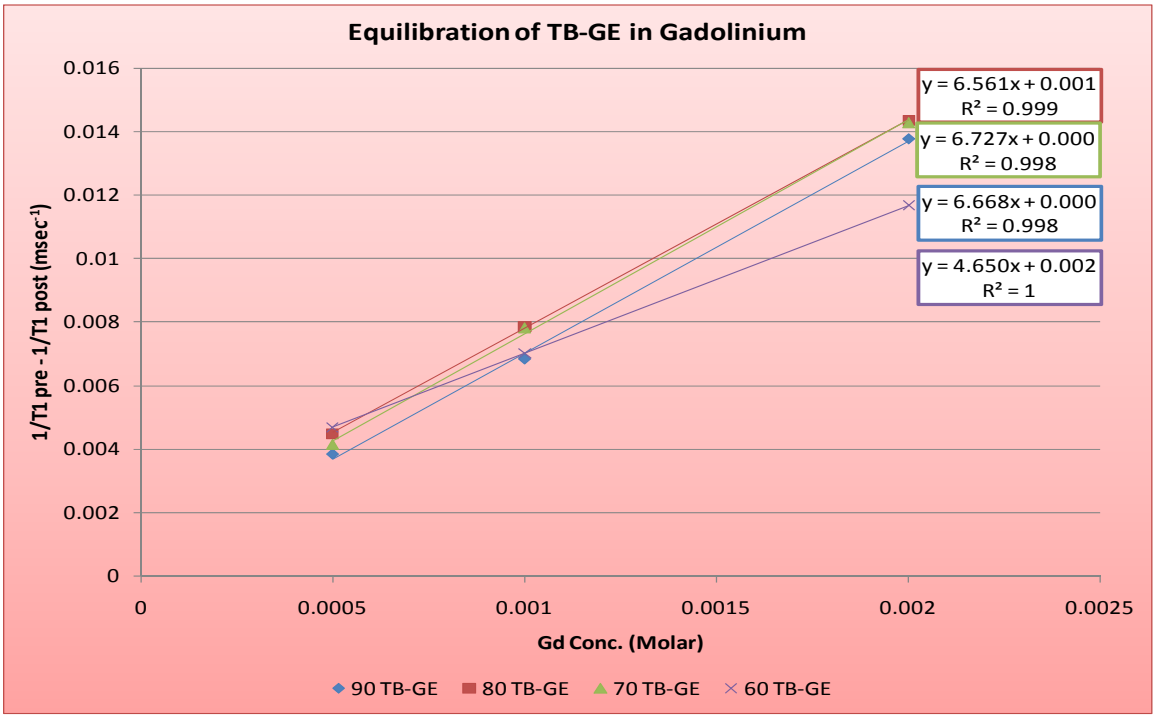

Figure 5.5. TB-GE Samples Equilibrated in Gd-DTPA. $T1_{pre\text{-}Gd}$ and $T1_{post\text{-}Gd}$ values as $1/T1_{pre} - 1/T1_{post}$ plotted versus the Gd-DTPA bath concentrations (0.5, 1 and 2 mM) for TB-GE concentrations of 60, 70, 80 and 90 mg/ml.

Gd-DTPA is negatively charge distributing into areas in cartilage that are depleted of GAG at a higher concentration than in areas of high GAG content. As expected, the Gd-DTPA did the same for our materials and distribute in high concentrations in the hydrogels with low GAG content and in low concentration in the hydrogel high GAG content. Gd-DTPA has a concentration-dependent effect on the MR parameter T1, thus T1 images in the presence of this contrast agent reflect the GD-DTPA concentration, and hence GAG concentration. The T1 map pre-Gd and post-Gd clearly shows the shortening of T1 in the presence of Gd-DTPA **(Fig 5.6).**

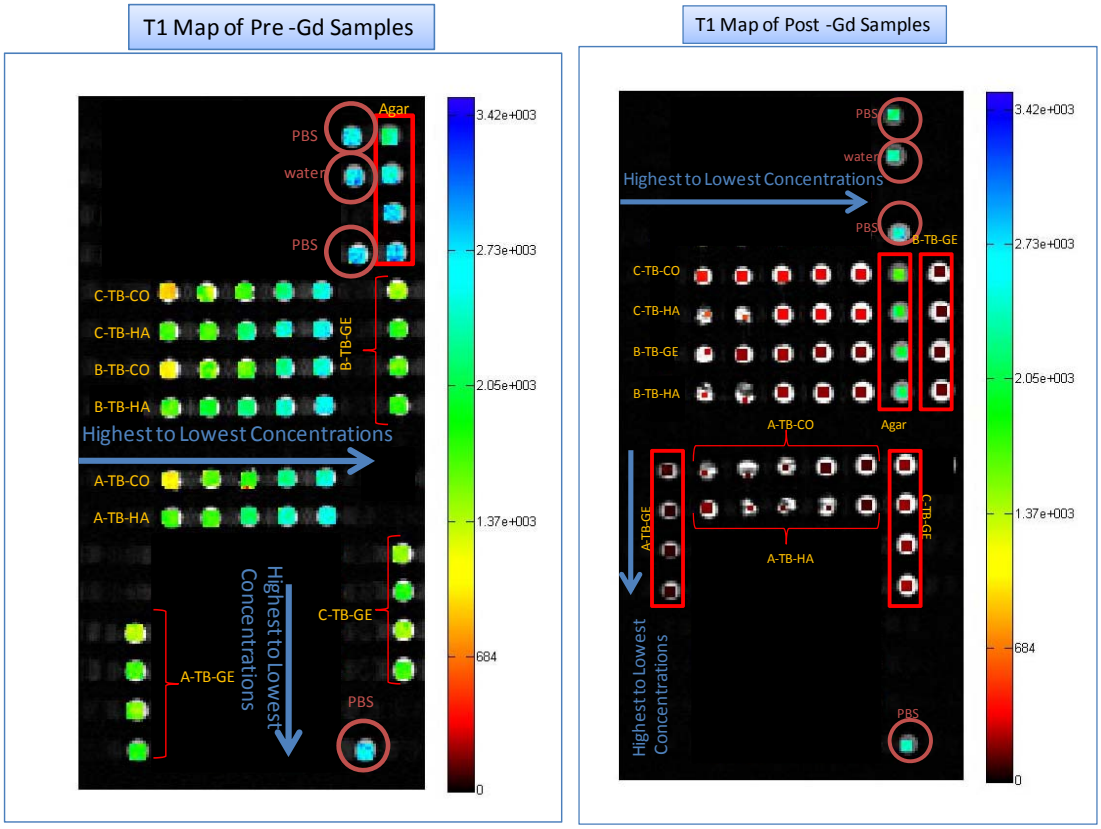

Figure 5.6. Pre and Post Gd-DTPA T1 maps of TB-HA, TB-GE and TB-CO. A, B, and C indicates the Gd-DTPA bath concentration in which the samples were equilibrated, which were 2, 1, and 0.5 mM, respectively. **Left:** T1 map before Gd equilibration showing the TB-HA and TB-CO samples within a T1 map range of 684 up to 2730 msec; while the TB-GE samples remained in the lower range of 684 to 2050 msec. Right: T1 map after Gd equilibration showing a shortening of T1 to low range of 0 to 360 approximately. The controls behaved as expected as both Agar and water were in the higher T1 range. Also, the inhomogeneity observed in the post-Gd T1 map for some of the samples is due to the samples breaking in the process of transferring them back to the cryotubes.

A = Gd at 2mM					B = Gd at 1mM					C = Gd at 0.5 mM				
Sample	Pre [mg/ml]	T1pre	Post (mg/ml)	T1post	Sample	Pre [mg/ml]	T1pre	Post (mg/ml)	T1post	Sample	Pre [mg/ml]	T1pre	Post (mg/ml)	T1post
TB-HA 6.25	6.3	2524	4.5	96	TB-HA 6.25	6.3	2607	4.1	186	TB-HA 6.25	6.3	2556	3.5	324
TB-HA 12.5	12.5	2358	10.4	115	TB-HA 12.5	12.6	2416	9.0	199	TB-HA 12.5	12.4	2416	7.9	333
TB-HA 25	25	2143	24.7	138	TB-HA 25	25.6	2176	20.7	216	TB-HA 25	25.3	2168	20.0	350
TB-HA 50	50	1701	47.3	208	TB-HA 50	50	1963	47.5	247	TB-HA 50	50	1674	41.6	523
TB-HA 100	100	1709	68.8	176	TB-HA 100	100	1665	78.6	368	TB-HA 100	100	1655	82.8	572
Sample	Pre [mg/ml]	T1pre	Post (mg/ml)	T1post	Sample	Pre [mg/ml]	T1pre	Post (mg/ml)	T1post	Sample	Pre [mg/ml]	T1pre	Post (mg/ml)	T1post
TB- GE 60	61	1862	69.1	82	TB- GE 60	61	1774	71.1	132	TB- GE 60	61	1717	62.4	190
TB-GE 70	71	1553	87.9	67	TB-GE 70	71	1675	73.7	119	TB-GE 70	71	1470	69.4	208
TB-GE 80	79	1711	90.5	67	TB-GE 80	79	1795	88.7	119	TB-GE 80	79	1841	83.3	199
TB-GE 90	91	1360	102.6	69	TB-GE 90	91	1432	87.1	133	TB-GE 90	91	1465	84.0	222
Sample	Pre [mg/ml]	T1pre	Post (mg/ml)	T1post	Sample	Pre [mg/ml]	T1pre	Post (mg/ml)	T1post	Sample	Pre [mg/ml]	T1pre	Post (mg/ml)	T1post
TB- CO 6.25	6.2	2437	4.3	98	TB- CO 6.25	6.4	2451	3.8	177	TB- CO 6.25	6.2	2507	3.7	317
TB-CO 12.5	12.3	2255	9.2	103	TB-CO 12.5	12.5	2259	9.0	184	TB-CO 12.5	12.1	2233	8.6	333
TB-CO 25	25.9	1665	26.9	115	TB-CO 25	26	1647	26.1	225	TB-CO 25	26	1706	23.9	371
TB-CO 50	50	1570	42.3	122	TB-CO 50	50	1601	37.5	203	TB-CO 50	50	1520	36.9	355
TB-CO 100	100	1076	80.9	211	TB-CO 100	100	1089	64.9	273	TB-CO 100	100	943	57.0	402

Table XVIII. Pre-Gd and post-Gd T1 values and initial and final concentrations for all the samples that were imaged.

The T1 pre and post–Gd values for each sample examined in this research are shown in **Table XVIII.** The above table demonstrates how the T1 post-Gd dramatically dropped compared to the T1 pre-Gd. Also, as expected, the T1 post-Gd became shorter as the concentration of the Gd-DTPA$_{bath}$ increased since the higher the concentration of the negatively charged Gd-DTPA, the greater are the repulsion forces of negatively charged GAG, causing the drop in T1. Furthermore, the pre and post-Gd concentration of the materials were included in this table in order to account for the fact that most of the samples experienced either shrinking or swelling, which would therefore change their concentrations.

ICP-MS measured Gd concentration values lower than the known Gd concentrations in the materials as demonstrated for the samples at 100 mg/ml HA or GE made in Gd at 0.125, 0.25, 0.5,1, 2 mM **(Table XIX)**. Then, it measured Gd concentration values higher for the Gd-DTPA concentration curve of 0.125, 0.25, 0.5, 1, 2 mM and for the 3 Gd bath concentrations of 0.5, 1, and 2mM **(Table XX)**. The Gd concentrations in the TB-HA, TB-GE, and TB-CO samples measured by ICP-MS are included in **Table XXI.** This study found ICP measurements of Gd-DTPA differed about 50% from the known concentrations.

Sample	[mM]	[Gd]material (mM)	Sample	[mM]	[Gd]material (mM)
100 HA+Gd 0.125	0.125	< 0.01	100 GE+Gd 0.125	0.125	< 0.01
100 HA+Gd 0.25	0.25	0.12	100 GE+Gd 0.25	0.25	0.13
100 HA+Gd 0.5	0.5	0.23	100 GE+Gd 0.5	0.5	0.31
100 HA+Gd 0.1	1	0.62	100 GE+Gd 0.1	1	0.66
100 HA+Gd 2	2	1.23	100 GE+Gd 2	2	1.28

Table XIX. Results of $[Gd]_{material}$ concentration measured by ICP-MS in 100 mg/ml HA and GE made in different concentrations of Gd-DTPA. The $T1_{pbs}$ value on this imaging day was 2,730.2 ± 188.4.

Sample	[mM]	[Gd]material (mM)	Sample	[mM]	[Gd]material (mM)
Gd 0.125	0.125	0.30	Gd 0.5	0.5	1.03
Gd 0.25	0.25	0.53	Gd 1	1	1.94
Gd 0.5	0.5	0.93	Gd 2	2	4.78
Gd 1	1	1.99			
Gd 2	2	2.73			

Table XX. Results of $[Gd]_{material}$ concentration measured by ICP-MS in Gd-DTPA at 0.125, 0.25, 0.5, 1, and 2 mM, and in the Gd-DTPA bath concentrations at 05, 1, and 2 mM. The $T1_{pbs}$ value on this imaging day was 2,730.2 ± 188.4.

A = Gd at 2mM			B = Gd at 1mM			C = Gd at 0.5 mM		
Sample	[mg/ml]	[Gd]material (mM)	Sample	[mg/ml]	[Gd]material (mM)	Sample	[mg/ml]	[Gd]material (mM)
TB-HA 6.25	6.3	1.39	TB-HA 6.25	6.3	0.64	TB-HA 6.25	6.3	0.32
TB-HA 12.5	12.5	1.18	TB-HA 12.5	12.6	0.56	TB-HA 12.5	12.4	0.29
TB-HA 25	25	0.83	TB-HA 25	25.6	0.52	TB-HA 25	25.3	0.27
TB-HA 50	50	0.59	TB-HA 50	50	0.37	TB-HA 50	50	0.13
TB-HA 100	100	0.94	TB-HA 100	100	0.27	TB-HA 100	100	0.13
Sample	[mg/ml]	[Gd]material (mM)	Sample	[mg/ml]	[Gd]material (mM)	Sample	[mg/ml]	[Gd]material (mM)
TB- GE 60	61	1.48	TB- GE 60	61	0.82	TB- GE 60	61	0.38
TB-GE 70	71	1.44	TB-GE 70	71	0.79	TB-GE 70	71	0.40
TB-GE 80	79	1.53	TB-GE 80	79	0.82	TB-GE 80	79	0.40
TB-GE 90	91	1.45	TB-GE 90	91	0.69	TB-GE 90	91	0.41
Sample	[mg/ml]	[Gd]material (mM)	Sample	[mg/ml]	[Gd]material (mM)	Sample	[mg/ml]	[Gd]material (mM)
TB- CO 6.25	6.2	1.30	TB- CO 6.25	6.4	0.67	TB- CO 6.25	6.2	0.34
TB-CO 12.5	12.3	1.24	TB-CO 12.5	12.5	0.58	TB-CO 12.5	12.1	0.30
TB-CO 25	25.9	0.91	TB-CO 25	26	0.41	TB-CO 25	26	0.25
TB-CO 50	50	0.89	TB-CO 50	50	0.42	TB-CO 50	50	0.23
TB-CO 100	100	0.43	TB-CO 100	100	0.28	TB-CO 100	100	0.15

Table XXI. Results of $[Gd]_{material}$ concentration measured by ICP-MS in TB-HA, TB-GE, and TB-CO. The $T1_{pbs}$ value on this imaging day was 2,730.2 ± 188.4. The T1 value of Gd at 2 mM was 91 ± 5, at 1 mM was 174 ± 15, and at 0.5 mM was 335 ± 8.

Moreover, the $[Gd]_{material}$ values obtained by ICP-MS were used to calculate FCD and convert it into GAG concentration, and as expected the values did not match those of the original concentrations in the materials, as exemplified in **Table XXII** for the TB-HA and TB-CO that were immersed in the 2 mM Gd-DTPA bath.

Next, the T1 values obtained from imaging the samples of 100 mg/ml HA or GE made in Gd at 0.125, 0.25. 0.5,1, 2 mM, and the R1 of Gd-DTPA calculations are included in **Table XXIII**. This table also includes the results for the Gd-DTPA control curve. The R1 (7.02 $mM^{-1}s^{-1}$) of Gd-DTPA in 100 mg/ml HA and the R1 of Gd-DTPA in 100 mg/ml GE (6.57$mM^{-1}s^{-1}$) was then used to calculate the Gd concentration in the material $[Gd]_{material}$ **(Table XXIV)**, followed by the FCD and GAG index computation **(Table XXIV)**.

A = Gd at 2mM					
Sample	**Intial [mg/ml]**	**Final (mg/ml)**	**[Gd]material (M)**	**FCD(mol/L)**	**[GAG](mg/ml)**
TB-HA 6.25	6.3	4.5	0.0014	-0.056	22.33
TB-HA 12.5	12.5	10.4	0.0012	-0.082	32.91
TB-HA 25	25	24.7	0.0008	-0.139	55.58
TB-HA 50	50	47.3	0.0006	-0.199	79.73
TB-HA 100	100	68.8	0.0009	-0.118	47.39
Sample	**Initial [mg/ml]**	**Final (mg/ml)**	**[Gd]material (mM)**	**FCD(mol/L)**	**[Asp , Glut](mg/ml)**
TB- CO 6.25	6.2	4.3	0.0013	-0.067	26.93
TB-CO 12.5	12.3	9.2	0.0012	-0.075	29.85
TB-CO 25	25.9	26.9	0.0009	-0.125	50.00
TB-CO 50	50	42.3	0.0009	-0.129	51.56
TB-CO 100	100	80.9	0.0004	-0.262	104.67

Table XXII. Fixed charge density (FCD) and glycosaminoglycans (GAG) calculations based on the $[Gd]_{material}$ concentration measured by ICP-MS.

Sample[1]	**[mM]**	**T1**	**1/T1- 1/T1HA**	**R1**	**Sample**	**[mM]**	**T1**	**1/T1- 1/T1PBS**	**R1**
100 HA[2]+Gd 0.125	0.125	658 ± 23	0.0009	7.02	Gd 0.125	0.125	910 ± 26	0.0007	5.23
100 HA+Gd 0.25	0.25	409 ± 7	0.0018	$r^2 = 1$	Gd 0.25	0.25	553 ± 14	0.0014	$r^2 = 1$
100 HA+Gd 0.5	0.5	235 ± 6	0.0036		Gd 0.5	0.5	312 ± 6	0.0028	
100 HA+Gd 0.1	1	130 ± 3	0.0070		Gd 1	1	169 ± 3	0.0055	
100 HA+Gd 2	2	68 ± 3	0.0140		Gd 2	2	92 ± 2	0.0104	
Sample	**[mM]**	**T1**	**1/T1- 1/T1HA**	**R1**	**Sample** [4]	**[mM]**	**T1**	**1/T1- 1/T1PBS**	**R1**
100 GE[3]+Gd 0.125	0.125	685 ± 22	0.0008	6.57	Gd 0.125	0.125	927 ± 24	0.0007	5.23
100 GE+Gd 0.25	0.25	454 ± 13	0.0015	$r^2 = 1$	Gd 0.25	0.25	556 ± 12	0.0014	$r^2 = 1$
100 GE+Gd 0.5	0.5	244 ± 8	0.0034		Gd 0.5	0.5	313 ± 9	0.0028	
100 GE+Gd 0.1	1	132 ± 4	0.0069		Gd 1	1	172 ± 4	0.0054	
100 GE+Gd 2	2	73 ± 3	0.0130		Gd 2	2	92 ± 4	0.0104	

[1] T1pbs value on this imaging day was 2,346.25±124
[2] T1 value of HA at 100 mg/ml was 1,519 ± 55
[3] T1 value of GE at 100 mg/ml was 174±15
[4] Gd was heated. No change observed compared to non-heated Gd

Table XXIII. T1 and R1 values of a 100 mg/ml HA or GE made in different concentrations of Gd-DTPA.

A = Gd at 2mM[2]									
Sample[1]	Pre [mg/ml]	Post (mg/ml)	T1pre	T1post	1/T1pre- 1/T1post	R1	[Gd]material	FCD(mol/L)	[GAG](mg/ml)
TB-HA 100	100	68.83	1709	176	0.0051	7.02	0.0007	-0.163	65.12
TB-GE 90	91	102.56	1360	69	0.0138	6.57	0.0021	0.002	
B = Gd at 1mM[3]									
Sample	Pre [mg/ml]	Post (mg/ml)	T1pre	T1post	1/T1pre- 1/T1post	R1	[Gd]material	FCD(mol/L)	[GAG](mg/ml)
TB-HA 100	100	78.59	1665	368	0.0021	7.02	0.0003	-0.196	78.35
TB-GE 90	91	87.13	1432	133	0.0068	6.57	0.0010	0.0003	
C = Gd at 0.5 mM[4]									
Sample	Pre [mg/ml]	Post (mg/ml)	T1pre	T1post	1/T1pre- 1/T1post	R1	[Gd]material	FCD(mol/L)	[GAG](mg/ml)
TB-HA 100	100	82.77	1655	572	0.0011	7.02	0.0002	-0.182	72.73
TB-GE 90	91	84.00	1465	222	0.0038	6.57	0.0006	0.018	

[1] $T1_{pbs}$ value on this imaging day was 2,730.2±188.4
[2] T1 value of Gd at 2 mM was 91±5
[3] T1 value of Gd at 1 mM was 174±15
[4] T1 value of Gd at 0.5 mM was 335±8

Table XXIV. Calculation of Gd concentration in the material ($Gd_{material}$), fixed charged density (FCD), and glycosaminoglycans (GAG) content for the 100 mg/ml HA and the 100 mg/ml GE at the three Gd-bath concentrations of 2, 1, and 0.5 mM.

The GAG content estimation was only done for the HA samples at 100 mg/ml, since the FCD of GE turned out to be positive (yellow in **Table XXIV**) impeding the estimate of the concentration in these materials. The outcome of a positive FCD for GE is in agreement with the calculated concentrations of Gd in the material ($Gd_{material}$) being slightly higher than the Gd-bath concentration (yellow in **Table XXIV**). Furthermore, these results is in agreement with the basic or positively charged characteristics found in the human type I collagen sequence described in **Chapter I**. Furthermore, these results confirm that collagen does not contribute to or interfere with the assessment of GAG content using dGEMRIC.

The GAG content of the 100 mg/ml HA closely matched the post-Gd GAG content in the materials, which are highlighted in red in **Table XXIV** and also plotted in **Fig 5.7**. As expected, the three Gd-bath concentrations (0.5, 1, 2 mM) estimated GAG content **(Fig 5.7)** equally well. Also, although the R1 of Gd was obtained only for the 100 mg/ml of HA, the R1 of Gd should be very similar within a range of concentrations and composition as shown by **Table XXIV**.

Additionally, it was verified that heating of the Gd-DTPA did not change the relaxivity of this contrast agent **(Fig 5.8)**. This confirmation was needed as the 100 mg/ml HA and GE samples that were made in the different concentrations of Gd required heating at 60ºC for 2 hours in order for the samples to go into solution.

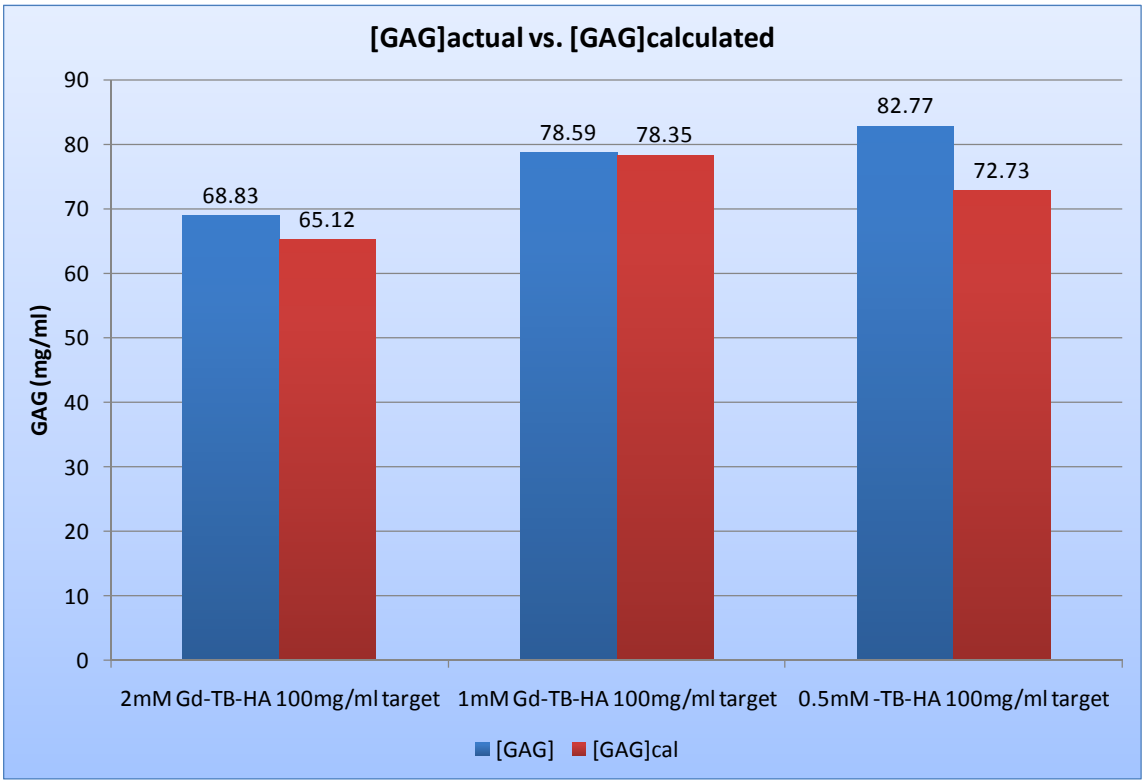

Figure 5.7. [GAG]actual vs. [GAG]calculated. This figure compares how closely the GAG content calculated (red) by means of finding the R1 of Gd in the material at 100 mg/ml of HA to the GAG content (blue) that was originally in the samples. The GAG content assessment was repeated in 0.5, 1, and 2 mM Gd-bath concentrations.

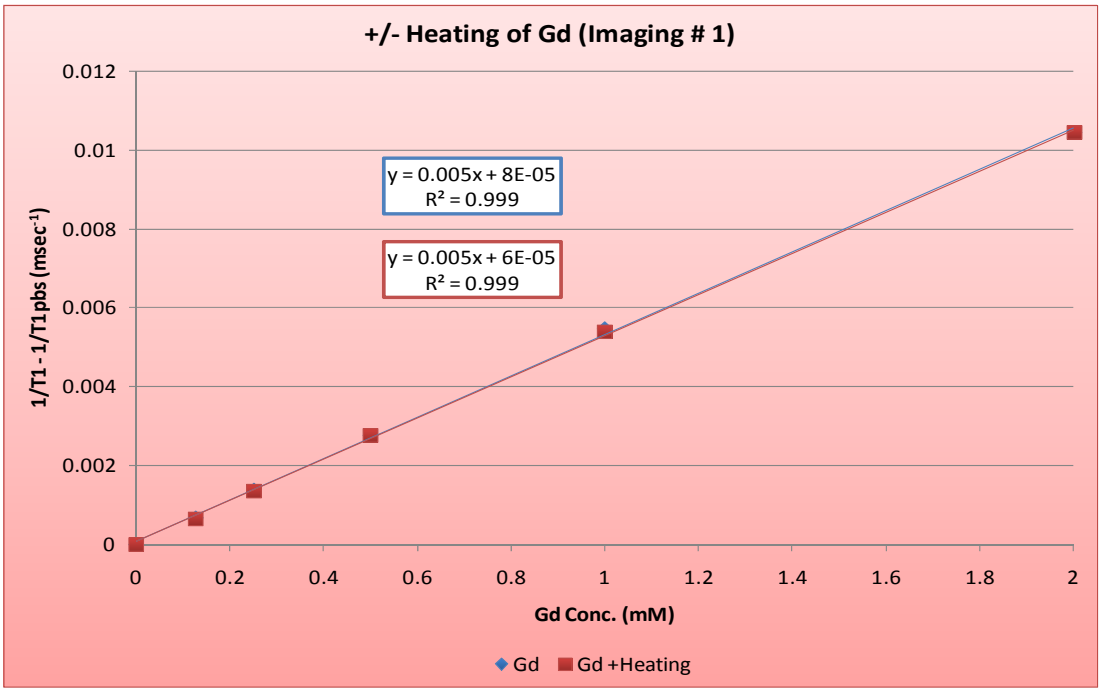

Figure 5.8. Effect of Heating on Gd-DTPA. Gd-DTPA with and without heating was plotted at concentrations of 0.125, 0.25, 0.5, 1, and 2 mM. As seen in this figure, heating has no effect on Gd-DTPA.

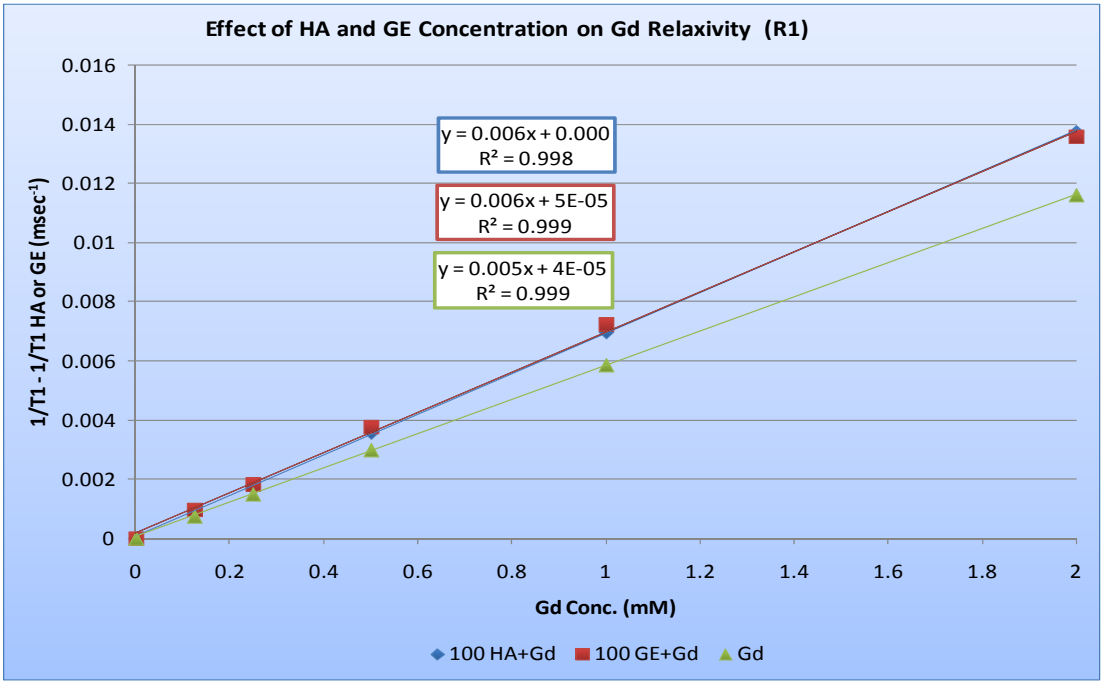

Figure 5.9. Effect of HA and GE Macromolecular Content on the Relaxivity (R1) of Gd-DTPA. The R1 of Gd increased in the presence of HA or GE content compared to Gd without HA or GE.

The final verification that was done referred to the dependency of the R1 of Gd-DTPA on GAG and collagen content. The R1 for Gd-DTPA in intact cartilage and in solution has been previously determined at 8.45 T and shown to be independent of GAG concentration **[52].** Nevertheless, our results in TB-hydrogels suggest that relaxivity is sensitive to macromolecular content **(Fig 4.5)** at lower field strengths (3 T), which agrees with the findings of recent work by Stanisz **[53]**. **Figure 5.9** shows that R1 of Gd-DTPA is reliant on molecular concentration since the relaxivity of Gd increased slightly in the presence of both the HA and GE materials. The data plotted in **Figure 5.9** originates from **Table XXV**.

Lastly, the variability of T1 and T2 values from day to day due to the MR shift was previously discussed in **Chapter IV.** This experiment allowed to image three replicates of TB-HA, TB-GE, and TB-CO samples in one day, thus we can now compare variability of reproduced samples from one single day **(Table XXV)**. The R1 and R2 values displayed narrower standard deviations compared to those values from day to day; except for TB-CO, which maybe due to inhomogeneities of these materials at higher concentrations.

	A-TB-HA	B-TB-HA	C-TB-HA	Average R	SD (±)
R1	0.0023	0.0023	0.0025	0.0024	0.0001
R2 (15)	0.0213	0.0229	0.0208	0.0217	0.0009
R2 (30)	0.0229	0.0238	0.0222	0.0230	0.0007
	A-TB-CO	B-TB-CO	C-TB-CO	Average R	SD (±)
R1	0.0055	0.0053	0.0068	0.0059	0.0007
R2 (15)	0.0561	0.0455	0.0719	0.0578	0.0109
R2 (30)	0.0599	0.0447	0.0744	0.0596	0.0121
	A-TB-GE	B-TB-GE	C-TB-GE	Average R	SD (±)
R1	0.0036	0.0032	0.0032	0.0034	0.0002
R2 (15)	0.0159	0.0173	0.0146	0.0159	0.0011
R2 (30)	0.0174	0.0174	0.0147	0.0165	0.0013

Table XXV. Average of R values for three replicates (A, B, and C) of TB-HA, TB-GE, and TB-CO all imaged the same day.

In summary, dGEMRIC has been shown to be able to determine the GAG concentrations both in cartilage and the TB-HA hydrogels. This study also validated the Donnan theory of FCD as the collagen contributions could be ignored relative to GAG due to its positive FCD, as also verified by Maroudas **[29]**. Additionally, our results indicate that ICP-MS measurements of Gd concentration in the materials greatly differed from the known concentrations; hence the ability to use this technique for assessing Gd concentrations may not be the most efficient. On the contrary, determining the Gd concentration by means of finding the R1 of Gd in the materials resulted in a more effective method, as the GAG index calculated closely matched the GAG in the original samples.

Currently, there is a dispute in the literature as to whether or not the relaxivity of Gd-DTPA is dependent on GAG content. Our data indicates that the relaxivity of Gd-DTPA is dependent on macromolecular content. Previous studies have been done in cartilage to test this premise, in which the GAG and collagen cannot be separated. The outcome of this investigation can be dependable as GAG and collagen could be tested alone. Finally, these biomaterials have demonstrated to be sufficiently stable to serve as an imaging system to test future MRI contrast agents.

CHAPTER VI

T1 AND T2 MRI MEASUREMENTS OF TYRAMINE-BASED HYDROGELS IMPLANTED IN CARTILAGE TISSUE.

6.1 Introduction

The development of a non-invasive, non-destructive technique to detect and characterize TB-HA, TB-GE and TB-CO hydrogels in tissues is desirable to facilitate the product development and regulatory approval of these biomaterials for a variety of clinical applications. The purpose of this study is to use the T1-weighted and T2-weighted image contrast and T1 and T2 mapping, which were determined best suited for detection and differentiation of the TB-hydrogels in **Chapter IV**, to detect and distinguish select formulations of the TB-hydrogels from surrounding tissue in cadaveric goat and sheep joints. This would be an extremely valuable tool for following the progress of these hydrogels with time after implantation, and thus improving the animal models and future clinical trials involving these biomaterials.

6.2 Experimental Design

Based on the results from the experiments presented in **Chapter IV**, T1 and T2 mapping are suitable for detecting, distinguishing, and characterizing TB-hydrogels. Pre-formed plugs of 6.25 and 100 mg/ml TB-HA hydrogels and TB-CO materials composed of 6.25 mg/ml HA and GE and 100 mg/ml HA and GE were implanted into cadaveric sheep and goat knee articular cartilage. The GE only materials were not tested because in the absence of the HA they do not have the necessary mechanical properties to serve as a potential cartilage replacement material. The 6.25 and 100 mg/ml concentrations were chosen as they represent the concentration extremes allowing assessment of the minimum detection limit based on material concentration on the one extreme (6.25 mg/ml), and assessment of the of the minimum detection limit based on signal differences with native cartilage (100 mg/ml). Furthermore, the 100 mg/ml concentration was selected as this concentration of TB-HA was recognized to posses a compressive aggregate modulus most closely resembling that of articular cartilage, as shown in **Table II**. Additionally, the 100 mg/ml concentration of the HA/GE composite approximates the concentration of GAG and collagen in cartilage, which composite material (TB-CO) was found to have a T1 value representative of cartilage in **Chapter IV**. Six healthy knees from 4 sheep and 2 goats were obtained after sacrifice from ongoing IACUC approved protocols at the Cleveland Clinic. The femur was dissected from the knee joint immediately before implantation of the hydrogel into the trochlear notch of the femur. The implanted specimen was wrapped in parafilm and evaluated with MRI

shortly after. All specimens were subjected to T1 and T2 mapping as well as T1-weighted and T2 weighted acquisitions. MR imaging of the specimens were performed using size proportional spatial resolution. Additionally, volumetric measurements of the implanted hydrogel plugs were performed using MicroView (GE Healthcare) at the Biomedical Imaging and Analysis Core at CCF.

6.3 Materials and Methods

6.3.1 Implantation Procedures

Implantation was performed after excising the femur from the knee joint. Cross-linked TB-HA and TB-CO hydrogels were formed *in vitro* as explained in **Appendix A**, and used in a manner similar to an autograft or allograft repair, where the preformed hydrogel is simply press fit into the defect space. Two circular full thickness chondral defects (10 mm in diameter, and approximately 12.7 mm thick) were created in the trochlear notch of the femur using a drill bit so as to provide a defect volume of 1 ml **(Fig 6.1)** similar to the sample volumes used for imaging in **Chapter IV**. In some cases, the joint anatomy of the femoral trochlear notch prevented drilling to the desired 12.7 mm depth. Therefore, some defect volumes were less than 1 ml. The two concentrations of either TB-HA or TB-CO cylindrical plugs were then press fit into the defect space as shown below, and trimmed to fit those defect volumes less than 1 ml. The excess material not implanted was recovered so as to calculate the volume added.

I

II

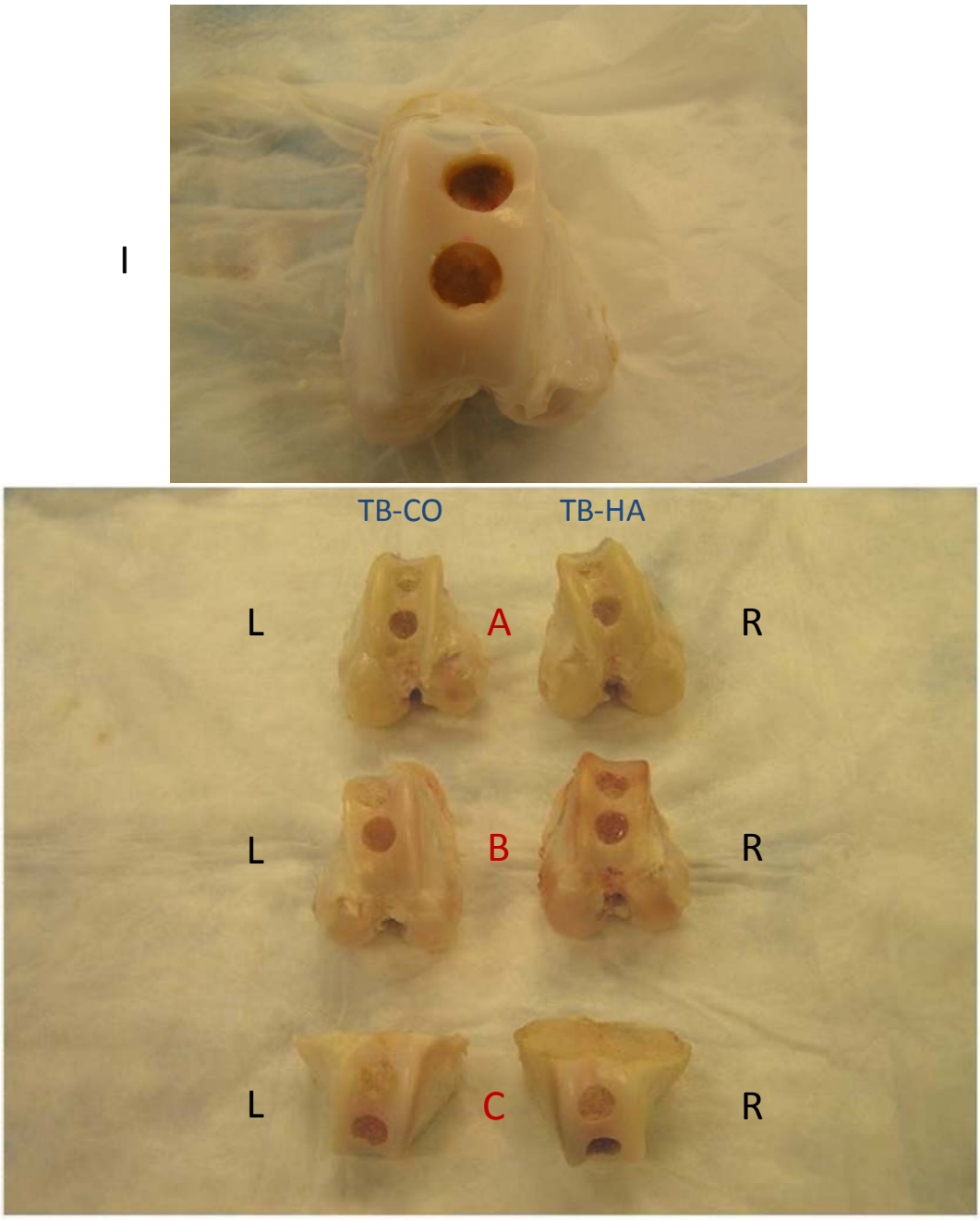

Figure 6.1. Hydrogel Implantation into Cartilage Defects. I: Two ~12.7 mm full thickness defects created in the trochlear notch. **II:** Left (L) and right (R) chondyl from two sheep (A and B) and one goat (C). The specimens in the left column were filled with the TB-CO hydrogel and in the right column with the TB-HA hydrogel with the 100 mg/ml plugs at the top and the 6.25 mg/ml plugs at the bottom for each.

6.3.2 T1 and T2 Measurements

The MRI measurements were done at room temperature as specified in previous chapters and utilizing the following instrument settings for T1 and T2:

T1 Measurement: An inversion recovery fast (turbo) spin echo sequence was used to create T1 maps with repetition time (TR) = 11,000 msec; inversion time (TI) = 23 msec, 75 msec, 150 msec, 300 msec, 750 msec, 1,400 msec, 2,000 msec, and 2,800 msec; echo time (TE) = 10 msec; field of view (FOV) = 260 mm; slice thickness = 4 mm, matrix = 256 x 204, and 1 average. The inversion recovery imaging sequence produced 8 images from each set of multiple slices (9 for the sheep and 7 for the goat specimens) each with a different TI.

T2 Measurement: T2 relaxation time of the specimens was conducted using a spin echo imaging sequence with a TR = 11,000 msec and 20 echoes with 15 msec echo spacing (e.g TE: 15 to 300 msec), FOV = 260 mm, slice thickness = 4 mm, matrix size = 256 X 204, and 1 average.

The TR, TE, matrix size and slice thickness parameters for the above T1 and T2 acquisitions are different to those described in **Chapter IV**. These changes had to be made in order to accommodate the geometry of the specimens as well as the position of the plugs once implanted on the concave joint surfaces. T1 and T2 maps were calculated using MRIMapper as described in **Chapter IV**. The regions of interests (ROI) were selected from the hydrogel implant, the native articular cartilage, and bone.

6.3.3 Volumetric Measurements

To test whether or not we could extract volumetric measurements of the implanted TB-hydrogel plugs, the volumes of the six TB-HA and six TB-CO plugs were measured from T2 images. The volumetric measurements were calculated by using the MicroView (GE Healthcare) program. First, splining or drawing ROIs around the hydrogel plugs was performed, followed by interpolation of the ROIs in the planes to create a spline set. A 3-dimensional ROI of the spline set was generated. A threshold of 90 -100 units was determined from a histogram performed on the samples, which corresponded with the shortest T2 values measured in **Chapter IV** for the TB-hydrogels. An iso-surface of each hydrogel plug was generated. The iso-surface rendered the plugs overlaid onto a maximum intensity of the cartilage tissue, from which the volume could be calculated.

6.4 Results and Discussions

The T1 and T2 values for the 6.25 and 100 mg/ml TB-HA and TB-CO hydrogel plugs for the six cadaveric chondyles **(Tables XXVI and XXVII, respectively)** as well as the same material formulations from the experiments described in **Chapter IV (Table XXVIII)** are tabulated below. As examples, color T1 and T2 maps for the sheep specimen (A) 100 mg/ml TB-HA and TB-CO hydrogel plug implants are shown in **Figs 6.2 and 6.3, respectively.** As shown in **Tables XXVI-XXVIII**, the T1 and T2 values for the 100 mg/ml TB-CO and the T1 values of the TB-HA plugs correlated well with those values determined in **Chapter IV**, with the relaxation times of TB-HA always longer than those of TB-CO. In the case of the 6.25 mg/ml TB-HA and TB-CO hydrogel plugs, the T1 and T2 are much shorter compared to those determined in **Chapter IV (Tables XXVI-XXVIII)**, which may be due to the necessary change in the acquisition parameters that seemed to have prevented the measurement of longer T1 and T2 relaxation times that are typical of low concentration hydrogels such as the 6.25 mg/ml TB-HA and TB-CO. The T2 values for the 100 mg/ml TB-HA were also shorter compared to those determined in **Chapter IV (Tables XXVII**, **XXVIII)** since measurement of longer T2 relaxation times was limited for the same reasons explained above. The 100 mg/ml TB-CO hydrogels have T1 values in the ~ 700 - 1000 msec range at 3.0 T and are consistent between *in situ* and *ex vivo* measurements of cartilage. The 100 mg/ml TB-CO hydrogels have T1 values similar to that of the native cartilage **(Table XXVI and Fig 6.2),** and if implanted in human cartilage, are predicted to closely resemble cartilage in a T1

map or on a T1-weighted acquisition. However, the T2 values measured for the 100 mg/ml TB-CO hydrogels both *in situ* (**Table XXVII and Fig. 6.3**) and *ex vivo* (**Table XXVIII**) are considerably greater than that for native articular cartilage (20–40 msec, **[50]**) and thus these hydrogels can be clearly visualized using a range of mapping and image contrast techniques. T1 and T2 maps of the entire sheep specimens (A) were measured, in which the hydrogel plugs are clearly distinguishable from the surrounding tissues **(Figs 6.2 B and 6.3 B)**.

Plugs	A-R	A-L	B-R	B-L	C-R	C-L
TB-HA 6.25	1577±683	-	1867±377	-	1926±395	-
TB-HA 100	1138±636	-	1422±158	-	1609±604	-
TB-CO 6.25	-	760±391	-	1446±237	-	1878±536
TB-CO 100	-	1101±201	-	707±153	-	1145±156

Table XXVI. T1 values (msec) for hydrogels implanted in the sheep (A and B) and goat (C) cadaveric joints. A-L and A-R represent the first pair of sheep specimens left and right, respectively. B-L and B-R represent the second pair of sheep specimens left and right, respectively. C-L and C-R represent the pair of goat specimens left and right, respectively.

Plugs	A-R	A-L	B-R	B-L	C-R	C-L
TB-HA 6.25	471±66	-	462±56	-	336±77	
TB-HA 100	95±6	-	144±8	-	149±12	
TB-CO 6.25	-	497±50	-	511±97	-	457±112
TB-CO 100	-	158±9	-	128±11	-	144±7

Table XXVII. T2 values (msec) for hydrogels implanted in the sheep (A and B) and goat (C) cadaveric joints. A-L and A-R represent the first pair of sheep specimens left and right, respectively. B-L and B-R represent the second pair of sheep specimens left and right, respectively. C-L and C-R represent the pair of goat specimens left and right, respectively.

T1					
Plugs	Day 1	Day 2	Day 3	Day 4	Day 5
TB-HA 6.25	-	2220 ± 168	2241 ± 183	2509±170	2395±242
TB-HA 100	-	1366 ± 66	1251 ± 72	1390±111	1381±81
TB-CO 6.25	-	-	-	2485±106	2288±242
TB-CO 100	-	-	-	978±38	948±32
T2					
Plugs	Day 1	Day 2	Day 3	Day 4	Day 5
TB-HA 6.25	-	1114 ± 44	1090 ± 26	1096±38	1047±22
TB-HA 100	-	198 ± 16	244 ± 19	264±257	208±13
TB-CO 6.25	-	-	-	991±100	922±44
TB-CO 100	-	-	-	139±62	140±10

Table XXVIII. T1 and T2 values (msec) for 6.25 and 100 mg/ml TB-HA and TB-CO materials formed *ex vivo* as part of experiments described in Chapter IV.

A

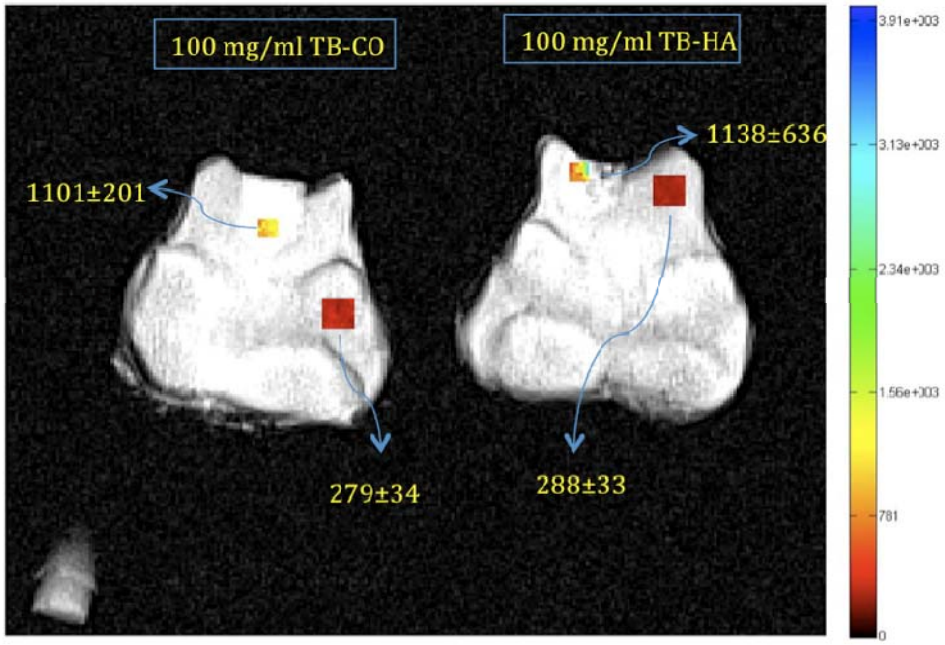

B

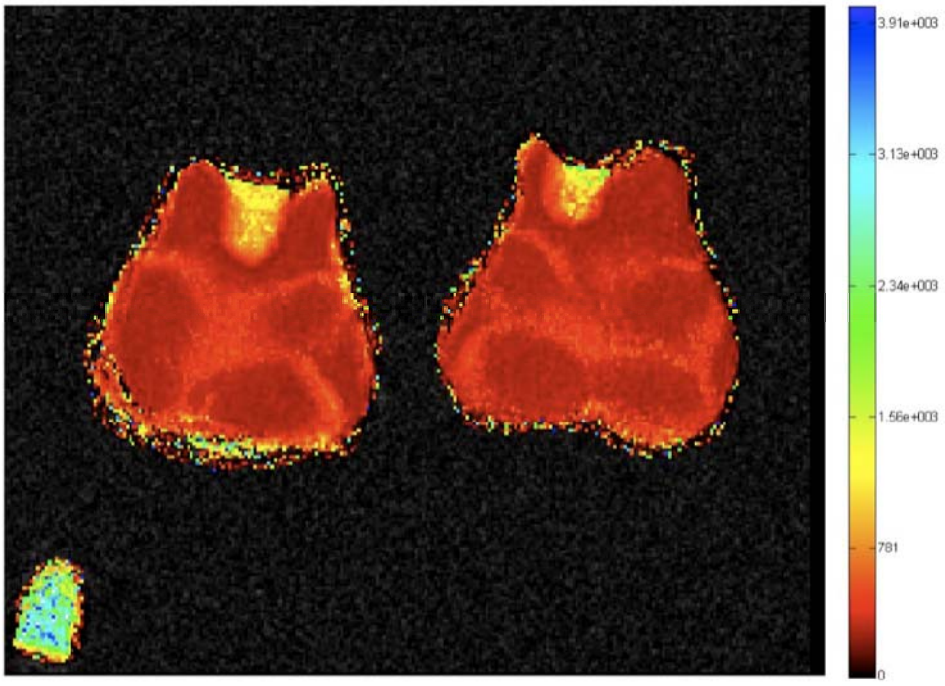

Figure 6.2. T1 Maps for Both Chondyles of Sheep A that Image the 100 mg/ml Hydrogel Plugs. A: On the left, chondyle with a 100 mg/ml TB-CO plug, and on the right, chondyle with a 100 mg/ml TB-HA plug showing the ROI used to measure the T1 values of 1,101 ± 201 and 1,138 ± 636 msec, respectively. The bone was also measured in both specimens as a control (279 ± 34 and 288 ± 33, respectively). **B:** T1 map for the entire specimen.

A

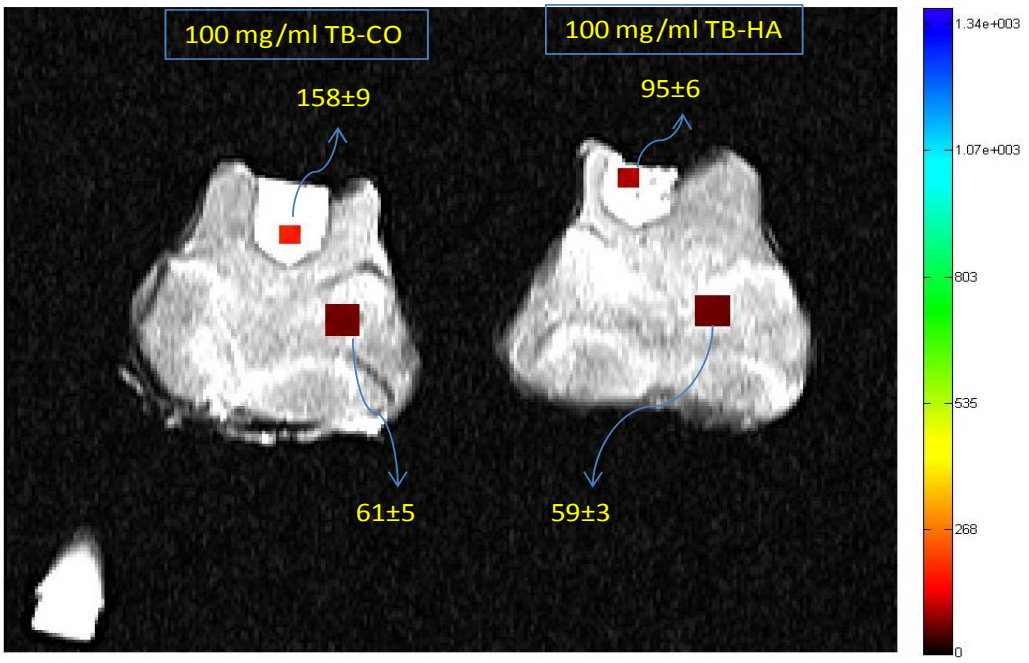

B

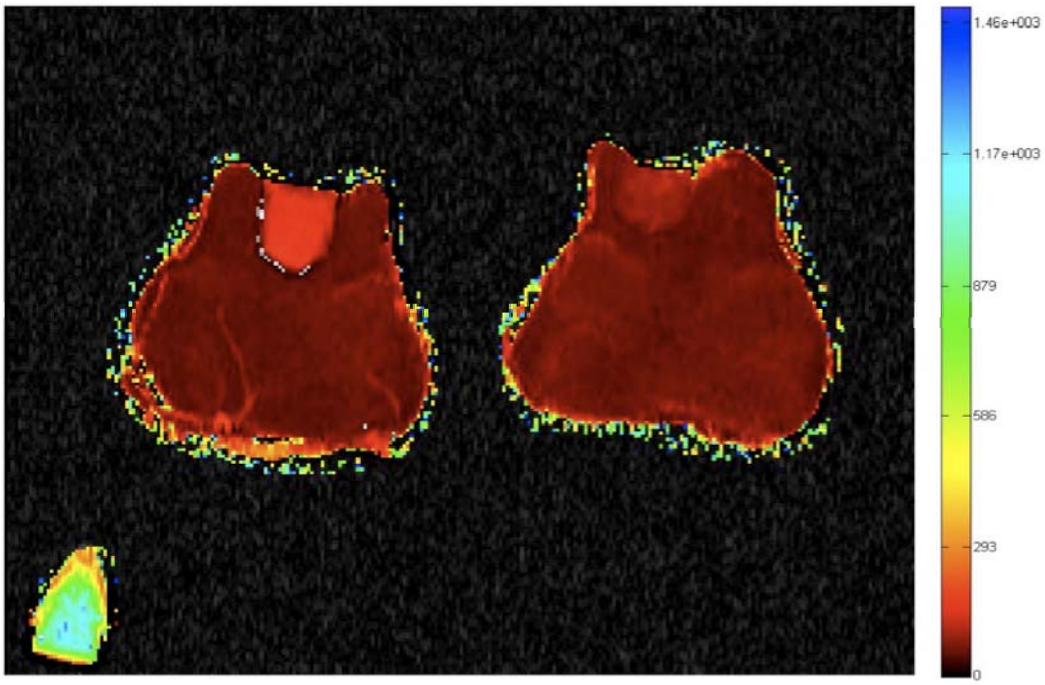

Figure 6.3. T2 Maps for Both Chondyles of Sheep A that Image the 100 mg/ml Hydrogel Plugs. A: On the left, chondyle with a 100 mg/ml TB-CO plug, and on the right, chondyle with a 100 mg/ml TB-HA plug showing the ROI used to measure the T2 values of 158 ± 9 and 95 ± 6 msec, respectively. The bone was also measured in both specimens as a control (61 ± 5 and 59 ± 3 msec, respectively). **B:** T2 map for the entire specimen.

The iso-surface rendering for the implanted TB-hydrogel plugs is shown in **Figure 6.4**. This technique allowed 3-D visualization of the contours of the plugs implanted in the specimens by highlighting the plugs that measured above 90-100 msec compared to the cartilage or bone that are below this threshold at ~30-40 **[50]** and ~ 50 msec **[51]**, respectively. As shown in Table **XXIX**, the volumetric measurements approximated the volumes originally implanted. Hence, we are able to successfully measure the volume of hydrogel implanted in the articular cartilage specimens.

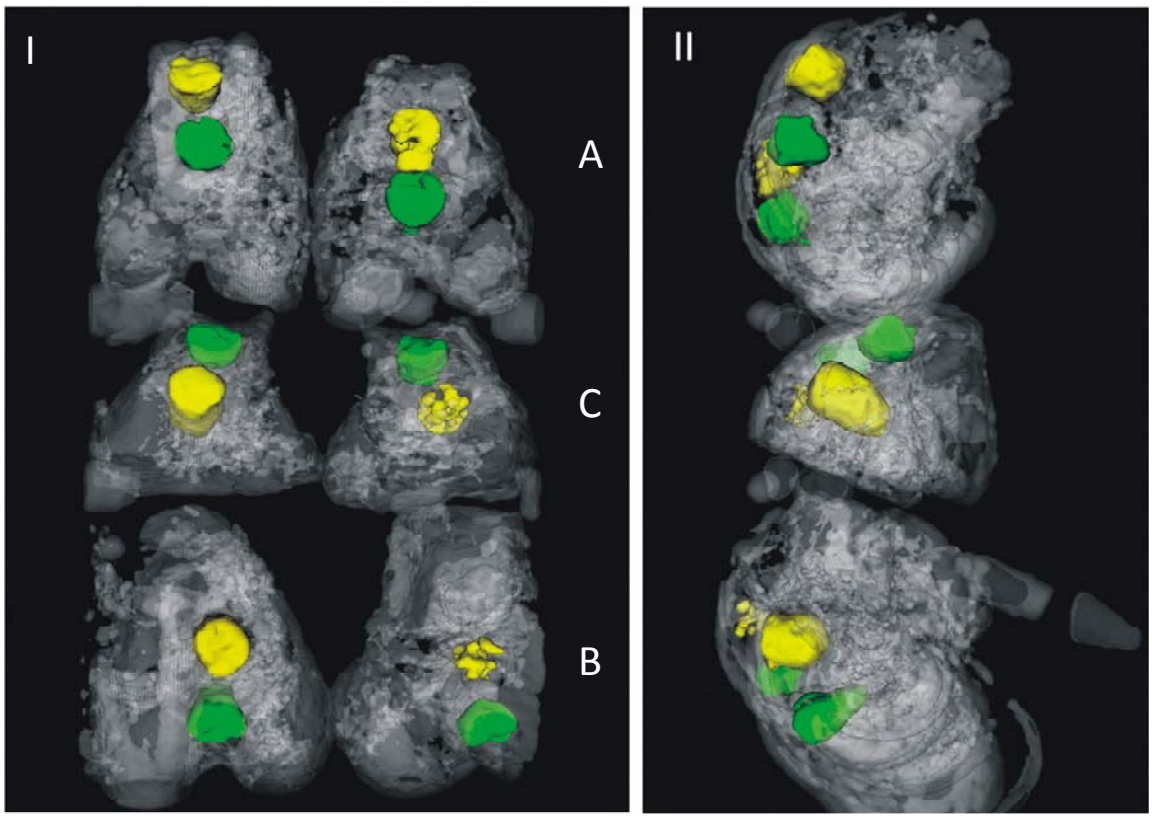

Figure 6.4. Iso-surface Rendering for the TB-HA and TB-CO Hydrogel Plugs. Panel I represents the top view of the TB-hydrogel plugs implanted in sheep chondyles **(A** and **B)**, and goat chondyles **(C)** with the implanted TB-CO hydrogel plugs in the chondyles on the left column, and the implanted TB-HA hydrogel plugs in the chondyles on the right column **(I)**. The TB-hydrogels at 6.25 and 100 mg/ml are represented in green and yellow, respectively. **Panel II** represents the side view similarly colored.

Plugs	Actual Volume	Measured Volume	Actual Volume	Measured Volume	Percent Change
	A-R	A-R	A-L	A-L	
TB-HA 6.25	467.4	486.4			4.1
TB-HA 100	403.5	449.9			11.5
TB-CO 6.25			423.5	439.8	3.8
TB-CO 100			427.2	458.3	7.3
	B-R	B-R	B-L	B-L	
TB-HA 6.25	390.0	355.2			-8.9
TB-HA 100	100.0	89.2			-10.8
TB-CO 6.25			451.0	481.6	6.8
TB-CO 100			620.3	638.8	3.0
	C-R	C-R	C-L	C-L	
TB-HA 6.25	454.0	451.6			-0.5
TB-HA 100	179.3	165.1			-7.9
TB-CO 6.25			407.7	414.3	1.6
TB-CO 100			922.0	894.9	-2.9

Table XXIX. Actual volume compared to the measured volume of the TB-Hydrogels implanted in cartilage and the percent changes between the two.

The TB-HA and TB-CO plugs at 100 mg/ml had T1 and T2 values comparable to those found *ex vivo* in **Chapter IV (Table XXVIII)**, while the same materials at 6.25 mg/ml did not match those in Chapter IV due to the need to change the T1 and T2 acquisition parameters as explained above. Implanted hydrogels plugs should therefore be easily distinguished from endogenous host cartilage using either T1 or T2 mapping as the materials' T1 and T2 values are greater than that of native articular cartilage. The exception is the TB-CO at 100 mg/ml, which has T1 values similar to that of cartilage, and is expected to be indistinguishable from surrounding cartilage in a T1 map. However, because its T2 value is significantly greater than that for articular cartilage, these hydrogel implants should be identifiable from surrounding cartilage using T2 mapping techniques. Hence, T1-weighted and T2-weighted MRI measurements should be able to detect and differentiate the TB-hydrogels from the surrounding tissues, including the composite materials. Having the ability to differentiate and possibly quantitate these TB implants will improve future animal models and clinical trials involving these biomaterials. For instance, a 100 mg/ml TB-HA hydrogel could be implanted in a rabbit model, as the one described in **Chapter II**, and its biologic fate followed with time without sacrificing the animal. Since we can now determine the shape and volume of the implanted hydrogel, any changes in shape or loss of material volume could be detected non-invasively. Furthermore, a loss in material concentration from the implant due to *in vivo* degradation could be identified and measured non-invasively. Standards of the TB-hydrogels at various concentrations similar to those used in **Chapter IV** could be included

within the imaging field with the animal in order to provide T1 and T2 values for generation of a standard curve (i.e. relaxivity value). By imaging the standards with the animal variations in the magnet based on imaging date or magnet design could be controlled. Then the concentration of the implant calculated from the implant T1 and T2 values and the relaxivity value calculated for that imaging session. Finally, if the implant material is being replaced or augmented by either *in vivo* GAG or collagen synthesis, these changes could be measured non-invasively as changes in T1 or T2 values, through once again, inclusion of standards as described above.

CHAPTER VII

CONCLUSIONS AND FUTURE INVESTIGATIONS

7.1 Conclusions

Tyramine-based (TB) hydrogels possess advantageous physical properties, providing for synthetic, implantable biomaterials suitable for a wide range of tissue types. The aggregate moduli of TB-HA hydrogels at 100 mg/ml and 50 mg/ml exhibit values that are equal to or exceed those of previously reported values for articular cartilage in confine mechanical compression **[36-39].** Hence, the excellent biocompatibility of these TB-hydrogels along with their ability to provide similar structural and mechanical properties to normal tissues calls for the development of a non-destructive technique to detect and characterize TB-hydrogels in tissues. Magnetic Resonance Imaging (MRI) is a broadly used non-invasive clinical imaging modality that allows direct visualization of soft tissues. Determining the MRI contrast best suited to identify, distinguish, quantify and trace these TB-hydrogels both *in vitro* and *in vivo,* may facilitate the product

development and regulatory approval of these biomaterials as functional synthetic, implantable tissue matrices to replace/repair various tissue types. This dissertation work has identified MRI contrast and acquisitions that can be used to characterize TB-hydrogels both *in vitro* and *in vivo.* Furthermore, this research provided insight and clarification as to the appropriateness of these MRI techniques to measure GAG and collagen content.

This study determined that both T1 and T2 mapping could be used to detect and measure tyramine-based hyaluronan (TB-HA), tyramine-based collagen in the form of gelatin (TB-GE), and combinatorial materials composed of both HA and collagen (TB-CO). T1 and T2 displayed relatively equivalent sensitivity to changes in both HA and collagen concentration. The greatest impact on both T1 and T2 was produced by the combination of HA and collagen in the composite materials.

The T1 and T2 values decreased with increasing concentration of the materials. The difference in T1 or T2 values between 6.25 and 12.5 mg/ml concentrations dropped by about 30-90 msec. However, once the concentration reached 25, 50 and 100 mg/ml the T1 or T2 values dropped by 200-900 msec as their influence on the imbibed water became significant. This transition in the material properties between the low and high concentration of these materials correspond with the results seen in the mechanical properties of these biomaterials. The aggregate modulus for the 6.25 and 12.5 mg/ml TB-HA hydrogels is between 20-70 Kpa,

while the 25, 50 and 100 mg/ml have moduli of 400-1,200 Kpa, as shown in **Table I**. Hence, a pronounced change in the mechanical properties of these materials is observed around the 25 mg/ml concentration and this can also be observed in the imaging properties of these materials. The dramatic transition in mechanical and imaging properties observed at the 25 mg/ml concentration occur as a result of changes in matrix porosity associated with an increase in material concentration that dramatically influence at a molecular level the imbibed water.

Characteristic of a MRI contrast agent, Magnevist (Gd-DTPA^{-2}), demonstrated an ability to produce a significant effect on relaxation time, T1, requiring 800 to 1,500 times less material to produce a given change in T1 than for all of the other non-MRI contrast agent materials tested. Agar and the HA, GE and CO hydrogel materials all had a relatively similar concentration effect on T1 requiring 800 to 1,500 times the concentration of Magnevist to produce the same change in T1 value.

It was also established that the chemistry (both tyramine substitution and di-tyramine cross-linking) used to formulate TB-hydrogels had a predictable but modest effect on the MRI properties of these biomaterials. All of the TB-hydrogel formulations possess T1 and T2 values that are measurably higher than those reported in cartilage, except for the 100 mg/ml TB-CO that only possess T2 values higher than cartilage. Consequently, these biomaterials could be readily

distinguished from the surrounding tissue. The composite materials (TB-CO) at 100 mg/ml, which concentration is typical of the molecular content in cartilage, have a T1 value in the ~1,000 msec range that is also characteristic of cartilage. By measuring the T1 and T2 values of defined synthetic HA and collagen materials, this work has provided a better understanding of the relationship between these MRI methods and tissue composition as well as MRI techniques to detect, distinguish, and characterize the TB-hydrogels.

The delayed Gadolinium Enhanced MRI of Cartilage (dGEMRIC) was identified as a technique that could be employed to quantify the glycosaminoglycan (GAG) content of TB-HA hydrogels in a fashion similar to that previously reported for GAG content in cartilage **[48]**. dGEMRIC relies on the Donnan theory that relates fixed charge density (FCD) to GAG content in cartilage. This work validated the Donnan theory and the relationship between FCD and GAG concentration with its application to the TB-hydrogels. This study also confirmed that collagen had no measurable contribution to the FCD of cartilage and thus no influence on the partitioning of the negatively charged Gd-DTPA contrast agent.

Furthermore, our results indicate that the relaxivity of Gd-DTPA is dependent on macromolecular content. This premise has been tested in previous studies; however, these studies used cartilage as the imaging substrate, in which GAG and collagen cannot be tested separately providing inconclusive results. The

outcome of this investigation is definitive as GAG and collagen were tested in separate imaging constructs.

The TB-based biomaterials have demonstrated sufficient stability to serve as a controlled system of synthetic ECM composed of HA (GAG) and collagen molecules that could be used to test future MRI contrast agents developed for measuring matrix composition.

Confirmation of standard MRI imaging methodologies to detect and distinguish TB-hydrogels from surrounding tissue was obtained in this investigation. The TB-HA and TB-CO at 6.25 mg/ml and TB-HA at 100 mg/ml demonstrated T1 and T2 values that were greater than that of native articular cartilage. Hence, these biomaterials could easily be differentiated from cartilage. TB-CO at 100 mg/ml had T1 value similar to that of cartilage, but a T2 value significantly different. Hence, we have identified MRI techniques to detect and differentiate the TB-hydrogels from the surrounding tissues. We now have the ability to evaluate *in vivo* performance of TB-hydrogels with time without the need to sacrifice experimental animals; hence providing us with the capacity to improve future animal models and clinical trials involving these biomaterials. Once the TB-hydrogel is implanted, we can identify any changes in the shape, contours or volume of the implant by volumetric measurements using MicroView. Any changes in concentration induced by loss of material (HA or collagen) could be measured through T1 and T2 MRI techniques and compared to the T1 and T2

values of the concentration curves for the phantoms we have established. Additionally, if the material is being augmented by GAG or collagen synthesized by cells from the surrounding tissues, we may be able to detect these modifications as well, as we have characterized these components of cartilage individually with T1 and T2 mapping.

7.2 Future Investigations

T1ρ is another MRI technique sensitive to the loss of PGs, which is detected as an increase in T1ρ. Contrary to T1 and T2, which are primarily the outcome of processes that occur at the resonant frequency (64 MHz at 1.5 T) or some small integral multiple thereof, T1ρ is mainly affected by processes (in particular, chemical exchange) that occur in the kilohertz region, as is more typical of macromolecules such as PG **[31]**. This technique was initially included as one of the MRI methods to be evaluated in this study. However, this software is not included in standard MR system software, and even though we obtained the license for installation, the installation has to date not been done due to administrative reasons. Hence, we would like to evaluate this technique once installed in the MR system, in order to test its sensitivity to PG content, and potentially identify another perhaps more sensitive technique to characterize the TB-HA hydrogels. Additionally, to establish a better assessment of TB-hydrogels in tissues, the experiments in **Chapter VI** will be repeated in species with thicker cartilage such as porcine. This will improve the quantitative and qualitative characterization of TB-hydrogels *in vivo*. Finally, we would apply all of the MRI

techniques evaluated in this dissertation in an animal cartilage repair model similar to the rabbit model described in **Chapter II**. This animal model would be followed over time (a year or more) and be the ultimate validation of our MRI techniques for evaluating the progress of physical and chemical changes to the implanted TB-hydrogels.

REFERENCES

1. Bashir A. Gray M.L. Burstein D. **Gd-DTPA^{-2} as a measure of cartilage degradation**. Magnetic Resonance in Medicine. 36:665-73,1996.

2. Bashir A. Gray ML. Boutin R.D. Burstein D. **Glycosaminoglycan in articular cartilage: in vivo assessment with delayed Gd (DTPA)$^{2-}$-enhanced MR imaging**. Radiology. 205: 551-8, 1997.

3. Bashir A. Gray M.L. Hartke J. Burstein D. **Nondestructive imaging of human cartilage glycosaminoglycan concentration by MRI.** Magnetic Resonance in Medicine. 41: 857-65, 1999.

4. Blumenkrantz N. Asboe-Hansen G. **New methods for quantitative determination of uronic acids**. Analitical Biochemistry. 54: 484-89, 1973.

5. Borthakur A. Shapiro E.M. Beers J. Kudchodkar S. Kneeland J.B. Reddy R. **Sensitivity of MRI to proteoglycan depletion in cartilage: comparison of sodium and proton MRI**. Osteoarthritis & Cartilage. 8: 288-93, 2000.

6. Bushberg J. Seibert J.A. Leidholdt E.M. Boone J.M. **Nuclear Magnetic Resonance**. In: The Essential Physics of Medical Imaging. 2nd. Philadelphia: Lippincott Williams & Wilkins. 373-465, 2002.

7. Buschmann M.D. Grodzinsky A.J. **A molecular model of proteoglycan-associated electrostatic forces in cartilage mechanics**. Journal of Biomechanical Engineering. 117:179-192, 1995.

8. Calabro A. **Hydroydroxyphenyl cross-linked macromolecular network and applications.** Official Gazette of the United States Patent and Trademark Office. Patent 20060084759, July 7, 2005.

9. Coan P. Mollenhauer J. Wagner A. Muehleman C. Bravin A. **Analyzer-based imaging technique in tomography of cartilage and metal implants: A study at the ESRF.** European Journal of Radiology. 68: S41-S48, 2008.

10. Darr A. **Development of Tyramine-Based Hyaluronan Hydrogels for the Repair of Focal Articular Cartilage Injuries**. (PhD dissertation, Case Western Reserve University, 2008).

11. Darr, A., Calabro, A. **Synthesis and characterization of tyramine-based hyaluronan hydrogels**. Journal of Material Science: Materials in Medicine. 20: 33-44, 2008.

12. DeBazelaire C.M. Duhamel G.D. Rofsky N.M. Alsop D.C. **MR imaging relaxation times of abdominal and pelvic tissues measured in vivo at 3.0 T: preliminary results.** Radiology. 230:652-9,2004.

13. DiSilvestro M.R, Suh J.K. **Biphasic poroviscoelastic characteristics of proteoglycan-depleted articular cartilage: simulation of degeneration**. Annals of Biomedical Engineering. 30: 792-800, 2002.

14. Elliott D.M. Narmoneva D.A, Setton L.A. **Direct measurement of the poisson's ratio of human cartilage in tension**. Journal of Biomechanical Engineering. 124: 223-228, 2002.

15. Farndale R.W. Butler D.J. Barret A.J. **Improved quantitation and discrimination of sulfated glycosaminoglycans by use of dimethylm-ethylene blue**. Biochimica et Biophysica Acta. 883:173-77, 1986.

16. Garcia J.J, Cortes D.H. **A biphasic viscohyperelastic fibril-reinforced model for articular cartilage: formulation and comparison with experimental data**. Journal of Biomechanics. 40:1737- 44, 2007.

17. Garcia J.J, Cortes D.H. **A nonlinear biphasic viscohyperelastic model for articular cartilage**. Journal of Biomechanics. 39: 2991- 98, 2006.

18. Gillis A. Gray M. Burstein D. **Relaxivity of Gadolinium Agents in Cartilage at 2T: Effects on dGEMRIC Imaging**. Proceedings of the International Society of Magnetic Resonance in Medicine. 9:34, 2001.

19. Gray M.L. Burstein D. Xia Y. **Biochemical (and functional) imaging of articular cartilage**. Seminars in Musculoskeletal Radiology. 5:329-43, 2001.

20. Haacke E.M. Brown R.W. Thompson M.R. Venkatesan R. **Magnetization, Relaxation and Bloch Equations. In: Magnetic Resonance Imaging: Physical Principles and Sequence Design**. New York: John Wiley & Sons. Inc. 51-63, 1999.

21. Hardingham T.E. Fosang A.J Dudhia J. **Part I: Structural Components of Cartilage: Proteoglycans**. In: Articular Cartilage Osteoarthritis (Kuettner K.E. SchleyerbachR. Peyron J.G. Hascall V.C. (eds) Raven Press, New York. 5–21, 1992.

22. Henderson B. Pettipher E.R. Murphy G. **Metalloproteinases and cartilage proteoglycan depletion in chronic arthritis-comparison of antigen-induced and polycation-induced arthritis**. Arthritis & Rheumatism. 33: 2241-46, 1990.

23. Jin H. Lewis J.L. **Determination of poisson's ratio of articular cartilage by indentation using different-sized indenters**. Journal of Biomechanical Engineering. 126:138-45, 2004.

24. Jurvelin J.S. Buschmann M.D. Hunziker E.B**. Mechanical anisotropy of the human knee articular cartilage in compression.** Proceedings of the Institution of Mechanical Engineers. Part H - Journal of Engineering in Medicine. 217: 215-9, 2003.

25. Jurvelin J.S. Buschmann M.D. Hunziker E.B. **Optical and mechanical determination of poisson's ratio of adult bovine humeral articularcartilage.** Journal of Biomechanics. 30: 235-41, 1997.

26. Jurvelin J. Kiviranta I. Saamanen A.M. Tammi M. Helminen H.J. **Indentation stiffness of young canine knee articular cartilage – influence of strenuous joint loading.** Journal of Biomechanics. 23:1239-46,1990.

27. Kreklau B. Sittinger M. Mensing MB. Voigt C. Berger G. Burmester G.R. et al. **Tissue Engineering of biphasic joint cartilage transplants**. Biomaterials. 20:1743-49, 1999.

28. Kimelman T. Vu A. Li B. Storey P. Williams A. McKenzie A. Burstein D. Prasad P.V. **Preliminary Experience with dGEMRIC at 3.0 T**. Proceedings of the International Society of Magnetic Resonance Medicine. 11:823,2004.

29. Kiviranta P, Rieppo J, Korhonen R.K, Julkunen P, Toyras J, Jurvelin J.S. **Collagen network primarily controls poisson's ratio of bovine articular cartilage in compression**. Journal of Orthopaedic Research. 24:690-99, 2006.

30. Kneeland J.B. Reddy R. **Frontiers in musculoskeletal MRI: articular cartilage**. Journal of Magnetic Resonance Imaging. 25:339-44, 2007.

31. Korhonen R.K. Laasanen M.S. Toyras J. Rieppo J. Hirvonen J. Helminen H.J. Jurvelin J.S. **Comparison of the equilibrium response of articular cartilage in unconfined compression, confined compression and indentation.** Journal of Biomechanics. 35:903-09, 2002

32. Lou X. Chirila TV. **Swelling Behavior and Mechanical Properties of Chemically Cross-linked Gelatin for Biomedical Use**. Journal of Biomaterials Applications. 14: 185-91, 1999.

33. Lu X.L, Sun D.D, Guo X.E, Chen F.H, Lai W.M, Mow V.C. **Indentation determined mechano-electrochemical properties and fixed charge density of articular cartilage**. Annals of Biomedical Engineering. 32: 370-79, 2004.

34. Mankin H.J, Buckwalter J.A, Mow V.C. Articular cartilage structure and function. **Orthopedic basic science: Biology and biomechanics of the musculoskeletal system**. Philadelphia, Pa: Saunders; 1992:443-471.

35. Maroudas A. **Physicochemical properties of articular cartilage.** In: Freedman MAR, ed. Adult articular cartilage. 2nd ed. Kent, England: Pitman Medical. 215-290, 1979.

36. Maroudas A. and Evans H. **A Study of Ionic Equilibria in Cartilage.** Connective Tissue Research. 1:69-77, 1972.

37. Maroudas A, Muir H, Wingham J. **The correlation of fixed negative charge with glycosaminoglycan content of human articular cartilage.** Biochimica et Biophysica Acta.177:492-500, 1969.

38. Mow V.C. Gibbs M.C. Lai W.M. Zhu W.B. Athanasiou K.A. **Biphasic indentation of articular cartilage II. A numerical algorithm and an experimental study.** Journal of Biomechanics. 22: 853-61, 1989.

39. Nimer E. Schneiderman R. Maroudas A. **Diffusion and partition of solutes in cartilage under static load**. Biophysical Chemistry.106:125-46, 2003.

40. Obenauer J. **Scansite Molecular Weight and Isoelectric Point Calculator**. Massachusetts Institute of Technology. 1 July 2003. <http://scansite.mit.edu/ >

41. Plonsey R. Fleming D.G. **Bioelectric Phenomena**. McGraw-Hill, Inc., New York, 1969.

42. Putnam C. **Protein Calculator v3.3**. 28 March 2006. <http://www.scripps.edu/~cdputnam/protcalc.html>

43. Recht M.P. Goodwin D.W. Winalski C.S. White L.M. **MRI of articular cartilage: revisiting current status and future directions.** American Journal of Roentgenology. 185:899-914, 2005.

44. Saarakkala S. Korhonen R.K. Laasanen M.S. Toyras J. Rieppo J. Jurvelin J.S. **Mechano-acoustic determination of young's modulus of articularcartilage.** Biorheology. 41:167-79, 2004.

45. Saarakkala S. Laasanen M.S. Toyras J. Jurvelin J.S. **Quantitative ultrasound imaging detects degenerative changes in articular cartilage surface and subchondral bone.** Physics in Medicine & Biology. 51:5333-46, 2006.

46. Sasaki M, Shibata E. Kanbara Y. Ehara S. **Enhancement effects and Relaxivities of Gadolinium-DTPA at 1.5 versus 3 Tesla: A Phantom Study**. Magnetic Resonance in Medical Science. 4: 145-49, 2005.

47. Schenk, R.K., Eggli, P.S. and Hunziker, E.B. Biosynthesis of Cartilage Proteoglycans. In: **Articular Cartilage Biochemistry** (Kuettner K.E. Schleyerbach R. Hascall V.C. (eds) Raven Press, New York. 93–113, 1986.

48. Stanisz G.J. Henkelman R.M. **Gd-DTPA relaxivity depends on macromolecular content.** Magnetic Resonance in Medicine. 44:665-7, 2000.

49. Stanisz G. J. Odrobina E.E. Pun J. Escaravage M. Graham S.J. Bronskill M.J. Henkelman M. **T1, T2 Relaxation and Magnetization Transfer in Tissue at 3T**. Magnetic Resonance in Medicine. 54:507-12, 2005.

50. Sun D.D. Guo X.E. Likhitpanichkul M. Lai W.M. Mow V.C. **The influence of the fixed negative charges on mechanical and electrical behaviors of articular cartilage under unconfined compression**. Journal of Biomechanical Enginering.126:6-16, 2004.

51. Taylor C. Carballido-Gamio J. Majundar S. Li X. **Comparison of quantitative imaging of cartilage for osteoarthritis: T2, T1ρ, dGEMRIC and contrast-enhanced computed tomography.** Magnetic Resonance Imaging. 27: 779 – 84, 2009.

52. VamBreuseghem I. Bosmans HTC. Elst LV. **T2 mapping of human articular cartilage with turbo mixed MRI at 1.5 T.** Radiology. 233: 609-14, 2004.

53. Winalski C.S. Shortkroff S. Mulkern R.V. Schneider E. Rosen G.M. **Magnetic resonance relaxivity of dendrimer-linked nitroxides.** Magnetic Resonance in Medicine. 48:965-72, 2002.

54. ZhengShu X. Prestwich G.D. Therapeutic Biomaterials from Chemically Modified Hyaluronan. In: **Chemistry and Biology of Hyaluronan** (Garg H.G. Hales C.A. (eds) Elsevier, California. 475-494, 2004.

APPENDIX A

Tyramine-Based Hydrogels Synthesis and Characterization

A.1 Introduction

This appendix provides in detail the fundamental methods utilized to formulate and characterized the tyramine-based hydrogels that were evaluated through the various experiments conducted in this dissertation work.

A.2 Synthesis of Tyramine-Substituted Hyaluronan (TS-HA) and Gelatin (TS-GE)

The TS-HA used in our experiments was provided by Lifecore Biomedical Inc. (LCBM), using their proprietary manufacturing process that is based on the procedure described below. LCBM has licensed the tyramine-based hydrogel technology from the Cleveland Clinic with the license including exclusive rights to their manufacture. Obtaining a single lot of TS-HA from LCBM provided us the opportunity to conduct our experiments with materials identical to those that will be used for future animal and clinical work. The TS-GE was formulated in our laboratory using the protocol described below and made as one single preparation.

HA (Acros, Pittsburgh, PA; MW = ~1,500,000 daltons) or GE (Sigma, St. Louis, MO; 300 bloom) at 5 mg/ml were dispersed in 250 mM 2-(N-morpholino) ethanesulfonic acid (MES), 75 mM NaOH, 150 mM NaCl, pH 6.5 containing a 2 fold molar excess of tyramine to the moles of carboxyl groups. Substitution of tyramine commenced with the addition of a 10 fold molar amount of 1-ethyl-3-(3-dimethylaminopropyl) carbodiimide (EDC), to the moles of carboxyl group. The

catalyst was a 1/10th molar ratio of N-hydroxysuccinimide (NHS) to the EDC. The substitution reactions were done stirring continuously at room temperature for 24 hours, resulting in production of either TS-HA or TS-GE, which were purified through dialysis versus 150 mM NaCl and then ultrapure water. Lastly, the dialyzed TS-HA and TS-GE were lyophilized, followed by re-suspension to the desired working concentrations in ultra-purified water. For the making of composite materials, the process is exactly the same as described above, except that the TS-HA and TS-GE being mixed together, lyophilized and re-suspended to the desired concentrations.

A.3 Formation of Tyramine-Based Hyaluronan (TB-HA) and Gelatin (TB GE) Hydrogels

Lyophilized TS-HA or TS-GE was dissolved at the corresponding concentrations in ultra-purified water containing 10 U/ml of type II horseradish peroxidase (HRP). The solution was thoroughly mixed by vortex, and allowed to fully hydrate for 24 h at 4ºC in the case of TS-HA, and at 37ºC in the case of TS-GE, so as to fully melt and hydrate the gelatin. Cross-linking to TB-HA hydrogels from various TS-HA solutions containing HRP commenced by introduction of 40 µl of 0.3% hydrogen peroxide (H_2O_2) per 1 ml of TS-HA, followed by centrifugation of the solution at 12,000 rpm for 5 min. The formation of TB-GE hydrogels followed the same steps as for TB-HA, except that the samples are kept cold on ice to promote gellation, as it facilitates diffusion of the H_2O_2 through the material. This method of cross-linking relies on the ability of H_2O_2 to diffuse throughout the

entire volume of the material, which is limited by the concentration and volume of the material as described in **Chapter III**. Therefore, only the lower end (6.25 and 12.5 mg/ml) concentrations were cross-linked using this method. The TB-HA and TB-GE hydrogels at 25, 50 and 100 mg/ml as well as the TB-CO at 6.25, 12.5, 25, 50 and 100 mg/ml were cross-linked using the dual syringe/needle injector device described in **Chapter II**.

A.4 Characterization of TB-HA and TB-GE

To validate the samples' characteristics, the molar concentration of total carboxyl groups and the percent tyramine substitution in the HA materials were measured spectrophotometrically. Amino Acid Analysis (AAA) using Cation Exchange Chromatography measured the molar concentration of total carboxyl groups and tyramine in the GE materials. The details of these analyses are provided below. Additionally, the formation of dityramine cross-links was assessed through their fluorescence properties.

A.4.1 Measurement of Percent Tyramine Substitution and Molar Concentration of TS-HA and TS-GE

The amount of tyramine covalently bound within a TS-HA was calculated by measuring the tyramine absorption at 275 nm of a 1mg/ml TS-HA solution in ultrapure water based on hexuronic acid assay **[9]** by means of SpectraMax Plus Spectrophotometer (Molecular Devices, Inc.)**.** The absorbance measured was compared relative to a tyramine standard curve consisting of 20, 40, 60, 80 and

100 µg/ml of tyramine in ultrapure water. The percent tyramine substitution within a TS-HA solution was then calculated from the molar ratio of covalently bound tyramine residues to total carboxyl groups on HA, based on hexuronic acid assay **[9].** The molar concentration of total carboxyl groups in a TS-HA formulation was also measured spectrophotometrically using the hexuronic acid assay routinely used for quantification of µg quantities of GAG. The hexuronic acid was performed in concentrated sulfuric acid and heating to 100^{o}C , which allows measurement of even those carboxyl groups on glcA residues that are amide bonded to tyramine because of the acid labile nature of the amide bond.

The amount of tyramine covalently bound within a TS-GE and the molar concentration of total carboxyl groups in a TS-GE was calculated through the recovery of nanomoles of amino acids obtained from Amino Acid Analysis (AAA) utilizing Cation Exchange Chromatography at the University of Oklahoma, Molecular Biology-Proteomics Facility. The AAA procedure consisted in two main sequences:

Standard Amino Acid Chromatography

For the common amino acids elution was accomplished by a two buffer system (program name: AAA-REG). Samples were injected onto the column equilibrated with 0.2 N sodium citrate, pH 3.28 with this buffer eluting the first nine amino acids. Next, 1.0 N NaCl, pH 7.4 was used to elute the remaining amino acids. Amino acids were detected by on-line post column reaction with ninhydrin. Derivatized amino acids were quantified by their absorption at 570 nm, except for

glutamic acid and proline, which are detected at 440 nm. This procedure was performed on an automated Beckman Gold HPLC amino acid analyzer system.

Tyramine Chromatography

Elution of tyramine required a much more aggressive buffer system (program name: AAA-TYRA). Again a two solvent system-step elution was utilized. The first solvent is 0.3 M sodium chloride, 0.2 N sodium citrate, pH 5.55 with 5.5% ethanol at a column temperature of 66°C. This eluted most amino acids, including arginine. The second solvent consists of 2.6 M sodium chloride, 0.2 N sodium citrate, pH 5.73 with 2.5% ethanol and 9.0% isopropanol. This solvent eluted any polyamines and tyramine. The column temperature during this solvent step was 73°C.

Each sample was run under both chromatography conditions. The data from each chromatographic run was normalized using the recovery of arginine.

A.4.2 Detection of Dityramine Cross-links

Similar to tyramine, the dityramine cross-links also have advantageous spectrophotometric properties in that dityramine bridges fluoresce blue-green upon exposure to UV light with an excitation maximum of 285 nm and emission of 415 nm. This property was used to assess the degree of cross-linking within TB-hydrogels. Subsequently, all of the TB-HA and TB-GE hydrogels made through out this research were exposed to UV light right after addition of the hydrogen peroxide to initiate cross-linking and centrifugation of the samples. This

step served to verify that cross-linking had proceeded uniformly throughout the entire hydrogel volume as evidence of full cross-linking.

A.5 Equilibration of Hydrogels in Saline

While the uncross-linked samples were made by rehydration directly in PBS, all of the cross-linked materials (i.e. hydrogels) were first cross-linked in water followed by equilibration in saline. The equilibration process started by first weighing the cross-linked plugs (initial weight) followed by addition of a volume of 10X PBS to the hydrogel plug sufficient to produce a 1X PBS concentration after equilibration at 4ºC for 24 h. Afterward; the plugs were removed from the cryotubes, blotted dry and weighted again (final weight). The percent changes and new concentrations were calculated, assessing the shrinking and swelling effects. This data was utilized to produce a standard curve that allowed determining the starting concentration required to obtain the desired or final concentration of the material.

APPENDIX - B

Table B- I. T1 and R1, MRI Day 1

Sample	[mg/ml]	T1	1/T1- 1/T1PBS	R1	r^2
HA 6.25	6.25	2556 ± 201	0.00001	0.0025	1
HA 12.5	12.5	2409 ± 139	0.00004		
HA 25	25	2167 ± 176	0.00008		
HA 50	50	2011 ± 79	0.00012		
HA 100	100	1573 ± 86	0.00026		
Sample	[mg/ml]	T1	1/T1- 1/T1PBS	R1	r^2
GE 6.25	6.25	2486 ± 213	0.00002	0.0023	0.99
GE 12.5	12.5	2370 ± 154	0.00004		
GE 25	25	2111 ± 108	0.00010		
GE 50	50	2011 ± 109	0.00012		
GE 100	100	1612 ± 149	0.00024		
Sample	Weight %	T1	1/T1- 1/T1PBS	R1	r^2
Agar 0.5	0.5	2469 ± 162	0.00003	0.0182	0.87
Agar 1	1	2288 ± 220	0.00006		
Agar 2	2	2243 ± 166	0.00007		
Agar 4	4	2174 ± 176	0.00008		
Sample	[mM]	T1	1/T1- 1/T1PBS	R1	r^2
Gd 0.125	0.125	1036 ± 30	0.00059	4.92	1
Gd 0.25	0.25	634 ± 13	0.00120		
Gd 0.5	0.5	352 ± 7	0.00246		
Gd 1	1	189 ± 4	0.00491		
Gd 2	2	98 ± 3	0.00983		

[1] All Samples in water

[2] $T1_{PBS}$ value on this imaging day was 2613.5± 231

Table B- II. T2 (15 msec echo spacing) and R2, MRI Day 1

Sample	[mg/ml]	T2	1/T2- 1/T2PBS	R2	r^2
HA 6.25	6.25	1214 ± 43	0.0001	0.028	1
HA 12.5	12.5	1054 ± 21	0.0003		
HA 25	25	822 ± 17	0.0005		
HA 50	50	537 ± 8	0.0012		
HA 100	100	289 ± 5	0.0028		
Sample	[mg/ml]	T2	1/T2- 1/T2PBS	R2	r^2
GE 6.25	6.25	1341 ± 30	0.0001	0.016	0.99
GE 12.5	12.5	1222 ± 28	0.0001		
GE 25	25	1035 ± 27	0.0003		
GE 50	50	832 ± 12	0.0005		
GE 100	100	441 ± 65	0.0016		
Sample	Weight %	T2	1/T2- 1/T2PBS	R2	r^2
Agar 0.5	0.5	267 ± 2	0.0031	6.23	1
Agar 1	1	149 ± 2	0.0060		
Agar 2	2	79 ± 2	0.0120		
Agar 4	4	39 ± 2	0.0250		
Sample	[mM]	T2	1/T2- 1/T2PBS	R2	r^2
Gd 0.125	0.125	739 ± 10	0.0007	5.49	1
Gd 0.25	0.25	480 ± 7	0.0014		
Gd 0.5	0.5	285 ± 3	0.0028		
Gd 1	1	158 ± 1	0.0057		
Gd 2	2	86 ± 1	0.0110		

[1] All Samples in water

[2] $T2_{PBS}$ value on this imaging day was 1483.5±36.5

Table B – III. T2 (30 msec echo spacing) and R2, MRI Day 1

Sample	[mg/ml]	T2	1/T2- 1/T2PBS	R2	r^2
HA 6.25	6.25	1204 ± 23	0.0002	0.029	1
HA 12.5	12.5	1016 ± 15	0.0003		
HA 25	25	778 ± 17	0.0006		
HA 50	50	512 ± 8	0.0013		
HA 100	100	277 ± 7	0.0029		
Sample	[mg/ml]	T2	1/T2- 1/T2PBS	R2	r^2
GE 6.25	6.25	1318 ± 20	0.0001	0.015	0.99
GE 12.5	12.5	1190 ± 22	0.0002		
GE 25	25	1007 ± 14	0.0003		
GE 50	50	819 ± 12	0.0006		
GE 100	100	449 ± 67	0.0016		
Sample	Weight %	T2	1/T2- 1/T2PBS	R2	r^2
Agar 0.5	0.5	273 ± 4	0.0030	6.06	1
Agar 1	1	158 ± 4	0.0057		
Agar 2	2	85 ± 6	0.0111		
Agar 4	4	40 ± 7	0.0243		
Sample	[mM]	T2	1/T2- 1/T2PBS	R2	r^2
Gd 0.125	0.125	733 ± 7	0.0007	5.14	1
Gd 0.25	0.25	478 ± 5	0.0014		
Gd 0.5	0.5	296 ± 3	0.0027		
Gd 1	1	169 ± 3	0.0052		
Gd 2	2	91 ± 3	0.0103		

[1] All Samples in water

[2] $T2_{PBS}$ value on this imaging day was 1496±21.5

Table B - IV. T1 and R1 for Unsubstituted Materials, MRI Day 2

Sample	[mg/ml]	T1	1/T1- 1/T1PBS	R1	r^2
HA 6.25	6.25	2194 ± 128	0.00003	0.0023	1
HA 12.5	12.5	2198 ± 147	0.00003		
HA 25	25	2058 ± 144	0.00006		
HA 50	50	1856 ± 97	0.00011		
HA 100	100	1519 ± 55	0.00023		
Sample	[mg/ml]	T1	1/T1- 1/T1PBS	R1	r^2
GE 6.25	6.25	2335 ± 122	0.00000	0.0026	0.99
GE 12.5	12.5	2166 ± 130	0.00004		
GE 25	25	2085 ± 130	0.00005		
GE 50	50	1937 ± 152	0.00009		
GE 100	100	1441 ± 125	0.00027		
Sample	[mg/ml]	T1	1/T1- 1/T1PBS	R1	r^2
CO 6.25	12.5	2226 ± 129	0.00002	0.0027	0.97
CO 12.5	25	2056 ± 194	0.00006		
CO 25	50	2016 ± 140	0.00007		
CO 50	100	1497 ± 133	0.00024		
CO 100	200	1050 ± 253	0.00053		

[1] $T1_{PBS}$ value on this imaging day was 2346.25±124

Table B – V. T1 and R1 for Tyramine - Substituted Materials and Magnevist (Gd), MRI Day 2

Sample	[mg/ml]	T1	1/T1- 1/T1PBS	R1	r^2
TS-HA 6.25	6.25	2282 ± 156	0.00001	0.0026	1
TS-HA 12.5	12.5	2104 ± 128	0.00005		
TS-HA 25	25	2004 ± 122	0.00007		
TS-HA 50	50	1800 ± 131	0.00013		
TS-HA 100	100	1458 ± 58	0.00026		
Sample	[mg/ml]	T1	1/T1- 1/T1PBS	R1	r^2
TS-GE 6.25	6.25	2272 ± 131	0.00001	0.0016	1
TS-GE 12.5	12.5	2173 ± 177	0.00003		
TS-GE 25	25	2100 ± 183	0.00005		
TS-GE 50	50	1947 ± 151	0.00009		
TS-GE 100	100	1695 ± 127	0.00016		
Sample	[mM]	T1	1/T1- 1/T1PBS	R1	r^2
Gd 0.125	0.125	910 ± 26	0.0007	5.23	1
Gd 0.25	0.25	553 ± 14	0.0014		
Gd 0.5	0.5	312 ± 6	0.0028		
Gd 1	1	169 ± 3	0.0055		
Gd 2	2	92 ± 2	0.0104		

[1] $T1_{PBS}$ value on this imaging day was 2346.25±124

Table B – VI. T1 and R1 for Cross-linked Materials and Agar, MRI Day 2

Sample	[mg/ml]	T1	1/T1- 1/T1PBS	R1	r^2
TB-HA 6.25	6.3	2220 ± 168	0.00002	0.0029	1
TB-HA 12.5	12.5	2048 ± 177	0.00006		
TB-HA 25	25.3	1983 ± 142	0.00008		
TB-HA 50	50	1754 ± 108	0.00014		
TB-HA 100	100	1366 ± 66	0.00031		
Sample [1]	[mg/ml]	T1	1/T1- 1/T1PBS	R1	r^2
TB- GE 6.25	6.25	2215 ± 161	0.00003	0.0020	0.98
TB-GE 12.5	12.5	2096 ± 141	0.00005		
TB-GE 25	25	2051 ± 140	0.00006		
TB-GE 50	50	1765 ± 89	0.00014		
TB-GE 100	100	1593 ± 152	0.00020		
Sample	Weight %	T1	1/T1- 1/T1PBS	R1	r^2
Agar 0.5	0.5	2295 ± 156	0.00001	0.0164	0.99
Agar 1	1	2210 ± 123	0.00003		
Agar 2	2	2130 ± 135	0.00004		
Agar 4	4	1902 ± 134	0.00010		

[1] All Samples in water

[2] $T1_{PBS}$ value on this imaging day was 2346.25±124

[2] $T1_{water}$ value on this imaging day was 2397±123

Table B – VII. T2 (15 msec echo spacing) and R2 for Unsubstituted Materials, MRI Day 2

Sample	[mg/ml]	T2	1/T2- 1/T2PBS	R2	r^2
HA 6.25	6.25	1160 ± 39	0.00015	0.026	1
HA 12.5	12.5	1027 ± 36	0.00026		
HA 25	25	810 ± 21	0.00052		
HA 50	50	532 ± 18	0.00117		
HA 100	100	299 ± 6	0.00263		
Sample	[mg/ml]	T2	1/T2- 1/T2PBS	R2	r^2
GE 6.25	6.25	1255 ± 36	0.00009	0.020	0.97
GE 12.5	12.5	1178 ± 36	0.00014		
GE 25	25	1025 ± 30	0.00026		
GE 50	50	819 ± 77	0.00051		
GE 100	100	368 ± 64	0.00201		
Sample	[mg/ml]	T2	1/T2- 1/T2PBS	R2	r^2
CO 6.25	12.5	1229 ± 57	0.00010	0.046	1
CO 12.5	25	910 ± 112	0.00039		
CO 25	50	609 ± 17	0.00093		
CO 50	100	320 ± 30	0.00241		
CO 100	200	100 ± 13	0.00929		

[1] $T2_{PBS}$ value on this imaging day was 1405.25±53.5

Table B – VIII. T2 (15 msec echo spacing) and R2 for Tyramine - Substituted Materials and Magnevist (Gd), MRI Day 2

Sample	[mg/ml]	T2	1/T2- 1/T2PBS	R2	r^2
TS-HA 6.25	6.25	1245 ± 58	0.00009	0.028	0.99
TS-HA 12.5	12.5	1066 ± 39	0.00023		
TS-HA 25	25	839 ± 35	0.00048		
TS-HA 50	50	552 ± 15	0.00110		
TS-HA 100	100	282 ± 10	0.00283		
Sample	[mg/ml]	T2	1/T2- 1/T2PBS	R2	r^2
TS-GE 6.25	6.25	1254 ± 51	0.00009	0.014	0.99779
TS-GE 12.5	12.5	1122 ± 26	0.00018		
TS-GE 25	25	987 ± 23	0.00030		
TS-GE 50	50	754 ± 31	0.00061		
TS-GE 100	100	476 ± 22	0.00139		
Sample	[mM]	T2	1/T2- 1/T2PBS	R2	r^2
Gd 0.125	0.125	705 ± 23	0.0007	5.84	1
Gd 0.25	0.25	462 ± 13	0.0015		
Gd 0.5	0.5	272 ± 10	0.0030		
Gd 1	1	149 ± 3	0.0060		
Gd 2	2	81 ± 2	0.0116		

[1] $T2_{PBS}$ value on this imaging day was 1405.25±53.5

Table B – IX. T2 (15 msec echo spacing) and R2 for Cross - linked Materials and Agar, MRI Day 2

Sample	[mg/ml]	T2	1/T2- 1/T2PBS	R2	r^2
TB-HA 6.25	6.3	1114 ± 44	0.00019	0.044	0.97
TB-HA 12.5	12.5	914 ± 160	0.00038		
TB-HA 25	25.3	744 ± 52	0.00063		
TB-HA 50	50	514 ± 45	0.00123		
TB-HA 100	100	198 ± 16	0.00434		
Sample [1]	[mg/ml]	T2	1/T2- 1/T2PBS	R2	r^2
TB- GE 6.25	6.25	1183 ± 22	0.00017	0.014	0.99
TB-GE 12.5	12.5	1269 ± 30	0.00011		
TB-GE 25	25	1048 ± 36	0.00028		
TB-GE 50	50	690 ± 48	0.00077		
TB-GE 100	100	483 ± 75	0.00139		
Sample	Weight %	T2	1/T2- 1/T2PBS	R2	r^2
Agar 0.5	0.5	280 ± 8	0.0029	5.93	1
Agar 1	1	156 ± 3	0.0057		
Agar 2	2	81 ± 2	0.0116		
Agar 4	4	41 ± 2	0.0237		

[1] All Samples in water

[2] $T2_{PBS}$ value on this imaging day was 1405.25±53.5

[2] $T2_{water}$ value on this imaging day was 1475 ± 32

Table B – X. T2 (30 msec echo spacing) and R2 for Unsubstituted Materials, MRI Day 2

Sample	[mg/ml]	T2	1/T2- 1/T2PBS	R2	r^2
HA 6.25	6.25	1183 ± 34	0.00017	0.028	1
HA 12.5	12.5	1027 ± 25	0.00029		
HA 25	25	800 ± 25	0.00057		
HA 50	50	509 ± 13	0.00129		
HA 100	100	286 ± 8	0.00282		
Sample	[mg/ml]	T2	1/T2- 1/T2PBS	R2	r^2
GE 6.25	6.25	1302 ± 31	0.00009	0.020	0.97
GE 12.5	12.5	1219 ± 25	0.00014		
GE 25	25	1046 ± 22	0.00028		
GE 50	50	816 ± 56	0.00055		
GE 100	100	363 ± 58	0.00208		
Sample	[mg/ml]	T2	1/T2- 1/T2PBS	R2	r^2
CO 6.25	12.5	1246 ± 41	0.00012	0.048	0.97
CO 12.5	25	911 ± 106	0.00042		
CO 25	50	603 ± 19	0.00098		
CO 50	100	309 ± 25	0.00256		
CO 100	200	98 ± 11	0.00953		

[1] $T2_{PBS}$ value on this imaging day was 1472.75±50

Table B – XI. T2 (30 msec echo spacing) and R2 for Tyramine – Substituted Materials and Magnevist (Gd), MRI Day 2

Sample	[mg/ml]	T2	1/T2- 1/T2PBS	R2	r^2
TS-HA 6.25	6.25	1295 ± 49	0.00009	0.031	0.99
TS-HA 12.5	12.5	1064 ± 24	0.00026		
TS-HA 25	25	832 ± 30	0.00052		
TS-HA 50	50	527 ± 14	0.00122		
TS-HA 100	100	266 ± 11	0.00308		
Sample	[mg/ml]	T2	1/T2- 1/T2PBS	R2	r^2
TS-GE 6.25	6.25	1316 ± 31	0.00008	0.014	1
TS-GE 12.5	12.5	1171 ± 29	0.00017		
TS-GE 25	25	1024 ± 26	0.00030		
TS-GE 50	50	769 ± 29	0.00062		
TS-GE 100	100	483 ± 17	0.00139		
Sample	[mM]	T2	1/T2- 1/T2PBS	R2	r^2
Gd 0.125	0.125	735 ± 23	0.0007	5.78	1
Gd 0.25	0.25	473 ± 10	0.0014		
Gd 0.5	0.5	278 ± 8	0.0029		
Gd 1	1	153 ± 4	0.0059		
Gd 2	2	82 ± 4	0.0115		

[1] $T2_{PBS}$ value on this imaging day was 1472.75±50

Table B – XII. T2 (30 msec echo spacing) and R2 for Cross – Linked Materials and Agar, MRI Day 2

Sample	[mg/ml]	T2	1/T2- 1/T2PBS	R2	r^2
TB-HA 6.25	6.3	1124 ± 42	0.00021	0.048	0.98
TB-HA 12.5	12.5	907 ± 182	0.00042		
TB-HA 25	25.3	719 ± 54	0.00071		
TB-HA 50	50	488 ± 41	0.00137		
TB-HA 100	100	183 ± 19	0.00479		
Sample [1]	[mg/ml]	T2	1/T2- 1/T2PBS	R2	r^2
TB- GE 6.25	6.25	1233 ± 35	0.00018	0.015	0.99
TB-GE 12.5	12.5	1320 ± 34	0.00013		
TB-GE 25	25	1069 ± 32	0.00030		
TB-GE 50	50	698 ± 51	0.00080		
TB-GE 100	100	477 ± 70	0.00146		
Sample	Weight %	T2	1/T2- 1/T2PBS	R2	r^2
Agar 0.5	0.5	275 ± 6	0.0030	6.25	1
Agar 1	1	154 ± 5	0.0058		
Agar 2	2	79 ± 4	0.0120		
Agar 4	4	39 ± 5	0.0250		

[1] All Samples in water

[2] $T2_{PBS}$ value on this imaging day was 1472.75±50

[2] $T2_{water}$ value on this imaging day was 1582 ± 22

Table B - XIII. T1 and R1 for Unsubstituted Materials, MRI Day 3

Sample	[mg/ml]	T1	1/T1- 1/T1PBS	R1	r^2
HA 6.25	6.25	2183 ± 122	0.00004	0.0031	0.99
HA 12.5	12.5	2039 ± 139	0.00008		
HA 25	25	1957 ± 69	0.00010		
HA 50	50	1696 ± 75	0.00018		
HA 100	100	1342 ± 16	0.00033		
Sample	[mg/ml]	T1	1/T1- 1/T1PBS	R1	r^2
GE 6.25	6.25	2385 ± 145	0.00000	0.0027	1
GE 12.5	12.5	2318 ± 123	0.00002		
GE 25	25	2177 ± 108	0.00004		
GE 50	50	1840 ± 79	0.00013		
GE 100	100	1487 ± 105	0.00026		
Sample	[mg/ml]	T1	1/T1- 1/T1PBS	R1	r^2
CO 6.25	12.5	2193 ± 117	0.00004	0.0028	0.99
CO 12.5	25	1953 ± 134	0.00010		
CO 25	50	1946 ± 143	0.00010		
CO 50	100	1415 ± 126	0.00029		
CO 100	200	1026 ± 136	0.00056		

[1] $T1_{PBS}$ value on this imaging day was 2412±148.75

Table B – XIV. T1 and R1 for Tyramine - Substituted Materials and Magnevist (Gd), MRI Day 3

Sample	[mg/ml]	T1	1/T1- 1/T1PBS	R1	r^2
TS-HA 6.25	6.25	2208 ± 133	0.00004	0.0035	1
TS-HA 12.5	12.5	2114 ± 128	0.00006		
TS-HA 25	25	1904 ± 68	0.00011		
TS-HA 50	50	1658 ± 71	0.00019		
TS-HA 100	100	1296 ± 26	0.00036		
Sample	[mg/ml]	T1	1/T1- 1/T1PBS	R1	r^2
TS-GE 6.25	6.25	2321 ± 138	0.00002	0.0024	1
TS-GE 12.5	12.5	2335 ± 180	0.00001		
TS-GE 25	25	2130 ± 155	0.00005		
TS-GE 50	50	1916 ± 87	0.00011		
TS-GE 100	100	1533 ± 62	0.00024		
Sample	[mM]	T1	1/T1- 1/T1PBS	R1	r^2
Gd 0.03125	0.03125	1703 ± 46	0.00017	5.82	1
Gd 0.0625	0.0625	1229 ± 38	0.00040		
Gd 0.125	0.125	839 ± 15	0.00078		
Gd 0.25	0.25	509 ± 14	0.00155		
Gd 0.5	0.5	297 ± 7	0.00295		
Gd 1	1	158 ± 4	0.00591		
Gd 2	2	83 ± 2	0.01163		

[1] $T1_{PBS}$ value on this imaging day was 2412±148.75

Table B – XV. T1 and R1 for Cross-linked Materials and Agar, MRI Day 3

Sample	[mg/ml]	T1	1/T1- 1/T1PBS	R1	r^2
TB-HA 6.25	6.3	2241 ± 183	0.00003	0.0037	1
TB-HA 12.5	12.5	2034 ± 137	0.00008		
TB-HA 25	25.3	1868 ± 82	0.00012		
TB-HA 50	50	1633 ± 43	0.00020		
TB-HA 100	100	1251 ± 72	0.00038		
Sample [1]	[mg/ml]	T1	1/T1- 1/T1PBS	R1	r^2
TB- GE 6.25	6.25	2273 ± 144	0.00002	0.0030	0.99
TB-GE 12.5	12.5	2211 ± 135	0.00004		
TB-GE 25	25	2044 ± 154	0.00007		
TB-GE 50	50	1666 ± 59	0.00018		
TB-GE 100	100	1403 ± 125	0.00030		
Sample	Weight %	T1	1/T1- 1/T1PBS	R1	r^2
Agar 0.5	0.5	2469 ± 162	0.00003	0.03	0.99
Agar 1	1	2288 ± 220	0.00003		
Agar 2	2	2243 ± 166	0.00008		
Agar 4	4	2174 ± 176	0.00012		

[1] All Samples in water

[2] $T1_{PBS}$ value on this imaging day was 2412±148.75

Table B – XVI. T2 (15 msec echo spacing) and R2 for Unsubstituted Materials, MRI Day 3

Sample	[mg/ml]	T2	1/T2- 1/T2PBS	R2	r^2
HA 6.25	6.25	1192 ± 18	0.00010	0.021	1
HA 12.5	12.5	1075 ± 21	0.00019		
HA 25	25	870 ± 24	0.00041		
HA 50	50	600 ± 17	0.00093		
HA 100	100	353 ± 9	0.00209		
Sample	[mg/ml]	T2	1/T2- 1/T2PBS	R2	r^2
GE 6.25	6.25	1226 ± 25	0.00008	0.016	0.98
GE 12.5	12.5	1160 ± 35	0.00012		
GE 25	25	1026 ± 20	0.00024		
GE 50	50	790 ± 32	0.00053		
GE 100	100	426 ± 45	0.00161		
Sample	[mg/ml]	T2	1/T2- 1/T2PBS	R2	r^2
CO 6.25	12.5	1154 ± 44	0.00013	0.044	0.97
CO 12.5	25	848 ± 101	0.00044		
CO 25	50	599 ± 17	0.00093		
CO 50	100	314 ± 22	0.00245		
CO 100	200	104 ± 10	0.00888		

[1] $T2_{PBS}$ value on this imaging day was 1352.5 ±28

Table B – XVII. T2 (15 msec echo spacing) and R2 for Tyramine - Substituted Materials and Magnevist (Gd), MRI Day 3

Sample	[mg/ml]	T2	1/T2- 1/T2PBS	R2	r^2
TS-HA 6.25	6.25	1208 ± 26	0.00009	0.024	1
TS-HA 12.5	12.5	1070 ± 27	0.00020		
TS-HA 25	25	851 ± 15	0.00044		
TS-HA 50	50	587 ± 12	0.00096		
TS-HA 100	100	323 ± 8	0.00236		
Sample	[mg/ml]	T2	1/T2- 1/T2PBS	R2	r^2
TS-GE 6.25	6.25	1200 ± 28	0.00009	0.016	1
TS-GE 12.5	12.5	1100 ± 21	0.00017		
TS-GE 25	25	942 ± 19	0.00032		
TS-GE 50	50	705 ± 20	0.00068		
TS-GE 100	100	423 ± 8	0.00162		
Sample	[mM]	T2	1/T2- 1/T2PBS	R2	r^2
Gd 0.03125	0.03125	1142 ± 20	0.00014	6.62	1
Gd 0.0625	0.0625	931 ± 14	0.00033		
Gd 0.125	0.125	691 ± 15	0.00071		
Gd 0.25	0.25	453 ± 11	0.00147		
Gd 0.5	0.5	257 ± 6	0.00315		
Gd 1	1	137 ± 4	0.00656		
Gd 2	2	72 ± 3	0.01315		

[1] $T2_{PBS}$ value on this imaging day was 1352.5 ±28

Table B – XVIII. T2 (15 msec echo spacing) and R2 for Cross - linked Materials and Agar, MRI Day 3

Sample	[mg/ml]	T2	1/T2- 1/T2PBS	R2	r^2
TB-HA 6.25	6.3	1090 ± 26	0.00018	0.033	0.98
TB-HA 12.5	12.5	912 ± 129	0.00036		
TB-HA 25	25.3	743 ± 30	0.00061		
TB-HA 50	50	551 ± 17	0.00108		
TB-HA 100	100	244 ± 19	0.00336		
Sample [1]	[mg/ml]	T2	1/T2- 1/T2PBS	R2	r^2
TB- GE 6.25	6.25	1164 ± 29	0.00018	0.014	0.99
TB-GE 12.5	12.5	1249 ± 35	0.00012		
TB-GE 25	25	1018 ± 17	0.00030		
TB-GE 50	50	684 ± 30	0.00078		
TB-GE 100	100	477 ± 72	0.00142		
Sample	Weight %	T2	1/T2- 1/T2PBS	R2	r^2
Agar 0.5	0.5	310 ± 7	0.0025	5.26	1
Agar 1	1	173 ± 3	0.0050		
Agar 2	2	91 ± 2	0.0102		
Agar 4	4	46 ± 2	0.0210		

[1] All Samples in water

[2] $T2_{PBS}$ value on this imaging day was 1352.5 ±28

Table B – XIX. T2 (30 msec echo spacing) and R2 for Unsubstituted Materials, MRI Day 3

Sample	[mg/ml]	T2	1/T2- 1/T2PBS	R2	r^2
HA 6.25	6.25	1223 ± 22	0.00012	0.023	1
HA 12.5	12.5	1091 ± 26	0.00021		
HA 25	25	865 ± 26	0.00045		
HA 50	50	570 ± 12	0.00105		
HA 100	100	330 ± 10	0.00233		
Sample	[mg/ml]	T2	1/T2- 1/T2PBS	R2	r^2
GE 6.25	6.25	1286 ± 17	0.00008	0.016	0.98
GE 12.5	12.5	1218 ± 29	0.00012		
GE 25	25	1054 ± 15	0.00025		
GE 50	50	806 ± 42	0.00054		
GE 100	100	432 ± 46	0.00161		
Sample	[mg/ml]	T2	1/T2- 1/T2PBS	R2	r^2
CO 6.25	12.5	1203 ± 24	0.00013	0.045	0.98
CO 12.5	25	873 ± 90	0.00044		
CO 25	50	599 ± 18	0.00097		
CO 50	100	304 ± 18	0.00259		
CO 100	200	103 ± 8	0.00901		

[1] $T2_{PBS}$ value on this imaging day was 1423.75±24

Table B – XX. T2 (30 msec echo spacing) and R2 for Tyramine – Substituted Materials and Magnevist (Gd), MRI Day 3

Sample	[mg/ml]	T2	1/T2- 1/T2PBS	R2	r^2
TS-HA 6.25	6.25	1252 ± 23	0.00010	0.026	1
TS-HA 12.5	12.5	1071 ± 17	0.00023		
TS-HA 25	25	840 ± 12	0.00049		
TS-HA 50	50	565 ± 14	0.00107		
TS-HA 100	100	301 ± 5	0.00262		
Sample	[mg/ml]	T2	1/T2- 1/T2PBS	R2	r^2
TS-GE 6.25	6.25	1253 ± 18	0.00010	0.016	1
TS-GE 12.5	12.5	1159 ± 17	0.00016		
TS-GE 25	25	981 ± 20	0.00032		
TS-GE 50	50	729 ± 19	0.00067		
TS-GE 100	100	431 ± 10	0.00162		
Sample	[mM]	T2	1/T2- 1/T2PBS	R2	r^2
Gd 0.03125	0.03125	1171 ± 19	0.00015	6.53	1
Gd 0.0625	0.0625	971 ± 20	0.00033		
Gd 0.125	0.125	704 ± 18	0.00072		
Gd 0.25	0.25	451 ± 12	0.00151		
Gd 0.5	0.5	255 ± 7	0.00322		
Gd 1	1	139 ± 5	0.00649		
Gd 2	2	73 ± 5	0.01300		

[1] $T2_{PBS}$ value on this imaging day was 1423.75±24

Table B – XXI. T2 (30 msec echo spacing) and R2 for Cross – Linked Materials and Agar, MRI Day 3

Sample	[mg/ml]	T2	1/T2- 1/T2PBS	R2	r^2
TB-HA 6.25	6.3	1131 ± 26	0.00018	0.036	0.98
TB-HA 12.5	12.5	916 ± 146	0.00039		
TB-HA 25	25.3	733 ± 33	0.00066		
TB-HA 50	50	533 ± 21	0.00117		
TB-HA 100	100	229 ± 15	0.00366		
Sample [1]	[mg/ml]	T2	1/T2- 1/T2PBS	R2	r^2
TB- GE 6.25	6.25	1210 ± 21	0.00019	0.015	0.99
TB-GE 12.5	12.5	1340 ± 62	0.00011		
TB-GE 25	25	1059 ± 32	0.00031		
TB-GE 50	50	693 ± 33	0.00081		
TB-GE 100	100	477 ± 71	0.00146		
Sample	Weight %	T2	1/T2- 1/T2PBS	R2	r^2
Agar 0.5	0.5	307 ± 6	0.0026	5.27	1
Agar 1	1	174 ± 5	0.0050		
Agar 2	2	90 ± 4	0.0104		
Agar 4	4	46 ± 5	0.0210		

[1] All Samples in water

[2] $T2_{PBS}$ value on this imaging day was 1423.75±24

[2] $T2_{water}$ value on this imaging day was 1582 ± 22

Table B - XXII. T1 and R1 for Unsubstituted Materials and Agar, MRI Day 4

Sample	[mg/ml]	T1	1/T1- 1/T1PBS	R1	r^2
HA 6.25	6.25	2553±148	0.00003	0.0029	1.00
HA 12.5	12.5	2436±164	0.00004		
HA 25	25	2238±216	0.00008		
HA 50	50	1968±111	0.00014		
HA 100	100	1507±71	0.00030		
Sample	[mg/ml]	T1	1/T1- 1/T1PBS	R1	r^2
GE 6.25	6.25	2621±120	0.00002	0.0034	0.97
GE 12.5	12.5	2403±122	0.00005		
GE 25	25	2224±122	0.00008		
GE 50	50	2145±276	0.00010		
GE 100	100	1378±75	0.00036		
Sample	[mg/ml]	T1	1/T1- 1/T1PBS	R1	r^2
CO 6.25	12.5	2522±124	0.00003	0.0035	0.99
CO 12.5	25	2174±219	0.00009		
CO 25	50	2288±189	0.00007		
CO 50	100	1448±281	0.00032		
CO 100	200	942±295	0.00070		
Sample	Weight %	T1	1/T1- 1/T1PBS	R1	r^2
Agar 0.5	0.5	2826±169	-0.00001	0.021	0.96
Agar 1	1	2739±154	0.00000		
Agar 2	2	2568±209	0.00002		
Agar 4	4	2264±182	0.00008		

[1] $T1_{PBS}$ value on this imaging day was 2730.2±188.4

Table B – XXIII. T1 and R1 for Tyramine - Substituted Materials and Magnevist (Gd), MRI Day 4

Sample	[mg/ml]	T1	1/T1- 1/T1PBS	R1	r^2
TS-HA 6.25	6.25	2556±161	0.00002	0.0030	1.00
TS-HA 12.5	12.5	2408±166	0.00005		
TS-HA 25	25	2205±125	0.00009		
TS-HA 50	50	1901±63	0.00016		
TS-HA 100	100	1498±50	0.00030		
Sample	[mg/ml]	T1	1/T1- 1/T1PBS	R1	r^2
TS-GE 6.25	6.25	2536±179	0.00003	0.0023	1.00
TS-GE 12.5	12.5	2404±170	0.00005		
TS-GE 25	25	2275±132	0.00007		
TS-GE 50	50	2024±126	0.00013		
TS-GE 100	100	1646±115	0.00024		
Sample	[mg/ml]	T1	1/T1- 1/T1PBS	R1	r^2
TS-CO 6.25	12.5	2495±149	0.00003	0.0042	1.00
TS-CO 12.5	25	2277±91	0.00007		
TS-CO 25	50	1948±116	0.00015		
TS-CO 50	100	1318±61	0.00039		
TS-CO 100	200	836±41	0.00083		
Sample	[mM]	T1	1/T1- 1/T1PBS	R1	r^2
Gd 0.125	0.125	958±28	0.00068	5.31	1.00
Gd 0.25	0.25	573±20	0.00138		
Gd 0.5	0.5	335±8	0.00262		
Gd 1	1	174±15	0.00538		
Gd 2	2	91±5	0.01062		

[1] $T1_{PBS}$ value on this imaging day was 2730.2±188.4

Table B – XXIV. T1 and R1 for Cross-linked Materials, MRI Day 4

Sample	[mg/ml]	T1	1/T1- 1/T1PBS	R1	r^2
TB-HA 6.25	6.3	2509±170	0.00003	0.0034	0.99
TB-HA 12.5	12.5	2284±196	0.00007		
TB-HA 25	25.3	2223±114	0.00008		
TB-HA 50	50	1891±131	0.00016		
TB-HA 100	100	1390±111	0.00035		
Sample [1]	[mg/ml]	T1	1/T1- 1/T1PBS	R1	r^2
TB- GE 6.25	6.25	2479±155	0.00004	0.0028	0.98
TB-GE 12.5	12.5	2344±180	0.00006		
TB-GE 25	25	2133±132	0.00010		
TB-GE 50	50	1765±112	0.00020		
TB-GE 100	100	1529±237	0.00029		
Sample	[mg/ml]	T1	1/T1- 1/T1PBS	R1	r^2
TB- CO 6.25	12.5	2485±106	0.00004	0.0061	0.93
TB-CO 12.5	25	2065±276	0.00012		
TB-CO 25	50	1360±158	0.00037		
TB-CO 50	100	1627±126	0.00025		
TB-CO 100	200	978±38	0.00066		
Sample	[mg/ml]	T1	1/T1- 1/T1PBS	R1	r^2
TB- GE 60	61	1671±114	0.00023	0.0034	0.95
TB-GE 70	71	1541±308	0.00028		
TB-GE 80	79	1749±174	0.00021		
TB-GE 90	91	1443±156	0.00033		

[1] All Samples in water

[2] $T1_{PBS}$ value on this imaging day was 2730.2±188.4

[2] $T1_{water}$ value on this imaging day was 2716±198

Table B – XXV. T2 (15 msec echo spacing) and R2 for Unsubstituted Materials and Agar, MRI Day 4

Sample	[mg/ml]	T2	1/T2- 1/T2PBS	R2	r^2
HA 6.25	6.25	1171±89	0.00013	0.027	1
HA 12.5	12.5	1036±72	0.00024		
HA 25	25	802±22	0.00052		
HA 50	50	512±11	0.00123		
HA 100	100	299±5	0.00262		
Sample	[mg/ml]	T2	1/T2- 1/T2PBS	R2	r^2
GE 6.25	6.25	1259±64	0.00007	0.018	0.98
GE 12.5	12.5	1167±28	0.00013		
GE 25	25	1026±41	0.00025		
GE 50	50	784±53	0.00055		
GE 100	100	390±39	0.00184		
Sample	[mg/ml]	T2	1/T2- 1/T2PBS	R2	r^2
CO 6.25	12.5	1147±20	0.00015	0.051	0.97
CO 12.5	25	892±94	0.00040		
CO 25	50	531±19	0.00116		
CO 50	100	279±43	0.00286		
CO 100	200	91±14	0.01026		
Sample	Weight %	T2	1/T2- 1/T2PBS	R2	r^2
Agar 0.5	0.5	280±11	0.0028	6.62	1
Agar 1	1	150±4	0.0059		
Agar 2	2	76±3	0.0124		
Agar 4	4	37±2	0.0263		

[1] $T2_{PBS}$ value on this imaging day was 1380 ± 61.8

Table B – XXVI. T2 (15 msec echo spacing) and R2 for Tyramine - Substituted Materials and Magnevist (Gd), MRI Day 4

Sample	[mg/ml]	T2	1/T2- 1/T2PBS	R2	r^2
TS-HA 6.25	6.25	1180±25	0.00012	0.029	0.99
TS-HA 12.5	12.5	1031±38	0.00025		
TS-HA 25	25	790±17	0.00054		
TS-HA 50	50	531±15	0.00116		
TS-HA 100	100	273±11	0.00294		
Sample	[mg/ml]	T2	1/T2- 1/T2PBS	R2	r^2
TS-GE 6.25	6.25	1234±100	0.00009	0.016	1
TS-GE 12.5	12.5	1103±25	0.00018		
TS-GE 25	25	935±21	0.00034		
TS-GE 50	50	715±18	0.00067		
TS-GE 100	100	426±14	0.00162		
Sample	[mg/ml]	T2	1/T2- 1/T2PBS	R2	r^2
TS-CO 6.25	12.5	1063±19	0.00022	0.049	0.98
TS-CO 12.5	25	864±20	0.00043		
TS-CO 25	50	607±31	0.00092		
TS-CO 50	100	245±16	0.00336		
TS-CO 100	200	96±14	0.00969		
Sample	[mM]	T2	1/T2- 1/T2PBS	R2	r^2
Gd 0.125	0.125	713±26	0.00068	6.0915781	1
Gd 0.25	0.25	481±14	0.00135		
Gd 0.5	0.5	280±10	0.00285		
Gd 1	1	148±6	0.00603		
Gd 2	2	78±2	0.01210		

[1] $T2_{PBS}$ value on this imaging day was 1380 ± 61.8

Table B – XXVII. T2 (15 msec echo spacing) and R2 for Cross - linked Materials, MRI Day 4

Sample	[mg/ml]	T2	1/T2- 1/T2PBS	R2	r^2
TB-HA 6.25	6.3	1096±38	0.00019	0.030	0.99
TB-HA 12.5	12.5	917±190	0.00037		
TB-HA 25	25.3	745±87	0.00062		
TB-HA 50	50	513±35	0.00122		
TB-HA 100	100	264±257	0.00306		
Sample [1]	[mg/ml]	T2	1/T2- 1/T2PBS	R2	r^2
TB- GE 6.25	6.25	1176±40	0.00021	0.014	0.99
TB-GE 12.5	12.5	1259±28	0.00015		
TB-GE 25	25	1038±44	0.00032		
TB-GE 50	50	711±168	0.00076		
TB-GE 100	100	475±61	0.00146		
Sample	[mg/ml]	T2	1/T2- 1/T2PBS	R2	r^2
TB- CO 6.25	12.5	991±100	0.00028	0.062	0.98
TB-CO 12.5	25	745±126	0.00062		
TB-CO 25	50	417±99	0.00167		
TB-CO 50	100	376±62	0.00193		
TB-CO 100	200	139±62	0.00647		
Sample	[mg/ml]	T2	1/T2- 1/T2PBS	R2	r^2
TB- GE 60	61	579±58	0.00100	0.016	0.97
TB-GE 70	71	506±77	0.00125		
TB-GE 80	79	576±82	0.00101		
TB-GE 90	91	438±35	0.00156		

[1] All Samples in water

[2] $T2_{PBS}$ value on this imaging day was 1380 ± 61.8

[2] $T2_{water}$ value on this imaging day was 1556±103

Table B – XXVIII. T2 (30 msec echo spacing) and R2 for Unsubstituted Materials and Agar, MRI Day 4

Sample	[mg/ml]	T2	1/T2- 1/T2PBS	R2	r^2
HA 6.25	6.25	1177±69	0.00017	0.026	1
HA 12.5	12.5	1027±43	0.00029		
HA 25	25	803±21	0.00056		
HA 50	50	512±11	0.00127		
HA 100	100	302±16	0.00263		
Sample	[mg/ml]	T2	1/T2- 1/T2PBS	R2	r^2
GE 6.25	6.25	1299±27	0.00009	0.019	0.98
GE 12.5	12.5	1196±21	0.00015		
GE 25	25	1040±17	0.00028		
GE 50	50	790±56	0.00058		
GE 100	100	385±51	0.00192		
Sample	[mg/ml]	T2	1/T2- 1/T2PBS	R2	r^2
CO 6.25	12.5	1148±27	0.00019	0.053	0.98
CO 12.5	25	850±116	0.00049		
CO 25	50	497±17	0.00133		
CO 50	100	269±36	0.00304		
CO 100	200	89±12	0.01055		
Sample	Weight %	T2	1/T2- 1/T2PBS	R2	r^2
Agar 0.5	0.5	279±9	0.0029	6.62	1
Agar 1	1	152±4	0.0059		
Agar 2	2	77±6	0.0123		
Agar 4	4	37±5	0.0263		

[1] $T2_{PBS}$ value on this imaging day was 1466.4±34.2

Table B – XXIX. T2 (30 msec echo spacing) and R2 for Tyramine – Substituted Materials and Magnevist (Gd), MRI Day 4

Sample	[mg/ml]	T2	1/T2- 1/T2PBS	R2	r^2
TS-HA 6.25	6.25	1206±35	0.00015	0.031	0.99
TS-HA 12.5	12.5	1027±35	0.00029		
TS-HA 25	25	784±20	0.00059		
TS-HA 50	50	524±13	0.00123		
TS-HA 100	100	266±10	0.00308		
Sample	[mg/ml]	T2	1/T2- 1/T2PBS	R2	r^2
TS-GE 6.25	6.25	1284±31	0.00010	0.017	1.00
TS-GE 12.5	12.5	1147±19	0.00019		
TS-GE 25	25	961±18	0.00036		
TS-GE 50	50	718±18	0.00071		
TS-GE 100	100	417±12	0.00172		
Sample	[mg/ml]	T2	1/T2- 1/T2PBS	R2	r^2
TS-CO 6.25	12.5	1013±23	0.00031	0.050	0.99
TS-CO 12.5	25	811±26	0.00055		
TS-CO 25	50	567±29	0.00108		
TS-CO 50	100	234±12	0.00359		
TS-CO 100	200	95±24	0.00984		
Sample	[mM]	T2	1/T2- 1/T2PBS	R2	r^2
Gd 0.125	0.125	728±21	0.00069	6.19	1
Gd 0.25	0.25	474±13	0.00143		
Gd 0.5	0.5	273±7	0.00298		
Gd 1	1	145±8	0.00621		
Gd 2	2	77±7	0.01231		

[1] $T2_{PBS}$ value on this imaging day was 1466.4±34.2

Table B – XXX. T2 (30 msec echo spacing) and R2 for Cross – Linked Materials, MRI Day 4

Sample	[mg/ml]	T2	1/T2- 1/T2PBS	R2	r^2
TB-HA 6.25	6.3	1073±40	0.00025	0.034	0.99
TB-HA 12.5	12.5	882±161	0.00045		
TB-HA 25	25.3	712±75	0.00072		
TB-HA 50	50	503±33	0.00131		
TB-HA 100	100	236±171	0.00356		
Sample [1]	[mg/ml]	T2	1/T2- 1/T2PBS	R2	r^2
TB- GE 6.25	6.25	1241±28	0.00019	0.015	0.99
TB-GE 12.5	12.5	1337±26	0.00014		
TB-GE 25	25	1077±52	0.00032		
TB-GE 50	50	714±162	0.00079		
TB-GE 100	100	475±62	0.00149		
Sample	[mg/ml]	T2	1/T2- 1/T2PBS	R2	r^2
TB- CO 6.25	12.5	949±79	0.00037	0.053	0.99
TB-CO 12.5	25	719±163	0.00071		
TB-CO 25	50	388±88	0.00190		
TB-CO 50	100	358±55	0.00211		
TB-CO 100	200	160±129	0.00557		
Sample	[mg/ml]	T2	1/T2- 1/T2PBS	R2	r^2
TB- GE 60	61	573±61	0.00106	0.016	0.97
TB-GE 70	71	513±84	0.00127		
TB-GE 80	79	588±93	0.00102		
TB-GE 90	91	453±85	0.00153		

[1] All Samples in water

[2] $T2_{PBS}$ value on this imaging day was 1466.4±34.2

[2] $T2_{water}$ value on this imaging day was 1637±39

Table B - XXXI. T1 and R1 for Unsubstituted Materials and Agar, MRI Day 5

Sample	[mg/ml]	T1	1/T1- 1/T1PBS	R1	r^2
HA 6.25	6.25	2219±112	0.00005	0.0025	0.99
HA 12.5	12.5	2183±132	0.00005		
HA 25	25	2051±158	0.00008		
HA 50	50	1835±133	0.00014		
HA 100	100	1482±48	0.00027		
Sample	[mg/ml]	T1	1/T1- 1/T1PBS	R1	r^2
GE 6.25	6.25	2332±126	0.00002	0.0049	0.98
GE 12.5	12.5	2305±195	0.00003		
GE 25	25	2177±218	0.00005		
GE 50	50	1751±84	0.00017		
GE 100	100	1122±49	0.00049		
Sample	[mg/ml]	T1	1/T1- 1/T1PBS	R1	r^2
CO 6.25	12.5	2311±204	0.00003	0.0046	0.98
CO 12.5	25	2137±138	0.00006		
CO 25	50	2257±107	0.00004		
CO 50	100	1371±135	0.00032		
CO 100	200	760±279	0.00091		
Sample	Weight %	T1	1/T1- 1/T1PBS	R1	r^2
Agar 0.5	0.5	2173±177	0.00006	0.046	0.98
Agar 1	1	2033±105	0.00009		
Agar 2	2	1942±191	0.00011		
Agar 4	4	1646±78	0.00020		

[1] $T1_{PBS}$ value on this imaging day was 2469±178.8

Table B – XXXII. T1 and R1 for Tyramine - Substituted Materials and Magnevist (Gd), MRI Day 5

Sample	[mg/ml]	T1	1/T1- 1/T1PBS	R1	r^2
TS-HA 6.25	6.25	2388±209	0.00001	0.0028	1.00
TS-HA 12.5	12.5	2228±124	0.00004		
TS-HA 25	25	2108±104	0.00007		
TS-HA 50	50	1809±65	0.00015		
TS-HA 100	100	1461±56	0.00028		
Sample	[mg/ml]	T1	1/T1- 1/T1PBS	R1	r^2
TS-GE 6.25	6.25	2244±124	0.00004	0.0021	0.99
TS-GE 12.5	12.5	2226±132	0.00004		
TS-GE 25	25	2067±125	0.00008		
TS-GE 50	50	1913±59	0.00012		
TS-GE 100	100	1590±56	0.00022		
Sample	[mg/ml]	T1	1/T1- 1/T1PBS	R1	r^2
TS-CO 6.25	12.5	2327±118	0.00002	0.0043	1.00
TS-CO 12.5	25	2115±88	0.00007		
TS-CO 25	50	1829±96	0.00014		
TS-CO 50	100	1266±34	0.00038		
TS-CO 100	200	809±27	0.00083		
Sample	[mM]	T1	1/T1- 1/T1PBS	R1	r^2
Gd 0.125	0.125	938±30	0.00066	5.31	1.00
Gd 0.25	0.25	573±16	0.00134		
Gd 0.5	0.5	324±9	0.00268		
Gd 1	1	171±5	0.00544		
Gd 2	2	91±2	0.01058		

[1] $T1_{PBS}$ value on this imaging day was 2469±178.8

Table B – XXXIII. T1 and R1 for Cross-linked Materials, MRI Day 5

Sample	[mg/ml]	T1	1/T1- 1/T1PBS	R1	r^2
TB-HA 6.25	6.3	2395±242	0.00001	0.0031	1.00
TB-HA 12.5	12.5	2125±123	0.00007		
TB-HA 25	25.3	2025±112	0.00009		
TB-HA 50	50	1774±91	0.00016		
TB-HA 100	100	1381±81	0.00032		
Sample [1]	[mg/ml]	T1	1/T1- 1/T1PBS	R1	r^2
TB- GE 6.25	6.25	2134±156	0.00004	0.0033	1.00
TB-GE 12.5	12.5	2018±100	0.00007		
TB-GE 25	25	1914±146	0.00010		
TB-GE 50	50	1647±81	0.00018		
TB-GE 100	100	1290±104	0.00035		
Sample	[mg/ml]	T1	1/T1- 1/T1PBS	R1	r^2
TB- CO 6.25	12.5	2288±242	0.00003	0.0031	0.99
TB-CO 12.5	25	1870±145	0.00013		
TB-CO 25	50	1679±48	0.00019		
TB-CO 50	100	1495±81	0.00026		
TB-CO 100	200	948±32	0.00065		
Sample	[mg/ml]	T1	1/T1- 1/T1PBS	R1	r^2
TB- GE 60	61	1383±51	0.00032	0.0024	0.65
TB-GE 70	71	1640±111	0.00020		
TB-GE 80	79	1431±75	0.00029		
TB-GE 90	91	1855±120	0.00013		

[1] All Samples in water

[2] $T1_{PBS}$ value on this imaging day was 2469±178.8

[2] $T1_{water}$ value on this imaging day was 2343±116

Table B – XXXIV. T2 (15 msec echo spacing) and R2 for Unsubstituted Materials and Agar, MRI Day 5

Sample	[mg/ml]	T2	1/T2- 1/T2PBS	R2	r^2
HA 6.25	6.25	1144±26	0.00012	0.025	1
HA 12.5	12.5	1008±22	0.00024		
HA 25	25	821±13	0.00046		
HA 50	50	536±7	0.00111		
HA 100	100	309±5	0.00248		
Sample	[mg/ml]	T2	1/T2- 1/T2PBS	R2	r^2
GE 6.25	6.25	1169±33	0.00010	0.030	0.97
GE 12.5	12.5	1075±27	0.00018		
GE 25	25	976±17	0.00027		
GE 50	50	607±24	0.00089		
GE 100	100	264±9	0.00303		
Sample	[mg/ml]	T2	1/T2- 1/T2PBS	R2	r^2
CO 6.25	12.5	1079±20	0.00017	0.060	0.96
CO 12.5	25	855±67	0.00041		
CO 25	50	474±6	0.00135		
CO 50	100	287±31	0.00273		
CO 100	200	77±10	0.01223		
Sample	Weight %	T2	1/T2- 1/T2PBS	R2	r^2
Agar 0.5	0.5	288±5	0.0027	5.50	1
Agar 1	1	162±3	0.0054		
Agar 2	2	85±2	0.0110		
Agar 4	4	44±3	0.0220		

[1] $T2_{PBS}$ value on this imaging day was 1324.6.6±48

Table B – XXXV. T2 (15 msec echo spacing) and R2 for Tyramine - Substituted Materials and Magnevist (Gd), MRI Day 5

Sample	[mg/ml]	T2	1/T2- 1/T2PBS	R2	r^2
TS-HA 6.25	6.25	1110±31	0.00012	0.028	0.99
TS-HA 12.5	12.5	988±18	0.00024		
TS-HA 25	25	808±16	0.00046		
TS-HA 50	50	551±7	0.00111		
TS-HA 100	100	282±11	0.00248		
Sample	[mg/ml]	T2	1/T2- 1/T2PBS	R2	r^2
TS-GE 6.25	6.25	1134±32	0.00013	0.017	1.00
TS-GE 12.5	12.5	1039±20	0.00021		
TS-GE 25	25	886±10	0.00037		
TS-GE 50	50	679±13	0.00072		
TS-GE 100	100	409±9	0.00169		
Sample	[mg/ml]	T2	1/T2- 1/T2PBS	R2	r^2
TS-CO 6.25	12.5	1000±17	0.00025	0.049	0.98
TS-CO 12.5	25	790±19	0.00051		
TS-CO 25	50	568±32	0.00101		
TS-CO 50	100	237±4	0.00346		
TS-CO 100	200	95±3	0.00977		
Sample	[mM]	T2	1/T2- 1/T2PBS	R2	r^2
Gd 0.125	0.125	661±15	0.00076	6.22	1
Gd 0.25	0.25	441±8	0.00151		
Gd 0.5	0.5	260±4	0.00309		
Gd 1	1	142±3	0.00629		
Gd 2	2	76±3	0.01240		

[1] $T2_{PBS}$ value on this imaging day was 1324.6.6±48

Table B – XXXVI. T2 (15 msec echo spacing) and R2 for Cross - linked Materials, MRI Day 5

Sample	[mg/ml]	T2	1/T2- 1/T2PBS	R2	r^2
TB-HA 6.25	6.3	1047±22	0.00020	0.039	0.98
TB-HA 12.5	12.5	799±147	0.00050		
TB-HA 25	25.3	640±52	0.00081		
TB-HA 50	50	503±16	0.00123		
TB-HA 100	100	208±13	0.00405		
Sample [1]	[mg/ml]	T2	1/T2- 1/T2PBS	R2	r^2
TB- GE 6.25	6.25	1118±36	0.00022	0.018	0.99
TB-GE 12.5	12.5	1203±34	0.00016		
TB-GE 25	25	972±26	0.00036		
TB-GE 50	50	654±33	0.00086		
TB-GE 100	100	396±51	0.00185		
Sample	[mg/ml]	T2	1/T2- 1/T2PBS	R2	r^2
TB- CO 6.25	12.5	922±44	0.00033	0.030	0.97
TB-CO 12.5	25	640±73	0.00081		
TB-CO 25	50	455±48	0.00144		
TB-CO 50	100	399±47	0.00175		
TB-CO 100	200	140±10	0.00639		
Sample	[mg/ml]	T2	1/T2- 1/T2PBS	R2	r^2
TB- GE 60	61	606±77	0.0009	0.018	0.97
TB-GE 70	71	465±52	0.0014		
TB-GE 80	79	517±41	0.0012		
TB-GE 90	91	413±19	0.0017		

[1] All Samples in water

[2] $T2_{PBS}$ value on this imaging day was 1324.6.6±48

[2] $T2_{water}$ value on this imaging day was 1487±111

Table B – XXXVII. T2 (30 msec echo spacing) and R2 for Unsubstituted Materials and Agar, MRI Day 5

Sample	[mg/ml]	T2	1/T2- 1/T2PBS	R2	r^2
HA 6.25	6.25	1195±35	0.00015	0.027	1
HA 12.5	12.5	1057±20	0.00026		
HA 25	25	816±14	0.00054		
HA 50	50	516±8	0.00125		
HA 100	100	294±5	0.00272		
Sample	[mg/ml]	T2	1/T2- 1/T2PBS	R2	r^2
GE 6.25	6.25	1247±26	0.00012	0.033	0.98
GE 12.5	12.5	1146±15	0.00019		
GE 25	25	980±15	0.00034		
GE 50	50	584±27	0.00103		
GE 100	100	249±12	0.00333		
Sample	[mg/ml]	T2	1/T2- 1/T2PBS	R2	r^2
CO 6.25	12.5	1182±25	0.00016	0.062	0.97
CO 12.5	25	879±71	0.00045		
CO 25	50	468±7	0.00145		
CO 50	100	274±26	0.00296		
CO 100	200	76±10	0.01247		
Sample	Weight %	T2	1/T2- 1/T2PBS	R2	r^2
Agar 0.5	0.5	283±5	0.0028	5.52	1
Agar 1	1	157±4	0.0057		
Agar 2	2	82±3	0.0115		
Agar 4	4	44±6	0.0220		

[1] $T2_{PBS}$ value on this imaging day was 1459.6±28.4

Table B – XXXVIII. T2 (30 msec echo spacing) and R2 for Tyramine – Substituted Materials and Magnevist (Gd), MRI Day 5

Sample	[mg/ml]	T2	1/T2- 1/T2PBS	R2	r^2
TS-HA 6.25	6.25	1217±18	0.00015	0.033	0.99
TS-HA 12.5	12.5	1041±19	0.00026		
TS-HA 25	25	807±18	0.00054		
TS-HA 50	50	522±7	0.00125		
TS-HA 100	100	251±22	0.00272		
Sample	[mg/ml]	T2	1/T2- 1/T2PBS	R2	r^2
TS-GE 6.25	6.25	1242±26	0.00012	0.017	1
TS-GE 12.5	12.5	1092±12	0.00023		
TS-GE 25	25	925±22	0.00040		
TS-GE 50	50	701±14	0.00074		
TS-GE 100	100	405±10	0.00178		
Sample	[mg/ml]	T2	1/T2- 1/T2PBS	R2	r^2
TS-CO 6.25	12.5	1072±11	0.00025	0.054	0.99
TS-CO 12.5	25	808±20	0.00055		
TS-CO 25	50	558±35	0.00111		
TS-CO 50	100	223±4	0.00380		
TS-CO 100	200	88±4	0.01068		
Sample	[mM]	T2	1/T2- 1/T2PBS	R2	r^2
Gd 0.125	0.125	708±10	0.00073	6.09	1
Gd 0.25	0.25	459±10	0.00149		
Gd 0.5	0.5	268±6	0.00305		
Gd 1	1	146±5	0.00616		
Gd 2	2	78±4	0.01214		

[1] $T2_{PBS}$ value on this imaging day was 1459.6±28.4

Table B – XXXIX. T2 (30 msec echo spacing) and R2 for Cross – Linked Materials, MRI Day 5

Sample	[mg/ml]	T2	1/T2- 1/T2PBS	R2	r^2
TB-HA 6.25	6.3	1122±23	0.00021	0.049	0.97
TB-HA 12.5	12.5	814±186	0.00054		
TB-HA 25	25.3	620±59	0.00093		
TB-HA 50	50	477±14	0.00141		
TB-HA 100	100	172±18	0.00513		
Sample [1]	[mg/ml]	T2	1/T2- 1/T2PBS	R2	r^2
TB- GE 6.25	6.25	1207±22	0.00022	0.019	1
TB-GE 12.5	12.5	1278±28	0.00017		
TB-GE 25	25	1008±17	0.00038		
TB-GE 50	50	647±30	0.00094		
TB-GE 100	100	393±50	0.00193		
Sample	[mg/ml]	T2	1/T2- 1/T2PBS	R2	r^2
TB- CO 6.25	12.5	970±46	0.00035	0.034	0.97
TB-CO 12.5	25	663±77	0.00082		
TB-CO 25	50	431±38	0.00164		
TB-CO 50	100	378±46	0.00196		
TB-CO 100	200	129±9	0.00707		
Sample	[mg/ml]	T2	1/T2- 1/T2PBS	R2	r^2
TB- GE 60	61	632±96	0.0009	0.018	0.97
TB-GE 70	71	475±55	0.0014		
TB-GE 80	79	532±51	0.0012		
TB-GE 90	91	413±26	0.0017		

[1] All Samples in water

[2] $T2_{PBS}$ value on this imaging day was 1459.6±28.4

[2] $T2_{water}$ value on this imaging day was 1639±62

Fig B – I. R2 for Agar on the 5 MRI Days.